

# Development of fatigue assessment approaches for adhesively bonded joints

Master-Thesis

Román Hernando | 1825064

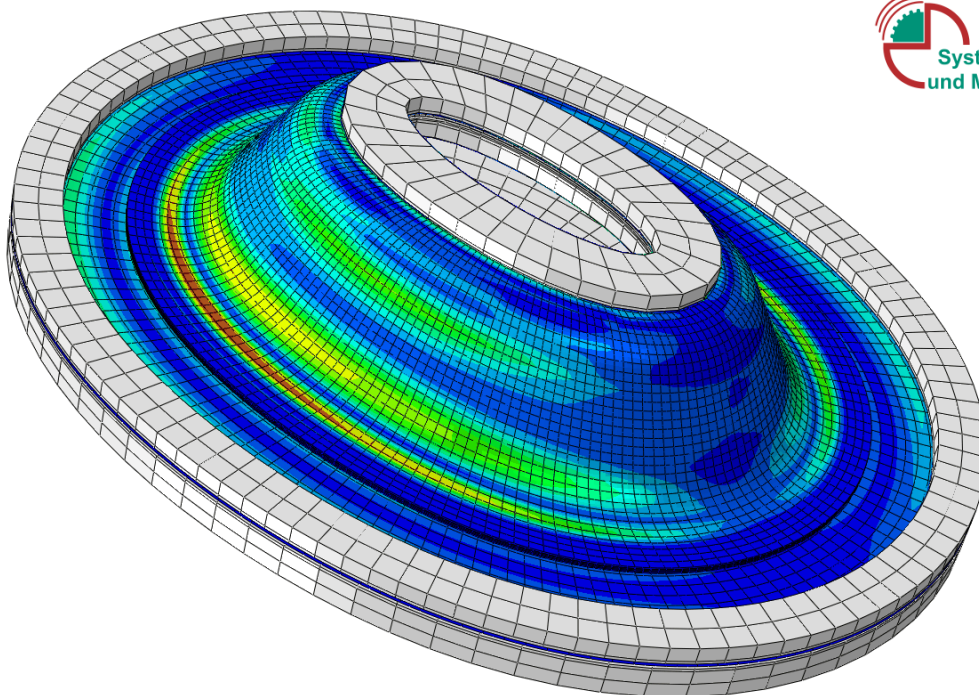
Systemzuverlässigkeit und Maschinenakustik SzM



TECHNISCHE  
UNIVERSITÄT  
DARMSTADT



Systemzuverlässigkeit  
und Maschinenakustik



---

Román Hernando  
Matrikelnummer: 1825064  
Studiengang: Maschinenbau

Master-Thesis  
Thema: "Development of Fatigue Assessment Approaches for Adhesively Bonded Joints"

Eingereicht: 23. November 2015

Betreuer:     Dipl.-Ing. Gudrun Rybar (SzM)  
                  Dr. Florian Bachmann (BMW AG)

Prof. Dr.-Ing. Tobias Melz  
Fachgebiet Systemzuverlässigkeit und Maschinenakustik SzM  
Fachbereich Maschinenbau  
Technische Universität Darmstadt  
Magdalenenstraße 4  
64289 Darmstadt

---



---

---

## **Declaration of honor**

---

I herewith formally declare that I have written the submitted thesis independently. I did not use any outside support except for the literature and other sources mentioned in the paper. I clearly marked and separately listed all of the literature and all of the other sources which I employed when producing this academic work, either literally or in content. This thesis has not been handed in or published before in the same or similar form.

In the submitted thesis the written copies and the electronic version are identical content.

Date: Darmstadt, den 23. November 2015

Signature:

---

---

---

## Index

---

Index of figures .....	III
Index of tables.....	VII
Index of abbreviations .....	VIII
Index of symbols .....	IX
1 Introduction .....	1
2 State of the art.....	2
2.1 Structural adhesive joints.....	2
2.1.1 Determination of the adhesive properties .....	5
2.1.2 Fundamentals of continuum mechanics for adhesive joints.....	8
2.1.3 Description and behaviour of elasto-plastic adhesives.....	9
2.2 Fatigue fundamentals .....	12
2.2.1 Experimental fatigue analysis.....	14
2.2.2 Nominal stress concept.....	17
2.2.3 Structural stress concept .....	18
2.2.4 Damage accumulation.....	20
2.2.5 Critical plane.....	22
2.3 Fatigue analysis for structural adhesive joints .....	25
2.3.1 Failure behaviour and criteria .....	25
2.3.2 Fatigue assessment approaches .....	28
3 Experimental investigations of bonded specimens.....	30
3.1 Adhesive .....	30
3.2 Substrate .....	31
3.3 KS-II specimen.....	31
3.4 Cup-shaped specimen .....	33
3.5 Butt-joined cylinder specimen.....	33
4 Numerical investigations.....	35
5 Evaluation of experimental and numerical investigations.....	37
5.1 Analysis of the test results.....	37
5.1.1 Analysis of KS-II specimen.....	37
5.1.2 Analysis of cup-shaped specimen.....	40
5.1.3 Analysis of butt-joined cylinder specimens .....	42
5.2 Validation of the Finite Element Models.....	47
5.2.1 Cup-shaped specimen validation .....	48
5.2.2 Butt-joined cylinder specimen validation.....	49
6 Application of stress approaches .....	51
6.1 Comparison of stress approaches for a lifetime of two million cycles .....	52
6.1.1 Critical distance approach .....	52
6.1.2 Stress averaging approach.....	74
6.2 Comparison of stress approaches in a master S-N curve .....	83
6.2.1 Critical distance approach .....	83
6.2.2 Stress averaging approach.....	86

---

6.2.3	Comparison of the applied approaches .....	87
7	Evaluation of the butt-joined specimen submitted to non-proportional loading.....	89
8	Conclusions .....	92
9	Outlook .....	94
Annex	.....	XI
A.	Technical drawings .....	XI
A.1.	KS-II specimen.....	XI
A.2.	Cup- shaped specimen .....	XII
A.3.	Butt-joined cylinder specimen.....	XIII
Bibliography	.....	XIV
Norms	.....	XVIII

---

---

## Index of figures

---

Figure 2-1: Adhesion and cohesion.....	2
Figure 2-2: Shear Deformation in an adhesive joint [Hab06] .....	6
Figure 2-3: a) Typical creep curve in creeping tests and the response of a rheological Burgers-Model [Mat12] b) Scheme of a rheological Burgers-Model [Mat12] c) Scheme of a mechanical equivalent 2-chained Maxwell-Model [Mat12].....	7
Figure 2-4: Description of the stress components [Men11] .....	8
Figure 2-5: Method to determinate the hydrostatic coefficient $a$ .....	12
Figure 2-6: Division of fatigue strength according to [Son08].....	14
Figure 2-7: Haigh diagram [Hai03] .....	16
Figure 2-8: S-N and Gassner curves by [Son05].....	16
Figure 2-9: Definition of hotspot-stress $\sigma_{hs}$ for welding joints by FRICKE [Rad07].....	19
Figure 2-10: Lifetime prediction under load with variable amplitude by [Son05] .....	21
Figure 2-11: Variants of the linear damage accumulation .....	22
Figure 2-12: Critical plane method to evaluate fatigue lifetime [Sus11] .....	23
Figure 2-13: Angle and vector references to describe the cutting plane [Sus10].....	24
Figure 2-14: Failure mode according to norm DIN EN ISO 10365.....	27
Figure 2-15: Example of the NEUBER theory for a notched sample [Neu68].....	29
Figure 3-1: Possible loading direction of KS-II specimens [Hah00] .....	32
Figure 3-2: Cup-shaped specimen (left), Possible setting up of Cup-shaped specimen (right)	33
Figure 3-3: Butt-joined cylinder specimen .....	34
Figure 5-1: S-N curves for KS-II test, pure tension (KZ), pure shear (SZ) and Mixed Mode with 45° resultant force angle (45°) .....	39
Figure 5-2: Reference components for cup-shaped adhesive layer specimen .....	40
Figure 5-3: S-N curve for Cup-shaped specimen .....	41
Figure 5-4: S-N curve 50% survival probability lifetime curve for butt-joined cylinder specimens .....	44
Figure 5-5: Average displacement of samples under pure torsion load before failure .....	45
Figure 5-6: Stiffness trends of the adhesive joint during pure torsion load .....	46
Figure 5-7: Stiffness trends of adhesive joint during axial load.....	47

---

Figure 5-8: Location of the strain gauges on cup-shaped specimens.....	48
Figure 5-9: Validation of the measured and the simulated strain .....	48
Figure 5-10: Stiffness behaviour of the quasi-static tests; a) pure torsion, b) pure tension ....	49
Figure 5-11: Comparison between the elastic stiffness of the simulation and the tests; a) pure torsion, b) pure tension.....	49
Figure 6-1: Middle plane of the adhesive with the three paths studied in KS-II specimen.....	53
Figure 6-2: Stress distribution along path 1 for critical distance approach .....	54
Figure 6-3: Stress distribution along path 2 for critical distance approach .....	55
Figure 6-4: Stress distribution along path 3 for critical distance approach .....	56
Figure 6-5: Path of the stress distribution (red line) for the cup-shaped specimen .....	57
Figure 6-6: Maximum principal stress distribution of KS-II (along path 1) and cup-shaped specimens .....	58
Figure 6-7: Comparison of the stress distribution between KS-II at path 1, $z = 1.7$ mm, and cup-shaped specimen using the critical distance approach.....	58
Figure 6-8: Comparison of stress distribution between KS-II at path 2, $z = 22$ mm, and cup-shaped specimen using the critical distance approach .....	59
Figure 6-9: Maximum principal stress distribution of KS-II (along path 1) and cup-shaped specimens with constant gap from the point with highest maximal principal stress ...	60
Figure 6-10: Maximum principal stress distribution of KS-II (along path 1) and cup-shaped specimens considering a relative distance .....	61
Figure 6-11: Maximum principal stress distribution of KS-II (along the path 1) and cup-shaped specimens with a constant gap distance from the point with highest max. principal stress and considering a relative distance .....	61
Figure 6-12: Maximum principal stress distribution of KS-II (along the path 1) and cup-shaped specimens applying the three hypotheses .....	62
Figure 6-13: Maximum principal stress distribution of KS-II (along path 2) and cup-shaped specimens considering a relative distance .....	63
Figure 6-14: Maximum principal stress distribution of KS-II (along the path 2) and cup-shaped specimens with a constant gap distance from the point with highest max. principal stress and considering a relative distance .....	63



---

Figure 6-15: Maximum principal stress distribution of KS-II (along the path 2) and cup-shaped specimens with a constant gap distance from the point with highest max. principal stress and considering a relative distance .....	64
Figure 6-16: Maximum principal stress distribution of KS-II (along the path 2) and cup-shaped specimens with applying the three hypotheses .....	64
Figure 6-17: Max. principal stress distribution of the butt-joined specimen along the middle layer .....	65
Figure 6-18: Maximum principal stress distribution of the three specimen types along the middle layer.....	66
Figure 6-19: Graphic Beltrami stress- first invariant to find the $a$ parameter [Tre12] .....	68
Figure 6-20: Five points to determinate the equivalent elliptic stress parameters .....	69
Figure 6-21: Graphic Beltrami tension - first invariant to determinate $a$ parameter. From left to the right the points with same colour are from: pure shear, mixed-mode and pure tension.....	70
Figure 6-22: Graphic $\sqrt{(J_2)} - I_1$ that determines the maximum stress state combination. From left to the right the points with same colour are from: pure shear, mixed-mode and pure tension.....	71
Figure 6-23: Comparison stress distribution between KS-II and cup-shaped specimens respect equivalent elliptic stress .....	72
Figure 6-24: Equivalent elliptic stress distribution of KS-II and cup-shaped specimens with constant reference distance from their maximal stress point.....	73
Figure 6-25: Equivalent elliptic stress distribution of KS-II and cup-shaped specimens with relative distance.....	73
Figure 6-26: Equivalent elliptic stress distribution of KS-II and cup-shaped specimens with a constant reference distance and relative distance .....	74
Figure 6-27: Stress distribution along path 1 for stress averaging approach .....	75
Figure 6-28: Stress distribution along path 2 for stress averaging approach .....	76
Figure 6-29: Stress distribution along path 3 for stress averaging approach .....	77
Figure 6-30: Comparison of the stress distribution between KS-II at path 1, $z = 1.7$ mm, and cup-shaped specimen using the stress averaging approach .....	78
Figure 6-31: Comparison of stress distribution between KS-II at path 2, $z = 22$ mm, and cup-shaped specimen using the stress averaging approach.....	79

---

Figure 6-32: Average of maximum principal stress distribution of KS-II (along path 1) and cup-shaped specimens with constant gap from the point with highest maximal principal stress.....	80
Figure 6-33: Average of maximum principal stress distribution of KS-II (along path 1) and cup-shaped specimens considering a relative distance .....	80
Figure 6-34: Average stress distribution of KS-II (along the path 1) and cup-shaped specimens with a constant gap distance from the point with highest max. principal stress and considering a relative distance .....	81
Figure 6-35: Average stress distribution of KS-II (along the path 1) and cup-shaped specimens applying the three hypotheses.....	81
Figure 6-36: Minimum scatter of the different parameters applying the critical distance approach.....	84
Figure 6-37: Scatter values along the distance applying the critical stress distance approach	85
Figure 6-38: Minimum scatter of the master S-N curve for the several hypotheses using the reference stresses of path 1 applying the stress averaging approach .....	86
Figure 6-39: Scatter values of the master S-N curve along the path 1 applying the stress averaging approach.....	86
Figure 6-40: Comparison of the minimum scatter between the two approaches .....	87
Figure 6-41: Scatter values of the approaches along the distance.....	88

---

---

## Index of tables

---

Table 2-1: Classification according to the application of adhesives .....	5
Table 2-2: Advantages and disadvantages of basic concepts for fatigue analysis according to [Vor03] and [Kre99].....	13
Table 3-1: Elastic mechanical properties of steel.....	31
Table 3-2: Type of substrate steel for every test .....	31
Table 5-1: No. of samples for each loading type .....	37
Table 5-2: No. of samples for each loading type for the butt-joined cylinder specimens .....	42
Table 6-1: Values of the equivalent elliptic stress parameters.....	71
Table 7-1: Maximum damage accumulation for the 16 butt-joined samples with combined loads with phase shift .....	91

---

---

## Index of abbreviations

---

Abbreviation	Description
CAE	Computer-aided engineering
FE	Finite Element
FEA	Finite Element Analysis
FEM	Finite Element Model
KS-II	U-Profile specimen for tension/shear loads (Kopfzug, Scherzug)
KZ	<i>Kopfzug</i> , pure tension load
NVH	Noise, vibration and harshness
RP	Reference Point
SZ	<i>Scherzug</i> , pure shear load

---



---

## Index of symbols

---

Symbol	Unit	Description
$a$	MPa	Hydrostatic coefficient from equivalent elliptic stress
$A$	mm <sup>2</sup>	area
$b$		Coefficient of equivalent elliptic stress
$d$	mm	Thickness of the adhesive layer
$D$		Damage of Palmgren-Miner
$D_i$		Unitary damage/damage for a cycle
$D_{th}$		Theoretical total damage
$D_{total}$		Total Damage
$E$	MPa	Elastic modulus
$F$	N	Force
$G$	MPa	Shear modulus
$I_1$	MPa	First invariant of hydrostatic stress tensor
$J_2$	MPa <sup>2</sup>	Second invariant of the stress deviator
$k$		Slope of S-N curve
$K_p$		Plastic concentration factor
$K_t$		Concentration factor
$M_b$	N mm	Bending moment
$M_t$	N mm	Torsion moment
$N_{exp}$		Experimental number of cycles
$N_i$		Cycles with $\sigma_i$ stress
$N_k$		Number of cycles at the threshold point
$N_{rech,D=1}$		Calculated number of cycles for $D = 1$
$P_1$		Lifetime probability
$Q$	N	Shear force
$R$		Stress ratio
$r_{M/F}$	mm	Ratio between moment and force in butt-joined cylinder specimens with combined load
$r_{\sigma/\tau}$		Ratio between tension stress and torsion stress for combined loads in butt-joined cylinder specimens
$S$	MPa	nominal normal stress
$S_p$	MPa	Plastic nominal normal stress
$T$	MPa	nominal shear stress



$T_p$	MPa	Plastic nominal shear stress
$v$	mm	Lateral displacement
$W_b$	mm <sup>3</sup>	Resistance to bending moment
$W_t$	mm <sup>3</sup>	Resistance to torsion moment
$\gamma$	°	Deformation angle under shear stress loading
$\varepsilon$		Strain
$\varepsilon_{axial}$		Strain in the direction of the applied force
$\varepsilon_{trans}$		Strain in the perpendicular direction of the force
$\nu$		Poisson ratio
$\rho^*$	mm	Optimal distance of the averaged stress
$\sigma$	MPa	Tension stress
$\sigma^*$	MPa	Principal stress
$\sigma_a$	MPa	Stress amplitude
$\sigma_{a, Re}$	MPa	Plastic stress limit
$\sigma_{e,max}$	MPa	Peak normal stress
$\sigma_{eff}$	MPa	Effective stress
$\sigma_{ell}$	MPa	Equivalent elliptic stress
$\sigma_{HS}$	MPa	Maximum principal stress (Hauptspannung)
$\sigma_k$	MPa	Threshold fatigue limit
$\sigma_m$	MPa	Mean stress
$\sigma_{max}$	MPa	Maximum stress of a variable load
$\sigma_{max HS}$	MPa	highest value of the maximum principal stress
$\sigma_{min}$	MPa	Minimum stress of a variable load
$\sigma_{VM}$	MPa	Von Mises stress
$\tau$	MPa	Torsion or shear stress
$\tau_{e,max}$	MPa	Peak shear stress
$\tau_F$	MPa	Elliptic equivalent stress
$\tau_{v,Belt}$	MPa	Equivalent stress according to Beltrami equation

---

---

## 1 Introduction

---

The increasing global warming and pollution in our world concerns the population about the necessity to reduce the consumption of natural resources. In the last years the automobile industry has focused in reducing the consumption of their vehicles. Beside the improvement of the motors, an important aspect is the reduction of the total weight of the vehicle. The introduction of light-weight materials contributes to this aim. The use of these materials fosters novel joining technologies. Traditionally, the main joining technology in automotive industry is welding. Low cost and fast application for joining metallic components are the main benefits.

The lightweight materials, such as fibre reinforced plastics, cannot be welded and alternative joining techniques are necessary. In this way, adhesive joints are becoming more important to and complement classic joining technologies such as welding, riveting or clinching. There are several advantages of its use. One advantage is the increase of the total stiffness of the body-in-white structure. Another advantage is the improvement of crash energy absorption. The most important is the possibility to join materials that cannot be welded, as for example metallic plates with glass or carbon fibre materials.

The increasing use of structural adhesive opens a new investigation field. To develop an optimum design of adhesive joints it is necessary to understand the connection behaviour and derive design allowable for quasi-static dynamic and fatigue loading.

The behaviour of adhesives submitted to variable amplitude loading and proper computational fatigue analysis is not yet state of art and concern of ongoing research [Sch14]. The methods applied to analyse the behaviour of adhesive are based mainly on the methods used to evaluate welded joints. They should be analysed to evaluate if they describe properly the behaviour and failure of the modern adhesive bonds. Otherwise, new methods based on the adhesive characteristics should be developed.

---

---

## 2 State of the art

---

An introduction of the specific aspects, in order to evaluate properly the fatigue life of adhesive joints, is the first point of this report. This chapter starts with a definition of structural adhesive joints followed by the definition of fatigue for materials.

---

### 2.1 Structural adhesive joints

---

Adhesive joints are one of the oldest joining techniques, even before screwing, riveting or welding. In 5.000 Year B.C., the human being used resins to join the parts of their first tools and weapons, as spears or harpoons [Sta98].

The norm DIN EN 923 defines an adhesive as a non-metallic material, which can join through surface bonding (adhesion), and which gives sufficient internal strength (cohesion) to maintain the joint. That means that there are two types of forces, adhesive and cohesive, that ensure a proper connection between the substrates.

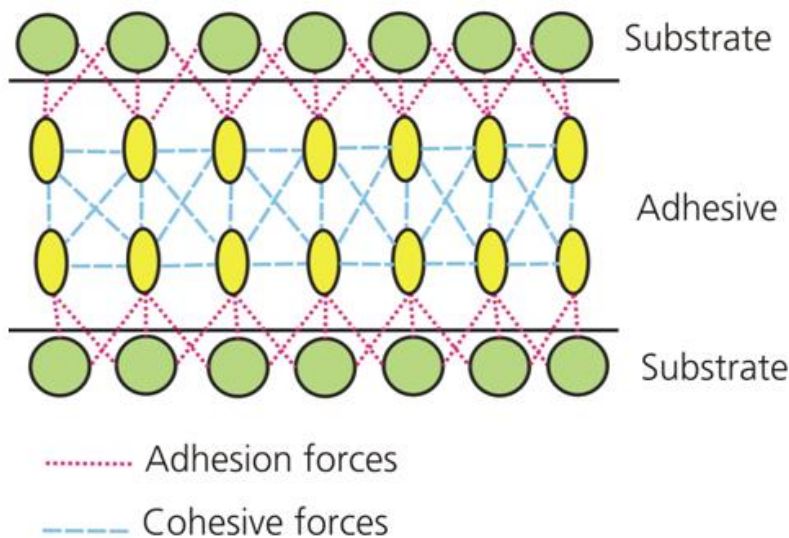


Figure 2-1: Adhesion and cohesion

Adhesion involves all the connection forces that guarantee the union between the adhesive and the adherent or substrate. They also determine the strength of the boundary layer. Some factors, as the stress state of the substrate or the pre-treatment of the substrate surface, affect the maximal strength of these forces. To obtain higher forces, the surface should be prepared in advance before application of the adhesive. The stress state of the substrate should not exceed the allowable value. Two different types of adhesion are considered: specific adhesion and mechanic adhesion. Mechanic adhesion is the mechanical bracing of the cured adhesive in the pores of the surface. In a macroscopic view of smooth surfaces, as the metal plates used



---

in automobiles, this type of adhesion is almost insignificant. Specific adhesion is based on the interaction of intermolecular forces at the borders of the joint, with chemical links between the molecules of the adhesive and the substrates and the interlinking of polymeric molecules with the surface of the substrate. Modern adhesives have been developed to produce a diffusion process between the molecules of the adhesive and the atoms of the substrate, increasing this adhesive force [Sta98].

The internal strength of the adhesive is based on the **cohesive forces**. These forces are produced by the attractions between atoms and molecules of a material. They strongly depend on the temperature and the state of the adhesive, which reaches its maximum when it is completely cured.

The first adhesives were based on plant resins, animal blood, egg proteins or asphalt [Sta98]. Currently, adhesives are composed of bulking agent and an additive. There are diverse classifications to determinate the type of adhesive, the most common classifications are based on their composition. A major distinction of adhesives is one component and two component adhesives. The latter one cures with a chemical reaction mixing the components in a well-defined proportion. Typical examples of these adhesives are: Epoxy resins, polyurethanes, methacrylates and silicones. One component adhesives can be classified according to their curing process. These curing processes are: chemical curing (Epoxies, Polyurethane, Cyanacrylate, Silicone), physical curing (coupling agents, Plastisol), chemical-physical curing (Dispersion adhesives) and pressure sensitive adhesives (Acrylates, natural or synthetic rubbers). A more specific differentiation can be done for the chemical curing adhesives according to the temperature of this process, cold or warm curing. Furthermore, another distinction is the chemical curing process which can be classified as polymerization, polyaddition and polycondensation [Sch14].

Nowadays, the use of adhesive joints is widely used in different fields, such as medicine, mechanical engineering, aerospace and electronic engineering. The implementation of this joining technique in automotive industry is increasing mainly due to the possibility to join different materials. Other benefits of adhesive connections are the process automation of adhesive lines application and corrosive protection [Sta98]. The advantages and disadvantages of their use are, according to [Gei12], [Hen11] and [Tre12]:

Advantages:

- Possibility to join different materials
- Substrates are not harmed by holes

- 
- Continuous surface connection, beside the non-uniform stress distribution that produces stress peaks on some specific points
  - Smaller heat stresses due to the joining process, smaller pre-stress
  - No electrical conductivity, thermal isolation and reduced contact corrosion
  - Possibility to join thin substrates
  - Greater geometrical tolerance allowable for part connection
  - Good damping properties (NVH)
  - Gas and liquid sealing of the joint, reduced corrosion
  - High fatigue resistance
  - Improvement of stiffness and crash properties of the car

Disadvantages:

- High influence of temperature and humidity
- Cleaning and pre-treatment of substrate surfaces essential
- Necessity of continuous quality control of the joining processes
- The shear strength is usually higher than the tensile strength. Because of that special design of the methods are used to reduce the tensile stresses in the adhesive.
- Limited demountability
- Difficult recycling

The adhesive can be classified according to their use, which is influenced by the mechanical properties of the adhesives (e.g. the stiffness or the ultimate elongation), in: structural adhesives, elastic adhesives or sealant adhesives. The division is given in more detail in the table 2-1, according to [Hab06] and [Sch07]:

---

Table 2-1: Classification according to the application of adhesives

Application	Strength	Shear Modulus $G_K$ [N/mm <sup>2</sup> ]	Ultimate elongation $e_K$ [%]
Structural Adhesive	High	>10	Up to 70
Elastic Adhesive	Medium	1-10	70-300
Sealant Adhesive	Low	0.1-1	300-700

---

### 2.1.1 Determination of the adhesive properties

---

Frequently, the substance samples are not considered appropriate to determine the mechanical properties of adhesives, such as the elastic modulus, shear modulus, yield strength and elongation at failure (specified in DIN EN ISO 527 for plastics). To obtain these mechanical properties of the bonded joints, other specific tests are realized, as the tensile test method using thick adherends that is described in the norm ISO 11003-2 or the determination of tensile lap-shear strength on bonded assemblies described in DIN EN 1465. Another common test to determinate the mechanical properties is to use bonded tubes loaded with an axial force, a twisting moment (torsion) or a combination of them.

The main properties of adhesive are explained below.

#### Shear modulus

Nominal shear strength is usually higher than tensile strength. Because of that, the typical mechanical property measured to define the stiffness of the adhesive is the shear modulus ( $G$ ) rather than the elastic modulus ( $E$ ), which is used more often for other types of materials. The variable  $G$  relates the stress with the strain or deformation of the material. Figure 2-2 shows the shear deformation in an adhesive joint with a pure shear stress state:

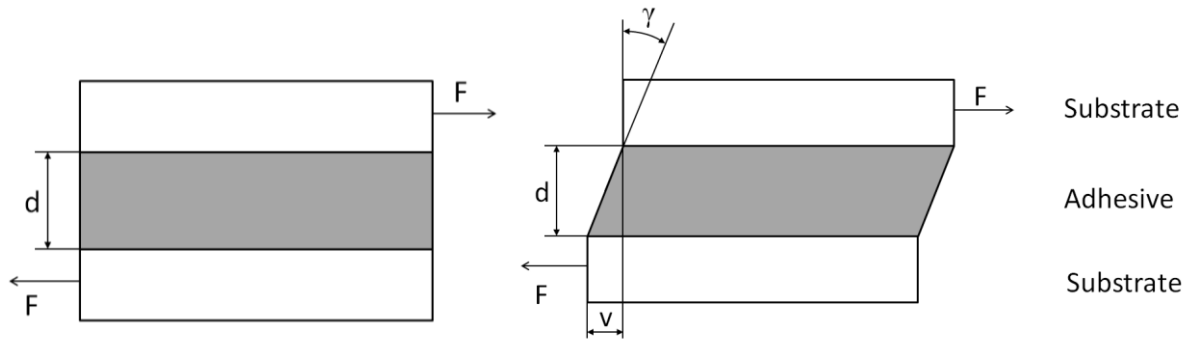


Figure 2-2: Shear Deformation in an adhesive joint [Hab06]

The shear modulus, also known as modulus of rigidity, is defined as:

$$G = \frac{\tau}{\tan \gamma} \quad (2.1)$$

The relation between the force and the stress is:

$$\tau = \frac{F}{A} \quad (2.2)$$

Where  $A$  is the surface in contact between the adhesive and adherent.

Another definition of Shear modulus based on the relation:

$$\tan \gamma = \frac{v}{d} \quad (2.3)$$

$$G = \frac{\tau}{v} d \quad (2.4)$$

$v$  represents the lateral displacement of the substrate and  $d$  the thickness of the adhesive layer.

The deformation of the adhesive is elastic for low stresses but becomes plastic behaviour for higher stresses.

### Poisson ratio

The Poisson ratio of a material is the negative ratio of transverse to axial strain. When a material is stretched, it usually tends to contract in the directions transverse to the direction of stretching. This phenomenon is called Poisson effect. The Poisson ratio is defined with the Greek letter  $\nu$  (nu).

$$\nu = -\frac{d\varepsilon_{trans}}{d\varepsilon_{axial}} \quad (2.5)$$

The Poisson's ratio is an important property of an adhesive due to its relatively high value. A common value of Poisson ratio for adhesives is between 0.3 and 0.5.

To determine this ratio with tests, the following equation can be used:

$$\nu = \frac{2(1 - \frac{G}{E})}{1 - 2\frac{G}{E}} \quad (2.6)$$

### Creep

Creep is the tendency of a material to reversibly deform under a constant load for viscoelastic materials [Hab06]. The creep effect can be classified in three phases. Figure 2-3 shows these phases:

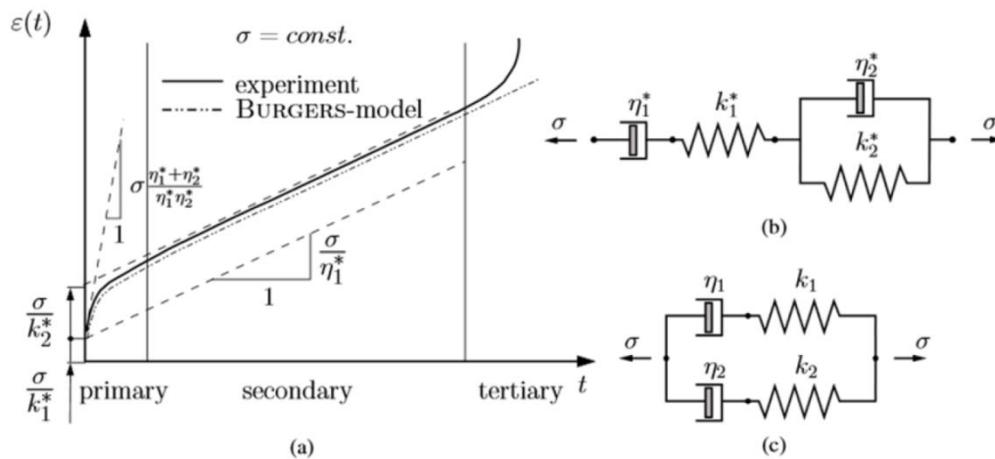


Figure 2-3: a) Typical creep curve in creeping tests and the response of a rheological Burgers-Model [Mat12]  
 b) Scheme of a rheological Burgers-Model [Mat12]  
 c) Scheme of a mechanical equivalent 2-chained Maxwell-Model [Mat12]

The primary phase is a quick deformation of the material. Then the secondary phase starts, which denotes a constant slope for the strain. The tertiary phase consists of a quick deformation and final failure of the specimen.

Adhesives submitted to cyclic loading show a pronounced creep effect. The creep influence increases with higher mean stresses and with lower frequencies [Har11]. Testing with high frequencies increases the temperature of the adhesive significantly. This effect harms the adhesive properties and introduces a higher damage in the material. In [P653] the influence of the frequency is studied and in it was determined a maximum frequency of 10 Hz to reduce

the increase of temperature during the test. According to the norm DIN EN 9664 the maximum test frequency is limited to 30 Hz for high-strength structural adhesives. For other adhesive the frequency is recommended to be between 1 Hz and 10 Hz.

## 2.1.2 Fundamentals of continuum mechanics for adhesive joints

The stress state of an element can be represented by the stress tensor. According to [Gro07] the stress tensor can be divided in the hydrostatic component and the deviatoric component (eq. (2.7) and figure 2-4). The hydrostatic component is an isotropic stress that represents the change in volume (figure 2-4b). The deviatoric component is the stress tensor rest after subtracting out the hydrostatic component. The deviatoric stress tensor describes the deformation of the volume under consideration.

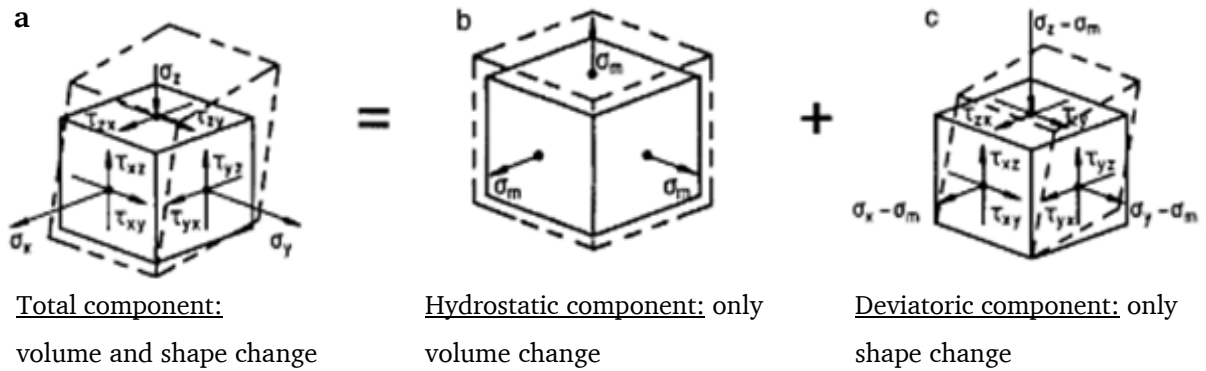


Figure 2-4: Description of the stress components [Men11]

$$\underbrace{\begin{bmatrix} \sigma_{11} & \tau_{12} & \tau_{13} \\ \tau_{21} & \sigma_{22} & \tau_{23} \\ \tau_{31} & \tau_{32} & \sigma_{33} \end{bmatrix}}_{\text{Stress tensor } \sigma_{ij}} = \underbrace{\begin{bmatrix} \sigma_m & 0 & 0 \\ 0 & \sigma_m & 0 \\ 0 & 0 & \sigma_m \end{bmatrix}}_{\text{Hydrostatic component}} + \underbrace{\begin{bmatrix} \sigma_{11} - \sigma_m & \tau_{12} & \tau_{13} \\ \tau_{21} & \sigma_{22} - \sigma_m & \tau_{23} \\ \tau_{13} & \tau_{32} & \sigma_{33} - \sigma_m \end{bmatrix}}_{\text{Deviatoric component } s_{ij}} \quad (2.7)$$

with

$$\sigma_m = p = \frac{\sigma_{11} + \sigma_{22} + \sigma_{33}}{3} \quad (2.8)$$

The components of the deviatoric tensor can also be written with the Kronecker-delta  $\delta_{ij}$ :

$$s_{ij} = \sigma_{ij} - \frac{1}{3} \sigma_{kk} \delta_{ij} \quad (i, j, k = 1, 2, 3) \quad (2.9)$$

---

The hydrostatic component is invariant to coordinate transformation and can be represented by the first invariant  $I_1$  of the hydrostatic tensor.

$$I_1 = \sigma_{11} + \sigma_{22} + \sigma_{33} = \sigma_{ii} = 3p \quad (2.10)$$

The deviatoric component can be described by the second invariant  $J_2$ . This invariant is also known as quadratic invariant, due to its quadratic terms:

$$J_2 = \frac{1}{6} \left[ (\sigma_x - \sigma_y)^2 + (\sigma_y - \sigma_z)^2 + (\sigma_z - \sigma_x)^2 \right] + \tau_{xy}^2 + \tau_{yz}^2 + \tau_{xz}^2 = \frac{1}{2} s_{ij} s_{ij} \quad (2.11)$$

The second invariant can also be described through the VON MISES stress:

$$\sigma_{VM} = \sqrt{3 \cdot J_2} \quad (2.12)$$

The equations and information are according to [Bet04], [Gro07] and [Men11].

---

### 2.1.3 Description and behaviour of elasto-plastic adhesives

---

In this master thesis, the failure is considered exclusively cohesive (inside the adhesive layer). Another assumption is that the adhesive possesses linear-elastic material behaviour. For the fatigue tests considered, the applied load is well below the yield strength of the adhesive. The simplification of linear-elastic material behaviour can be considered valid

The maximum principal stress and the equivalent elliptic stress are evaluated for failure assessment.

---

#### Maximum principal stress

---

The maximum principal stress is an equivalent stress from the stress tensor that can be used as a reference. The definition of this stress is the maximum normal stress in a specific direction. This stress is based on the stress tensor. It is always a positive-defined matrix, which means that through a coordinate transformation it is possible to transform the stress tensor in a diagonal matrix (eq. (2.13)).

$$[\sigma^*] = [S]^T [\sigma] [S] = [S]^T \begin{bmatrix} \sigma_{11} & \tau_{12} & \tau_{13} \\ \tau_{21} & \sigma_{22} & \tau_{23} \\ \tau_{31} & \tau_{32} & \sigma_{33} \end{bmatrix} [S] = \begin{bmatrix} \sigma_1^* & 0 & 0 \\ 0 & \sigma_2^* & 0 \\ 0 & 0 & \sigma_3^* \end{bmatrix} \quad (2.13)$$

---

considering [S] the matrix of the principal direction vectors and  $\sigma^*_1, \sigma^*_2$  and  $\sigma^*_3$  the principal stresses. The maximum principal stress is the highest value of these three stresses. The principal stresses are the eigenvalues of the stress tensor and their directions are the eigenvectors. These directions are always perpendicular toward each other and form a tripod coordinate base system. The method to calculate them is based equations (2.14) and (2.15):

$$[\sigma]v = \lambda v \quad (2.14)$$

$$\det ([\sigma] - \sigma^* [I]) = 0 \quad (2.15)$$

Herein, v is a principal direction and  $\sigma^*$  is a principal stress and [I] the identity matrix.

---

### Equivalent elliptic stress

---

The equivalent elliptic stress is a combination of the invariants of the stress tensor. This equivalent stress showed good results in other investigations [Her14], [Sch05], [Tre12]. It is based on the following assumptions and findings.

In an isotropic continuum material, it is possible to determine the deformation through a combination of stresses  $\sigma_{ij}$ . With an appropriate coordinate transformation, the combination of stresses can be substituted by the three invariants of the stress tensor,  $I_1, I_2$  and  $I_3$ .

$$F = F(I_1, I_2, I_3) \quad (2.16)$$

For an incompressible material, the hydrostatic component has no influence and the invariants of eq. (2.16) can be substituted by the invariants of the deviatoric component  $J_1, J_2, J_3$ .

$$J_1 = s_{ij}\delta_{ij} = 0$$

$$J_2 = \frac{1}{2}s_{ij}s_{ij} \quad (2.17)$$

$$J_3 = \det(s_{ij}s_{ij})$$

For a compressible material, the hydrostatic component  $I_1$  is considered and the stress can be considered as a function of  $I_1, J_2, J_3$ . The third invariant of the stress tensor can be neglected and the equation can be described as [Sch74]:



$$F = F(I_1, J_2) = J_2 + a I_1 + b I_1^2 \quad (2.18)$$

The equation (2.18) is a variation of the yield function of Beltrami (1885):

$$F = J_2 + b I_1^2 \quad (2.19)$$

The equation used in this case is an adaptation of eq (2.19):

$$\tau_F^2 = J_2 + a I_1 + b I_1^2 \quad (2.20)$$

The parameters are determined according to [Tre12]:

$$b = \frac{1}{6} \frac{1 - 2\nu}{1 + \nu} \quad (2.21)$$

where  $\nu$  is the Poisson ratio.

$$a = \frac{E\alpha}{1 + \nu} \quad (2.22)$$

where  $E$  is the elastic modulus of the adhesive and  $\alpha$  an influence parameter of the hydrostatic component that is experimentally determined. For detailed information about these parameters, see [Sch74], [Tre12].

The sign of the first invariant ( $I_1$ ) determinates the type of normal stress. If it is positive ( $I_1 > 0$ ), the normal stress is a tensile stress. If it is negative ( $I_1 < 0$ ) then the normal stress is a compressive stress. For adhesives, the tensile stress causes higher damage than the compressive stress [Tre12].

#### **Determination of the hydrostatic coefficient $a$**

Equations (2.19) and (2.20) are used to determine the coefficient  $a$ :

$$\tau_{V,Belt}^2 = \tau_F^2 - a I_1 \quad (2.23)$$

where  $\tau_F$  is the equivalent elliptic stress and  $\tau_{V,Belt}$  the equivalent stress according to Beltrami (eq (2.19)). The parameter  $a$  is the slope of the line between two different stresses of Beltrami's equivalent stress.

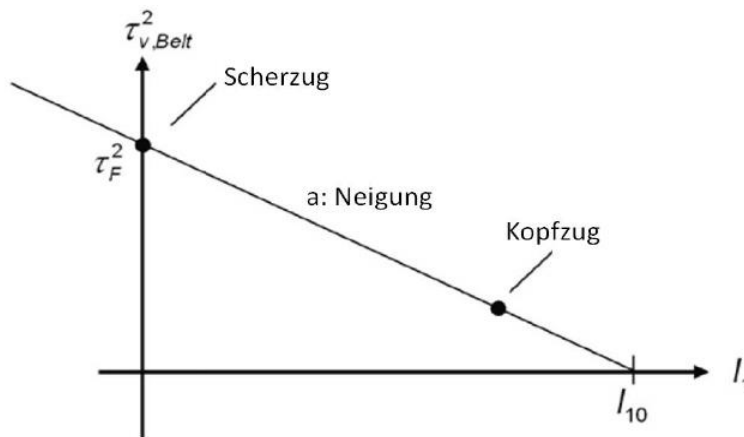


Figure 2-5: Method to determinate the hydrostatic coefficient  $a$

This slope can be experimentally determined by a linear regression between two loading types.

The method to calculate the coefficients and apply the equivalent elliptic stress works as follows:

1. Experimental determination of the maximum load for at least two loading types (for example pure tension and pure shear).
2. Calculate the stress tensor through FE-Simulation
3. Determination of  $\tau_{v,Belt}$  through the invariants  $I_1$  and  $J_2$  using equation (2.19).
4. Represent the reference points of the two different loading types in a yield diagram (figure 2-5).
5. Calculate the linear regression of the reference points to obtain the hydrostatic coefficient  $a$ . This value does strongly depend on the point stress evaluation (e.g. which node is the FE representation of the loading layer).

---

## 2.2 Fatigue fundamentals

---

Fatigue, as it was defined by Ernst GASSNER in 1939 [Gas39], is defined as the fatigue strength of the component under realistic working conditions with a modern, lifetime-oriented interpretation of the cyclic loaded components and assemblies. It correlates the lifetime to the magnitude of the cyclic loading amplitudes [Hai98]. Nowadays this definition also includes other loads (Overloading, bumping, bending and impact loads), creeping loads and wears [Son05, Son08].

An appropriate stress analysis in fatigue tests can be based on different concepts. The most common ones are [Vor00]:

- pure experimental determination
- nominal stress concept
- structural stress concept
- the concept of local elastic load
- the concept of local load (local concept) and
- the crack propagation concept

Table 2-2: Advantages and disadvantages of basic concepts for fatigue analysis according to [Vor03] and [Kre99]

Concept	Advantages	Disadvantages/Limitations
<b>Experimental determination</b>	<ul style="list-style-type: none"> <li>• High accuracy of results</li> </ul>	<ul style="list-style-type: none"> <li>• higher requirements of time and money</li> <li>• Real components and loads necessary</li> <li>• difficult to generalize</li> </ul>
<b>Nominal stress concept</b>	<ul style="list-style-type: none"> <li>• satisfactory to good result accuracy</li> <li>• low requirements</li> </ul>	<ul style="list-style-type: none"> <li>• difficult to determinate combined load cases</li> <li>• limited applicability or high requirements of time and money in order to use the SN curve of the component that was experimentally determined as a basis</li> </ul>
<b>Local concept</b>	<ul style="list-style-type: none"> <li>• Low experimental requirements of time and money</li> <li>• Information about demands and crack initiation</li> <li>• Combined loads and order effect are considered</li> </ul>	<ul style="list-style-type: none"> <li>• elastic local stresses have to be known</li> <li>• Occasionally higher numeric requirements</li> <li>• Crack initiation definition necessary</li> </ul>
<b>Crack propagation concept</b>	<ul style="list-style-type: none"> <li>• Analogously as in local concept</li> </ul>	
<b>Mixed Concepts</b>	<ul style="list-style-type: none"> <li>• Combining the elements of the four basic concepts for appropriate adjustment of the advantages and disadvantages</li> </ul>	

Further information can be found in the literature, as in [See96], [Hai06], and [Rad07]. The next chapters explain the structural stress concept and local elastic stress concept, which are the ones applied to evaluate the tests of this master thesis.

## 2.2.1 Experimental fatigue analysis

Despite of the advances in computational life analysis of components submitted to cyclic loading, the experimental determination of the fatigue strength properties is still essential.

The fatigue strength test can be separated in two groups depending on the amplitude of the cyclic load applied, which can be constant or variable, figure 2-6. Subgroups are classified through the number of cycles and the stress that the component can support, which are low cycle fatigue ( $<5 \cdot 10^4$ ), finite-life fatigue ( $5 \cdot 10^4 - 2 \cdot 10^6$ ) and high cycle fatigue ( $>2 \cdot 10^6$ ). The tests with a constant amplitude load are easier and faster to realize than tests with a multistage loads. However, constant amplitude loading cannot properly describe the real working conditions of the component. In general, the operational loads are varying over time. Simplifications in testing can lead to false evaluation of local failures, the damage, the lifetime estimation and finally the dimensioning of the components [Son11].

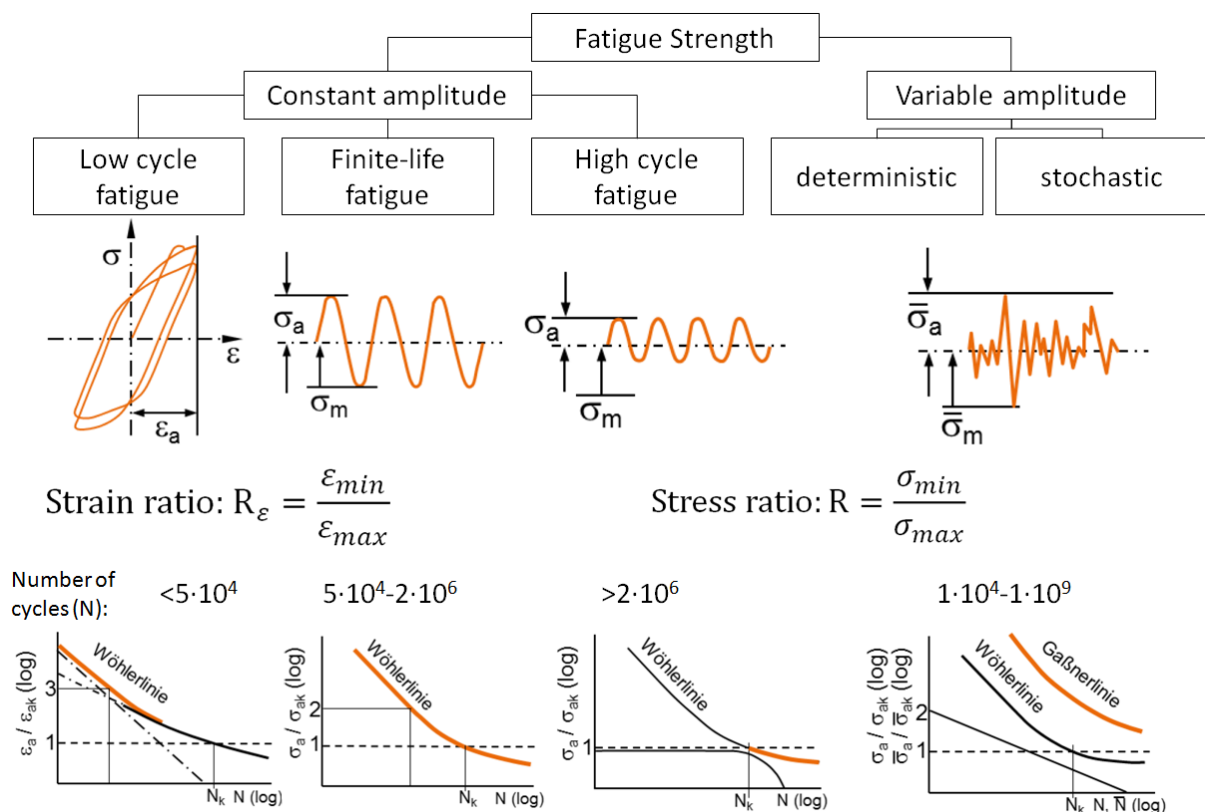


Figure 2-6: Division of fatigue strength according to [Son08]

For each stress ratio ( $R = \sigma_{min} / \sigma_{max}$ ) or rather mean stress ( $\sigma_m$ ) there are some particular stress states [Hai06]:

- Fully reversed loading with  $\sigma_m = 0$  and  $R = -1$  ( $\sigma_{min} = -\sigma_{max}$ )
- Tensile stress state with  $\sigma_m = \sigma_a$  and  $R = 0$

- Pressure stress state with  $\sigma_m = -\sigma_a$  and  $R = -\infty$
- Static stress with  $\sigma_m = \sigma_{\max}$  and  $R = 1$

The S-N curve describes the supportable stress state during a determined number of cycles correlated to failure of the component. It is experimentally obtained or estimated from other test data. Because of this reason, the basic fatigue strength experiments are the test with constant amplitude and mean stress to obtain S-N curves [Hol04]. Characteristic values of an S-N curve depend on:

- the material (heat treatment and state)
- the geometry and dimensions of the component
- the properties of the component surface
- the environmental conditions (temperature, humidity, etc.)
- the loading type [Hai06]

There are several estimations to describe the S-N curve [Hai06] according to:

- WÖHLER (1870)  $\lg N = a - b \sigma$
- BASQUIN (1910)  $\lg N = a - b \lg \sigma$
- STROMEYER (1914)  $\lg N = a - b \lg(\sigma - \sigma_k)$
- PALMGREN (1924)  $\lg(N + B) = a - b k(\sigma - \sigma_k)$
- WEIBULL (1949)  $\lg(N + B) = a - b \lg[(\sigma - \sigma_k)/(R_m - \sigma_k)]$
- STÜSSI (1955)  $\lg N = a - b \lg[(\sigma - \sigma_k)/(R_m - \sigma_k)]$
- BASTENAIRE (1963)  $\lg N = a - b \lg(\sigma - \sigma_k) - b(\sigma - \sigma_k)^c$

Both semi and double logarithmic curves converge to an asymptotic point called threshold fatigue limit [Hai06]. At present, S-N curves are commonly double logarithmic represented by a straight line with a slope  $k$  up to the threshold fatigue limit point ( $\sigma_k$ ), where the vertical axis describes the stress amplitude and the horizontal axis the number of cycles [Hai06, Vor00]. A threshold fatigue limit stress, which can be applied to the component for an infinite cycle number does not exist [Son05, Son08].

$$N = N_k \cdot \left(\frac{\sigma_a}{\sigma_k}\right)^{-k} \quad \text{for } \sigma_k \leq \sigma_a \leq \sigma_{a,Re} \quad (2.24)$$

Equation (2.24) is used to determinate the lifetime for a determined stress amplitude [Hol04]. The exponent  $k$  describes the slope of the S-N curve between two points, the plastic stress limit ( $\sigma_{a,Re}$ ), for low number of cycles, and the threshold fatigue limit. The parameters

$\sigma_k$ ,  $N_k$  and  $k$  are dependent on the stress ratio  $R$ , the lifetime probability  $P_b$ , the component factors and the failure criterion (for example crack initiation or failure) according to [Vor00].

To compare the influence of the stress ratio or mean stress of the S-N curves, the stress values are represented in a SMITH or HAIGH diagram. The stress ratio defined as:

$$R = \frac{\sigma_{\min}}{\sigma_{\max}} \quad (2.25)$$

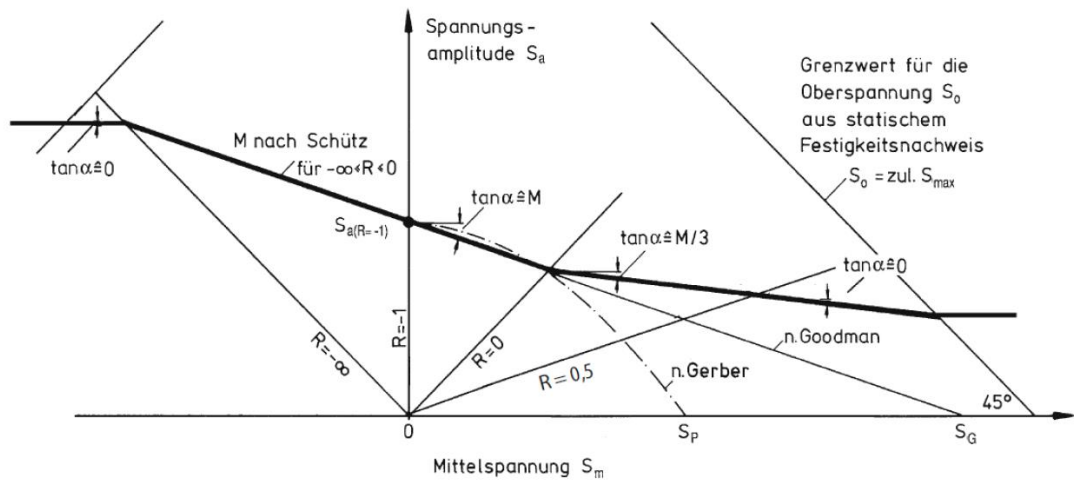


Figure 2-7: Haigh diagram [Hai03]

The above showed S-N curve is valid for constant amplitude fatigue loads. To study loads with variable amplitudes another curve is used, called Gassner curve. The fatigue test with variable amplitude to obtain this curve is based on the highest value of the sequence  $\sigma_a$  and the number of repetitions of the sequence  $\bar{N}$  [Son05, Son07, Son08]

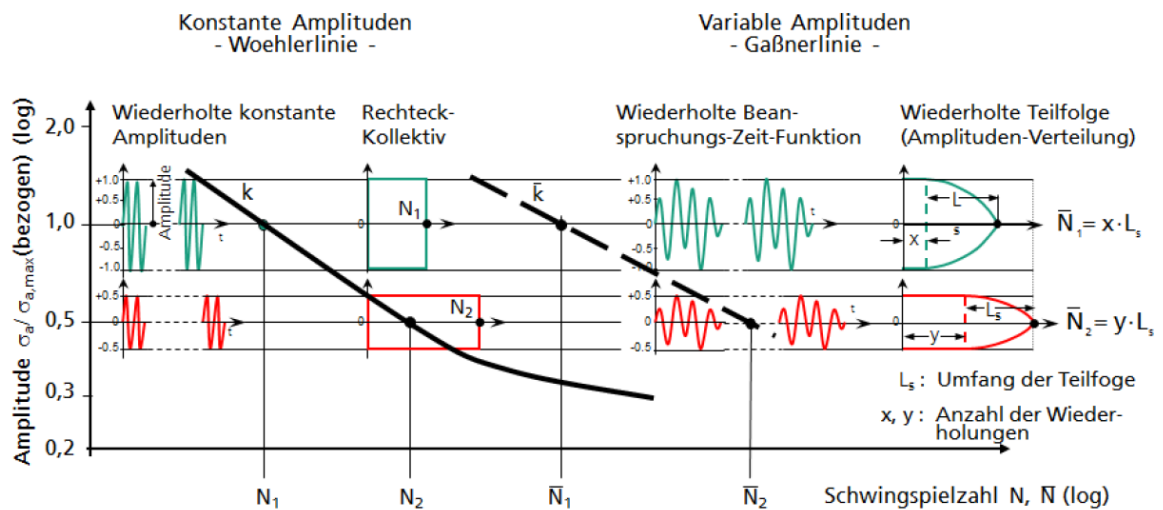


Figure 2-8: S-N and Gassner curves by [Son05]

---

---

## 2.2.2 Nominal stress concept

---

The nominal stress concept is also known as “global concept”, to discriminate it from the local concept. A first conceptual disadvantage is that the specific S-N curve of the component is needed. Another disadvantage is that the nominal stress is not always possible to define (for example a valid definition of the nominal shear stress for shell structures [Hai89])

The necessary nominal stress  $S$  is with a normal force  $F$  and a surface  $A$  generally defined [Hai06] as:

$$S = \frac{F}{A} \quad (2.26)$$

for bending with a bending moment  $M_b$  and a resistance moment  $W_b$  as:

$$S = \frac{M_b}{W_b} \quad (2.27)$$

for shear the nominal shear stress  $T$  is dependent on the shear force  $Q$  and the surface  $A$  and defined as:

$$T = \frac{Q}{A} \quad (2.28)$$

and for torsion with the torsion moment  $M_t$  and the resistance moment against rotation of the nominal cross-section  $W_t$  as:

$$T = \frac{M_t}{W_t} \quad (2.29)$$

Due to the notch from the geometry of the component and the loading type appears a stress concentration or peak  $\sigma_{e,max}$ . The relation between the stress peak and the nominal stress is established by the (elastic) concentration factor  $K_t$  [Hai06]:

$$K_t = \frac{\sigma_{e,max}}{S} \quad (2.30)$$

for a nominal tensile stress  $S$ .

$$K_t = \frac{\tau_{e,max}}{T} \quad (2.31)$$

for a nominal shear stress  $T$ .

For the pure plastic concentration factor  $K_p$  is the same equation (2.30) with  $S_p$  instead of  $S$  (for equation (2.31)  $T_p$  instead  $T$  respectively). The  $S_p$  is the nominal stress in the cross-section for a pure plastic state and  $T_p$  the shear stress for a pure plastic state.

In the case of a cyclic load and a small notch radius or a steep stress gradient the concentration factor  $K_t$  do not reduce the lifetime [Hai06]. Due to the local flow in the area of the notch the notch stress cannot be considered as a static load. The reduction of the lifetime is done in proportion to the fatigue strength reduction factor  $K_f$ .  $K_f$  is the known fatigue strength (stress amplitude at the drop-off point of the S-N curve), defined from the relation between an unnotched polished sample  $\sigma_k$  and that from a notched sample or the according component  $S_k$  [Rad03]:

$$K_f = \frac{\sigma_k (K_t = 1)}{S_k (K_t > 1)} \quad (2.32)$$

for  $R = -1$ .

This method gives a range of tolerable stresses or amplitudes for a determined lifetime according to the S-N curve of the component [Her96].

---

### 2.2.3 Structural stress concept

---

Structural stresses are usually obtained from finite element calculation and obtain the geometric influences on the global stress [Hai06]. They can be considered as an improvement of the nominal stress. On the underlying linear-elastic behaviour, the method to calculate the fatigue strength based on the collective stresses sequences and the damage accumulation is the same as the one used for nominal stress concept [Hai06]. Frequently this concept is applied to evaluate welding joints, for example the hot-spot stress evaluation by FRICKE, figure 2-9 [Rad07].



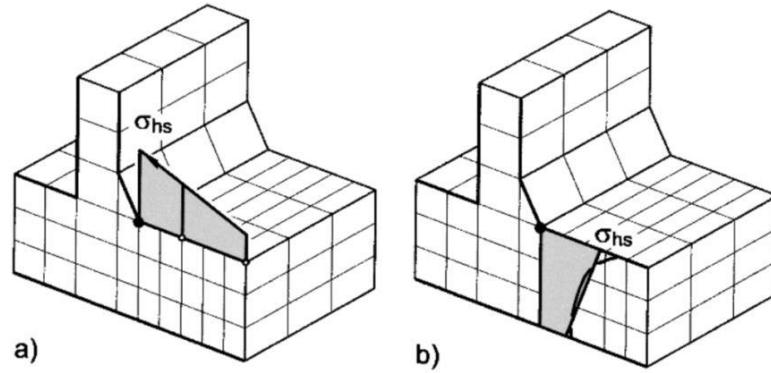


Figure 2-9: Definition of hotspot-stress  $\sigma_{hs}$  for welding joints by FRICKE [Rad07]

The selection of a proper hypothesis to describe properly the local multiaxiality depends on the loading type. For a proportional cyclic load, the stress condition can be properly described by the maximum principal stress at any time of the cycle. From experience it can be affirmed, that in these cases, the classic strength hypotheses reach a sufficient accuracy. Hence the classic strength hypotheses can be applied on these cases [Hai06].

The classic strength hypotheses for ductile materials are based on the shape modification energy and on the shear stress hypotheses [Hai89]. The reference stress (called von MISES) for the shape modification energy is defined as:

$$\sigma_{v,Mises} = \sqrt{\sigma_{11}^2 + \sigma_{22}^2 + \sigma_{33}^2 - \sigma_{11}\sigma_{22} - \sigma_{11}\sigma_{33} - \sigma_{22}\sigma_{33} + 3 \cdot (\tau_{12}^2 + \tau_{13}^2 + \tau_{23}^2)} \quad (2.33)$$

(based on coordinates: 1 = x, 2 = y, 3 = z)

In the case of a plane stress state, the equation is simplified to:

$$\sigma_{v,Mises} = \sqrt{\sigma_{11}^2 + \sigma_{22}^2 + \sigma_{33}^2 - \sigma_{11}\sigma_{22} + 3 \cdot \tau_{12}^2} \quad (2.34)$$

The shear stress hypothesis according to TRESCA differs usually up to 15% of the values from equation (2.33) or (2.34). It is defined for a plane stress state as:

$$\sigma_{v,Tresca} = \sqrt{(\sigma_1 - \sigma_2)^2 + 4 \cdot \tau_{12}^2} \quad (2.35)$$

For brittle materials tensile stress hypothesis is usually applied [Hai06]:

---

$$\sigma_{v,TH} = \frac{1}{2} \left[ \sigma_1 + \sigma_2 + \sqrt{(\sigma_1 - \sigma_2)^2 + 4 \cdot \tau_{12}^2} \right] \quad (2.36)$$

In the case of non-proportional loads the equivalent stresses mentioned cannot be used. In this case the components of the multi-axial cyclic load may have different mean stress, frequencies or amplitude characteristics [Hai06]. The maximum principal stress is also not valid as reference because its direction can vary over time and position. Because of this reason the classical strength hypothesis are not considered when there is a non-proportional cyclic loading state. Critical stress plane is a valid applicable method in these cases. In it instead the maximum principal stress is considered the stresses from a cutting plane of the component [Hai06]. For each plane, the damage is calculated and the highest one is selected as reference.

---

#### 2.2.4 Damage accumulation

---

The damage accumulation hypothesis was developed to estimate the service lifetime under a multi-stage load based on the results of a single-stage loading state [Hai03], [Son05], [Gas67]. The linear damage accumulation hypothesis from PALMGREN [Pal24] and MINER [Min45] provides the easiest, well-known and most frequently used method for a lifetime assessment of a component under a cyclic load with variable amplitude [Hai06]. This lifetime prediction hypothesis is known as PALMGREN-MINER rule.

The load is generally measured by time series, in particular by Rainflow matrices or spectrums described by amplitude and frequency. The information about the order of the cycles with the spectrum description is lost and the order influence is not considered.

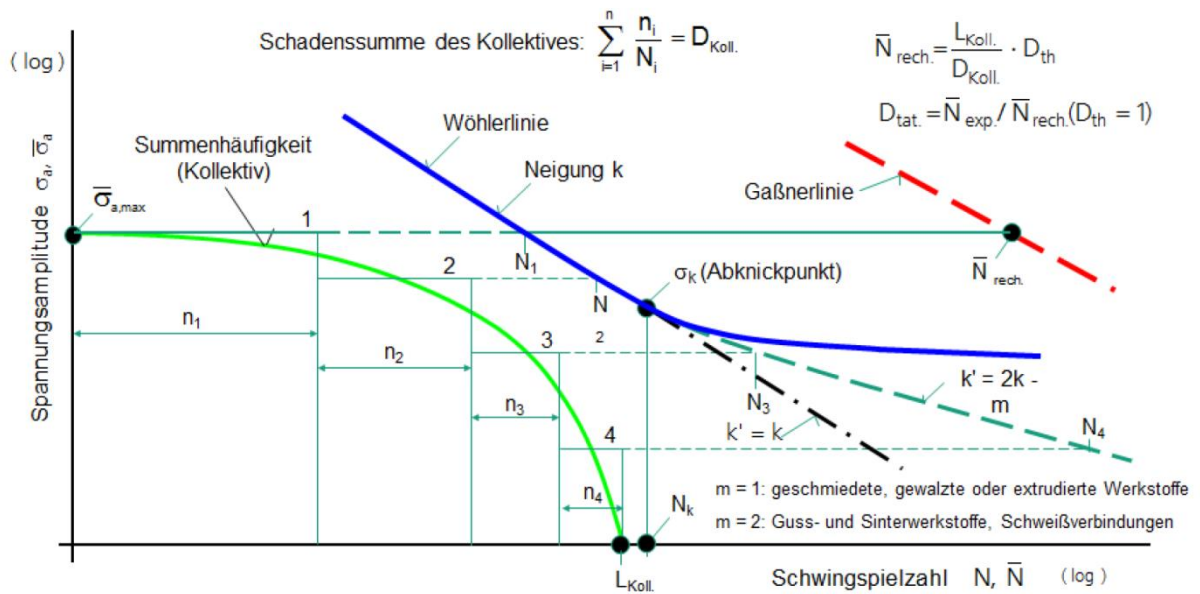


Figure 2-10: Lifetime prediction under load with variable amplitude by [Son05]

The basic concept of linear damage accumulation is that the cyclic load causes a damage  $D$  of the component. The theoretical failure occurs when a critical value of the total damage  $D$  is reached. The theoretical value is  $D_{th} = 1$ . However, the damage accumulation in the reality is more complex and non-linear [Wal03]. Approximately 90% of the experiments that apply this method have a total damage below  $D = 1$  [Son11] and can sometimes reach values three decades below [Sch73], [Eul00], [Eul99]. For example, the total damage of the forged steel is in an experimental range between  $D = 0.01$  and  $D = 10$  [Son05]. For unwelded aluminium the total damage between  $D = 0.3$  and  $D = 0.1$  for medium load fluctuations. For welded aluminium joints the total damage is between  $D = 0.5$  and  $D = 0.2$  [Son12]. Under corrosive condition the total damage can reach higher values, see [Son12].

The total damage sum is:

$$D_{total} = \frac{N_{exp}}{N_{rech,D=1}} \quad (2.37)$$

is one of the key indicators in a fatigue strength analysis [Bac08]. The fractional damage  $\Delta D_i$  of a cycle is defined as [Hai06]:

$$\Delta D_i = \frac{1}{N_i} \quad (2.38)$$

with  $N_i = N(\sigma_{a,i}, \sigma_{m,i})$ .

$N_i$  is the maximum number of cycles according to the stress amplitude  $\sigma_{a,i}$  and the mean stress  $\sigma_{m,i}$ , based on the single-stage S-N curve. The damage  $D$  is the sum from the fractional damages:

$$D = \sum_i \Delta D_i \quad (2.39)$$

The cycles loaded with stress amplitude below the drop-off point may cause damage to the component (high-cycle fatigue). In this case some variants of the PALMGREN-MINER rule exist (figure 2-11) [Sch14],[Vor00]:

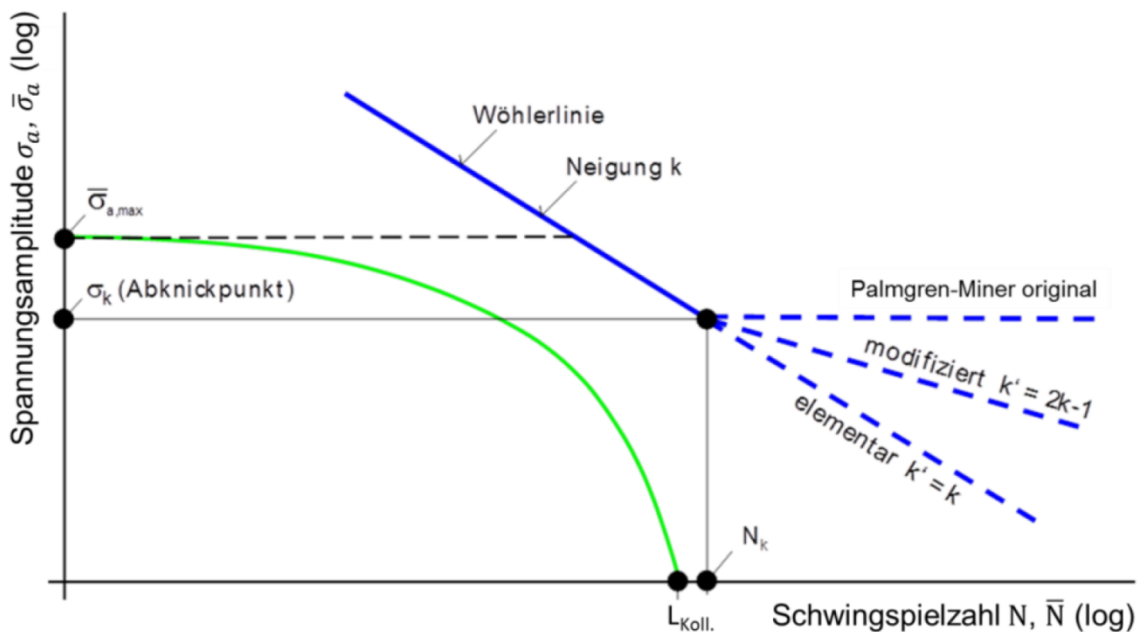


Figure 2-11: Variants of the linear damage accumulation

Actually the adhesive does not have a drop-off point. So in this thesis the variant applied is the elementary, without any change in the slope of the S-N curve after the drop-off point. For further information about other variants, see [Sch14].

## 2.2.5 Critical plane

The critical stress plane is a method that evaluates the stress state of the material on different cutting planes of the component to find which one is most critical. This method is widely applied in different fields of research as can be found in the literature, for example by [Car00], [Sus10] and [Sus13], or the one used in the FEMFAT program developed by *Magna* [Mag15]. The method is schematized in figure 2-12 and figure 2-13:

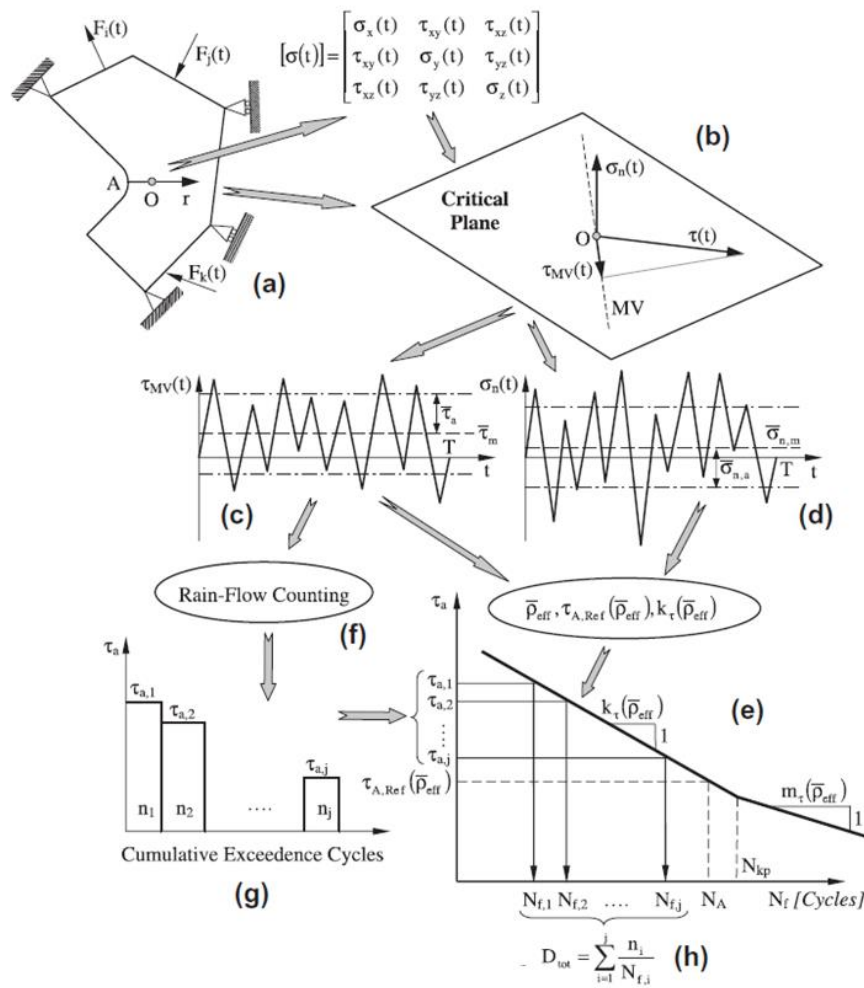


Figure 2-12: Critical plane method to evaluate fatigue lifetime [Sus11]

The first step is to obtain the stress tensor of the component. This method is generally applied for multi-axial loading state. For this reason the stress tensor is variable and depends on time or period inside the cycle (figure 2-12a). Then an iterative algorithm is applied to calculate the stress in the cutting planes systematically. The reference to determinate the planes are (figure 2-13):

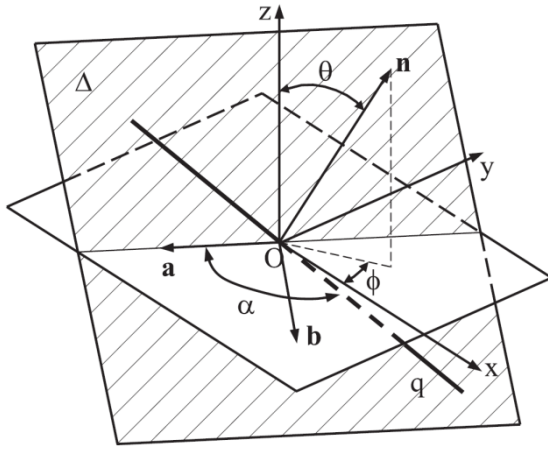


Figure 2-13: Angle and vector references to describe the cutting plane [Sus10]

According to the notation used in figure 2-13, the orientation of a generic material plane,  $\Delta$ , having normal unit vector  $\mathbf{n}$  can be defined through angles  $\phi$  and  $\theta$ , where the latter is the angle between  $\mathbf{n}$  and axis  $z$ , while  $\phi$  is the angle between axis  $x$  and the projection of unit vector  $\mathbf{n}$  on plane  $x$ - $y$ . In order to easily calculate the stress components relative to the plane under consideration, a new system of coordinates,  $O_{nab}$ , can now be introduced. The unit vectors defining the orientation of axes  $n$ ,  $a$  and  $b$  can be expressed, respectively, as follows [Sus10]:

$$\mathbf{n} = \begin{bmatrix} n_x \\ n_y \\ n_z \end{bmatrix} = \begin{bmatrix} \sin(\theta) \cos(\phi) \\ \sin(\theta) \sin(\phi) \\ \cos(\theta) \end{bmatrix}; \quad \mathbf{a} = \begin{bmatrix} a_x \\ a_y \\ a_z \end{bmatrix} = \begin{bmatrix} \sin(\phi) \\ -\cos(\phi) \\ 0 \end{bmatrix}$$

$$\mathbf{b} = \begin{bmatrix} n_x \\ n_y \\ n_z \end{bmatrix} = \begin{bmatrix} \cos(\theta) \cos(\phi) \\ \cos(\theta) \sin(\phi) \\ -\sin(\theta) \end{bmatrix} \quad (2.40)$$

Consider now a generic direction  $q$  lying on plane  $\Delta$  and passing through point  $O$ . If  $\alpha$  is the angle between such a direction and axis  $a$ , it is straight forward to calculate the components of unit vector  $\mathbf{q}$ , that is [Sus10]:

$$\mathbf{q} = \begin{bmatrix} q_x \\ q_y \\ q_z \end{bmatrix} = \begin{bmatrix} \cos(\alpha) \sin(\phi) + \sin(\alpha) \cos(\theta) \cos(\phi) \\ -\cos(\alpha) \cos(\phi) + \sin(\alpha) \cos(\theta) \sin(\phi) \\ -\sin(\alpha) \sin(\theta) \end{bmatrix} \quad (2.41)$$

According to the definition reported above, the instantaneous value of the stress normal to plane  $\Delta$ ,  $\sigma_n(t)$ , as well as of the shear stress resolved along direction  $q$ ,  $\tau_q(t)$ , can then be calculated respectively, as:

$$\sigma_n(t) = \begin{bmatrix} n_x & n_y & n_z \end{bmatrix} \begin{bmatrix} \sigma_x(\varphi) & \sigma_{xy}(\varphi) & \sigma_{xz}(\varphi) \\ \sigma_{xy}(\varphi) & \sigma_y(\varphi) & \sigma_{yz}(\varphi) \\ \sigma_{xz}(\varphi) & \sigma_{yz}(\varphi) & \sigma_z(\varphi) \end{bmatrix} \begin{bmatrix} n_x \\ n_y \\ n_z \end{bmatrix} \quad (2.42)$$

$$\tau_q(t) = \begin{bmatrix} q_x & q_y & q_z \end{bmatrix} \begin{bmatrix} \sigma_x(\varphi) & \sigma_{xy}(\varphi) & \sigma_{xz}(\varphi) \\ \sigma_{xy}(\varphi) & \sigma_y(\varphi) & \sigma_{yz}(\varphi) \\ \sigma_{xz}(\varphi) & \sigma_{yz}(\varphi) & \sigma_z(\varphi) \end{bmatrix} \begin{bmatrix} n_x \\ n_y \\ n_z \end{bmatrix} \quad (2.43)$$

According to the instantaneous values of the normal stress and shear stress, the critical plane can be calculated. As an example, in [Sus10] is determined as the plane with maximum shear stress variability. This critical plane may change depending on the critical stress type of each material.

Once the critical plane is determined, the values along a cycle of normal and shear stress (figure 2-12 c and d) are obtained and simplified by an equivalent alternative stress through a rain-flow counting or a spectrum distribution (figure 2-12 f and g). The next step is to apply the PALMGREN-MINER rule (figure 2-12e) to calculate the damage of normal and shear stress respectively. The sum of both damage values is the total accumulative damage (figure 2-12 h). As it is explained in the previous chapter 2.2.4, generally this total damage is below the total damage for a single-step load (see chapter 2.2.4 damage accumulation).

---

## 2.3 Fatigue analysis for structural adhesive joints

---

### 2.3.1 Failure behaviour and criteria

---

In a fatigue test of bonded components under variable load different phases can be discriminated (see [FAT221]). In [Rad07] the lifetime of a metallic material is divided in two phases, the crack initiation and crack propagation. The crack initiation is considered until the crack is detectable. This phase include the dislocation, the crack nucleation and the micro crack propagation. The other phase, the crack propagation, is subdivided in macro crack propagation and remaining fracture. It is important to remark that during the micro and macro crack, the crack propagation is stable.

In the case of adhesive joints, the damage process is more complex and it is not possible to differentiate properly the crack initiation and propagation phases [Sil10]. The crack initiation of adhesives depends on the adhesive formulation, geometry and environmental conditions.

---

Generally the failure is divided based on the failure location or mode in adhesive or cohesive failure. The adhesive failure is when the failure is located between the substrate and the adhesive. Despite this fracture, it is possible to find adhesive rest on the substrate as well as substrate rest on the adhesive layer. The cohesive failure is located in the adhesive and it is the failure of the intern strength of the adhesive. In the theory exposed by BIKERMANN [Bik68] and confirmed by KÖTTING [Köt84] it is affirmed that the pure adhesion failure is very improbable. Instead of that it is possible to have a cohesive failure in a thin layer between adhesive and substrate.

The failure mode is influenced by different factors as the environmental conditions and the aging processes. In figure 2-14 the failure modes according to the norm DIN EN ISO 10365 are displayed.





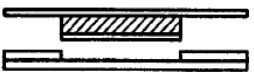
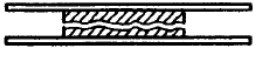



	Failure patterns	Designation
Substrate	 Failure of one or both adherends (Substrate failure)	SF
	 Failure of an adherend (Cohesive substrate failure)	CSF
	 Failure through delamination (Delamination failure)	DF
Adhesive	<p>Types of cohesion failure</p>  Cohesion failure	CF
	 Special cohesion failure	SCF
	 Adhesion failure	AF
	 Adhesion and cohesion failure with peel	ACFP

Figure 2-14: Failure mode according to norm DIN EN ISO 10365

Beside the mean stress, temperature and environmental conditions, the manufacturing conditions (geometrical adhesives defects) have a high influence on the fatigue strength [Teu12]. Generally, in the fatigue test of adhesive joints there is a high scatter [Gei12].

The failure criterion is an important aspect to determine. In some cases it is defined as the total failure of the sample (for example [Rut03]) and in another as stiffness decrease of the joint [Hah95] and [Sch14]. In this master thesis is determined as the total failure of the sample.

---

---

### 2.3.2 Fatigue assessment approaches

---

To conclude the state of art, a review of the possible approaches applied to evaluate the adhesive joints is presented. The two approaches compared in this thesis are:

- Stress averaging approach (*Spannungsmittelungsansatz*)
- Critical distance approach (*Spannungsabstandsansatz*)

These two methods are based on the influence of the stress gradient in fatigue test in order to avoid the stress singularities. In the case of fatigue evaluation, the stress gradient has a higher influence on the failure as the maximum stress value. Because of this reason, the aim of two methods is to find a reference point with an equivalent stress that can be used as a reference stress to evaluate the fatigue strength of real components.

#### **Stress averaging approach**

This theory is similar to the one proposed by NEUBER [Neu61] to evaluate notched or welded metallic materials. It is based on the influence for fatigue strength of the stress gradient perpendicular to the direction of the welded joint [Sch14]. The reason to apply this method is to evaluate the stress gradient taking into account the stress singularities but avoiding them as a reference stress. The effective stress is an average of the stress gradient and it is defined as:

$$\sigma_{eff} = \frac{1}{\rho^*} \int_{y=0}^{y=\rho^*} \sigma_{maxHS}(y) dy \quad (2.44)$$

An applied view and representation of this theory is in figure 2-15:

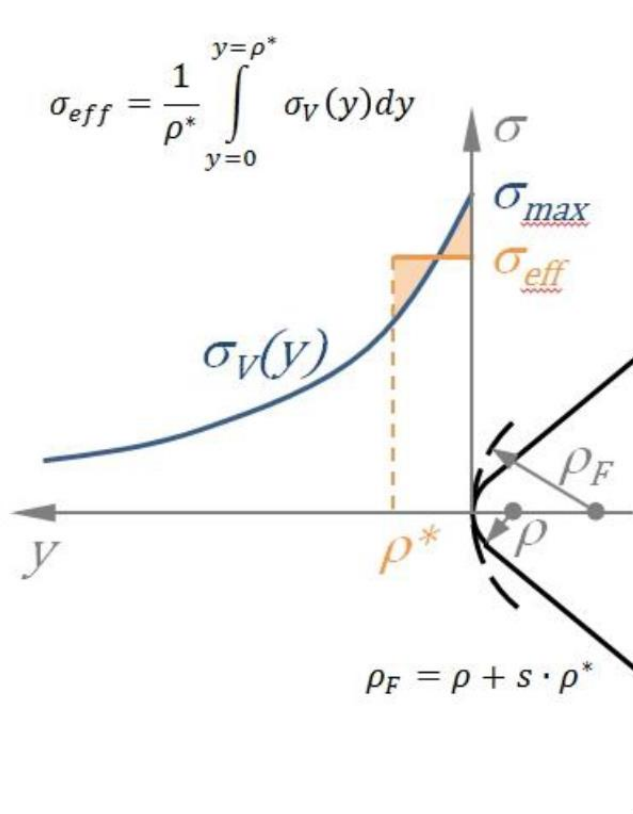


Figure 2-15: Example of the NEUBER theory for a notched sample [Neu68]

This approach was recently applied to study adhesive joints [Sch14].

### Critical distance approach

The critical distance approach is a theory used to evaluate fatigue life of metals and welded joints exposed by TAYLOR [Tay07]. Recently, it has been also applied to adhesive joints [Sch14]. The aim of the method is to find a reference point, which its stress state is valid to evaluate the adhesive fatigue strength. Theoretically this distance is dependent on the material, but the geometrical characteristics of the sample are also an influencing factor. This theory is similar to the one presented by PETERSON / MOORE [Sch14].

$$\sigma_{eff} = \sigma_{Max.HS} (r = a^*) \quad (2.45)$$

---

### 3 Experimental investigations of bonded specimens

---

In order to develop a method to calculate the lifetime of an adhesive joint under cyclic loading, three different specimen types were investigated. The tests were realized with the same adhesive, same stress ratio ( $R=0.1$ ) and same thickness of the adhesive layer to achieve good comparability. Only the geometry of the samples and the loading type was alternated.

The three geometries used are:

- KS-II specimen
- Cup-shaped specimen
- Butt-joined cylinder specimen

---

#### 3.1 Adhesive

---

The **Adhesive** is a one component, warm application, heat curing, high structural adhesive based on Epoxy resin from Firma Sika. With this adhesive high structural joints of different types of metals are possible. This adhesive is appropriate to combine its application with other joining techniques, as spot welding, riveting, clinching and other mechanical joints or to replace them partially. A high integrity of the components is achieved because of its high splitting resistance, including extreme deformations (Crash).

The adhesive thickness is 1.5 mm for all specimens.

The properties and advantages of this adhesive are [Sik09]:

- One component adhesive (no mixing prior to application needed)
- High strength
- Adhesion to oiled surfaces possible
- High wash resistance
- Adequate to join different metals
- Spot weldable
- Corrosion protection
- No damage on the substrate
- No solvent, PVC or free Isocyanates in its composition

---

## 3.2 Substrate

---

The adherents used for the specimens are typical automotive steels.

In the experiments the failure occurred exclusively in the adhesive, because its strength is lower than the steel strength. The mechanical strength of steel is several orders of magnitude higher than those of adhesive. The steel is loaded only in its elastic regimen during the test of adhesive joints. Therefore, only elastic properties of steel are used for simulation. Beside the use of different steels for the substrate, their elastic properties are the same, avoiding any different behaviour between them during the different experiments. Table 3-1 contains the elastic properties of the steel:

Table 3-1: Elastic mechanical properties of steel

	E-Modul [MPa]	$\nu$
Steel	210 000	0,3

The differences on the steels are in the yield strength or ultimate strength.

The steel types of the experiments are:

Table 3-2: Type of substrate steel for every test

KS-II specimen	HC420LAD
Cup-Shaped specimen	DP-K 34/60+ZE75/75
Butt-joined cylinder specimen	1.0036 (S235)

---

## 3.3 KS-II specimen

---

The KS-2 (Kopfzug-Scherzug) specimen was developed by the *Lehrstuhl für Werkstoff und Fügechnik (LWF) Paderborn*. The specimen consists of two U-profiles bonded on the middle face. It is possible to change the inclination of the force applied, allowing to load the joint with pure tension, pure shear or a combination of the two. This test is suitable to determine the properties of the joint for thin adhesive layers, submitted to cyclic and quasi-static loads. Finite-Element-Analysis is used to calculate the stress in the adhesive layer. The characteristics of the KS-II geometry are [Hah00]:

- Easy construction
- Easy fastening

- Low deformability demand of the material
- Joining surface similar to a joint flange
- Possibility to adjust the loading angle with respect to the joining surface
- Application of the load direct to the joining plane
- Suitable to evaluate the characteristics of point, line or planar connecting joints
- Possible to combine different joining techniques

In figure 3-1, the angle reference is determined. The nomenclature determinates that a loading angle of  $0^\circ$  is a pure shear load to the joint material, an angle of  $90^\circ$  a pure tension, and in the middle a combination of both.

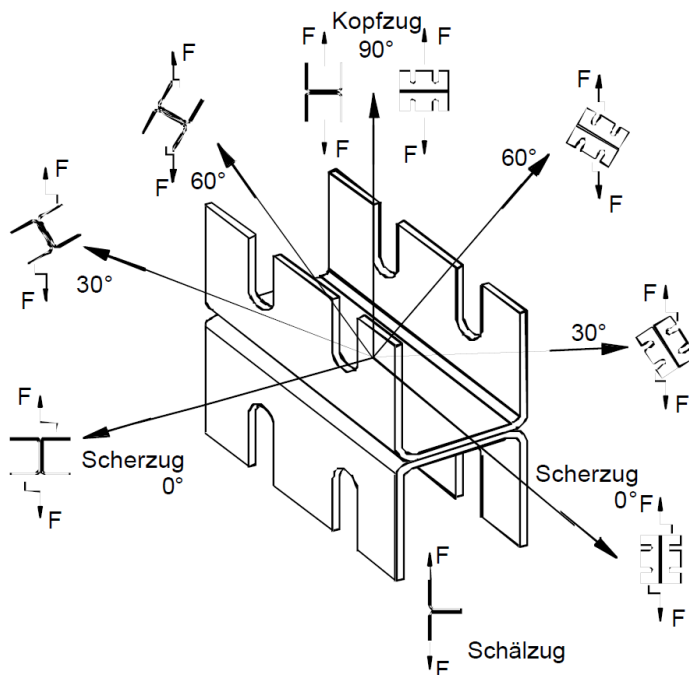


Figure 3-1: Possible loading direction of KS-II specimens [Hah00]

Because of its possibility to apply different loading types, the specimen is used to determine S-N curves for adhesive joints. For further information, as technical drawings, see [Hah00] or Annex.

In this thesis, three different loading angles were investigated: a pure shear stress ( $0^\circ$ ), a pure tension stress ( $90^\circ$ ) and a mixed-mode with a resultant angle of  $45^\circ$ .

---

### 3.4 Cup-shaped specimen

---

This test specimen represents a part-like specimen for adhesive connection in automotive industry. It is formed by a steel bowl piece with flat ends, which are joined to a steel plate, as can be seen in figure 3-2:

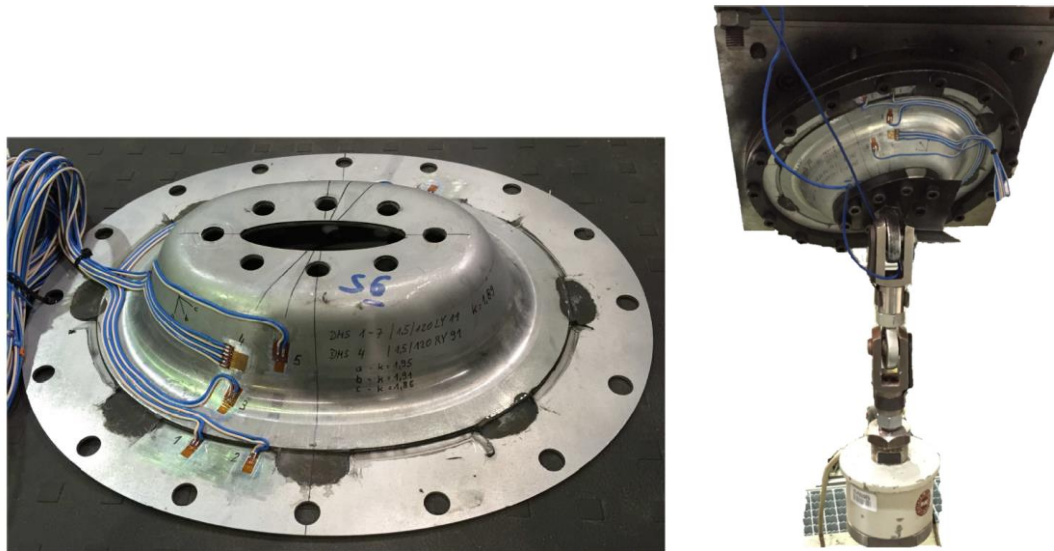


Figure 3-2: Cup-shaped specimen (left), Possible setting up of Cup-shaped specimen (right)

Cup-shaped specimen is a specimen innovated by *Fraunhofer-Institut für Betriebsfestigkeit und Systemzuverlässigkeit (LBF)*. The plate is fixed and the bowl is loaded by a uniaxial force. The clamping system is used to adjust the load direction.

In this master thesis, one load direction of the force is investigated. The load direction can be seen in figure 3-2. For detailed information of the specimen, such as the direction of the force, the area and dimension of the adhesive layer see Annex A.2.

---

### 3.5 Butt-joined cylinder specimen

---

This specimen consists in two solid cylinders joined at the flat ends. Figure 3-3 shows a representation:

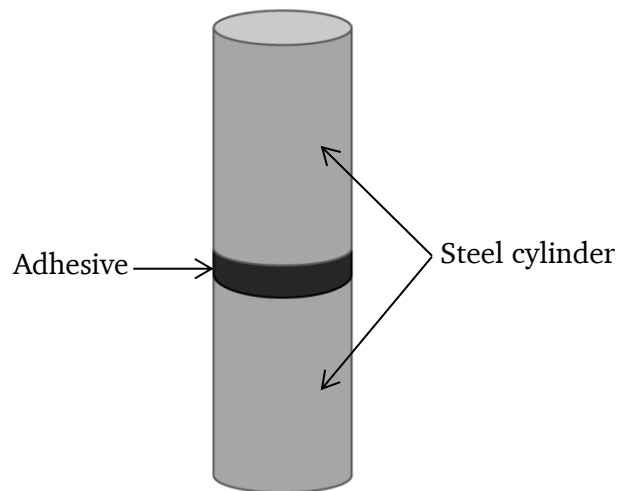


Figure 3-3: Butt-joined cylinder specimen

In this test the specimens are loaded in pure tension, pure torsion and a combination of both.

Specimens were tested in four different cyclic tests:

- Pure tension
- Pure torsion
- Combination of tension and torsion with the same ratio but without phase shift
- Combination of tension and torsion with the same ratio but with phase shift (90°)



---

---

## 4 Numerical investigations

---

This chapter explains the work with finite elements modelling with a Finite Element Software. The result of a simulation strongly depends on the joint modelling. The simulation is an approximation of the real behaviour under loading conditions. The idea is to simplify the model as much as possible to reduce the calculating time on the cost of decreased accuracy. The error should not exceed a permitted tolerance.

This thesis investigates the stress distribution of the adhesive layer. A very fine discretisation is used for this reason.

The software used is *Abaqus* version 6.12, Finite Element Analysis (FEA) Software from Dassault Systèmes. The pre-processing, solving and post-processing is entirely realized with *Abaqus* software.

The adhesive layers of KS-II and cup-shaped specimen models consist of 3-D elements, type C3D8R, linear elements with 8 nodes and reduced integration. The use of this element type is based on the good relation between results and computational time [Sch14]. The substrates are modelled with 2-D Elements, using S4R elements, a four node element with reduced integration. Both element types are considered as deformable solids [Aba10].

In the butt-joined cylinder specimens, due to their symmetry, an axis-symmetric model space is used to create the simulation. In this case, both adherent and adhesive, are 2-D deformable solids, discretised with CG4X4R element type, a four-node generalized bilinear axis-symmetric quadrilateral with reduced integration [Aba10].

The contacts used to impose a joint between the adhesive and the adherents are tie contacts, which permit joining different element types. This constraint imposes that the surface of the adhesive and the adherent are tied during the simulation. The material properties of substrate and adhesive are very different. This leads to singularities in the simulation near the contact surface. The adhesive layer is therefore discretised with four elements in thickness direction. The middle plane of the adhesive is studied in order to minimize singular effects [Sch14].

A fine discretization of the adhesive layer is used. Hence, the element length of the adhesive elements is 0.1 mm in the three models. The requirement in the steel is not critical and according to that, its discretization is coarse. The KS-II adherents have an element length of 2 mm, in the cup-shaped specimen of 1 mm and in the butt-joined cylinder specimen 0.5 mm.

The boundary conditions of the models are comparable common: the models contain one reference point (RP) for each of the substrates to apply the boundary conditions. These

---

reference points are constrained to the clamping surface of the adherends. One of this reference points is fixed (all six degrees of freedom are restrained in the FEM). The other reference point serves as load introduction point. No displacement restrictions in the direction of a force or moment applicate are applied for the latter reference point.

In the area of solver options, the FEA realized is an implicit solver (*Static, General*) [Aba10]. During the whole simulation, both adhesive and adherents deformations are considered as linear-elastic. This assumption is suitable for the substrates because the loading is well below their yield strength. Adhesives suffer plastic deformation before failure. Adhesives deform elastically until a certain stress value, where a crack initiates and local non-linear plastic deformation appears. After this crack, the supported stress of the adhesive is near the crack initiations stress. In fatigue testing, the applied stress is much lower than the yield strength value. Hence, elastic properties of the materials are sufficient to model the specimens. The elastic mechanical properties needed; Young's modulus and Poisson's ratio [Aba10], are specified in chapters 3.2 and 3.3, in table 3-1 and table 3-2. Due to this linear elastic assumption, the simulations are generated with a nominal load of 1kN and afterward scaled with the real load applied.

---

## 5 Evaluation of experimental and numerical investigations

---

Experimental investigations are evaluated and presented. The first step is an evaluation of the obtained results to have an overview of the behaviour of the specimen under cyclic loading. It is an important input to determinate the accuracy of the simulation. The determination of the adhesive properties, for example creeping, is valuable information. The finite element models are developed in order to obtain the stress distribution in the adhesive layer. A validation of these FE-models is needed to ensure that the simulated system properly describes the real test and that the obtained stresses from the simulation are realistic. In the next chapter there is an explanation and comparison of stress-based failure criteria to investigate the suitability of these methods for the lifetime analysis of bonded joints.

---

### 5.1 Analysis of the test results

---

S-N curves for each test scenario are derived, using force amplitude or the nominal stress amplitude as the dependent variable. Scatter slope and position of the S-N curve are derived. The determination of S-N curves from test data is based on an in-house Matlab-tool named *BMW Wöhlerlinie-tool version 1.2b* using the maximum likelihood algorithm.

Additionally, a further study of creep effects of the joint under cyclic loading is realized.

---

#### 5.1.1 Analysis of KS-II specimen

---

The derived S-N curves of the three different cyclic loading experiments for the KS-II geometry probes are presented. The three different loadings are: pure tension (*Kopfzug, KZ*), pure shear (*Shearzug, SZ*) and Mixed-Mode 45°, a combination of tension and shear load with a resultant angle of 45° (45°). The S-N curve values are summarized in table 2-1:

Table 5-1: No. of samples for each loading type

Type of Load	No. of samples	No. valid tests		Not valid
		Failure	Run out	
Pure tension (KZ)	19	9	2	7 (6 Different frequency) (1 Slipped test)
Mixed mode 45°	14	10	2	1 Slipped test
Pure shear (SZ)	16	15	1	0

In figure 5-1 it is possible to observe the scatter of each loading type in the test (TS), the slope of the curve (k), the drop-off point (y(NK)) and the cycle where this drop-off is considered

---

(NK)<sup>1</sup>. For further information of these variables, see chapter 2.3 and 2.4. The probes that are considered not valid are because of the slip of samples (2), not complete failure of the adhesive (1) or change of test conditions (test frequency) (5).

---

<sup>1</sup> As explained in the chapter 2, there is any drop-off point for the adhesives that determine an infinite lifetime, but calculations are realized for two million cycles

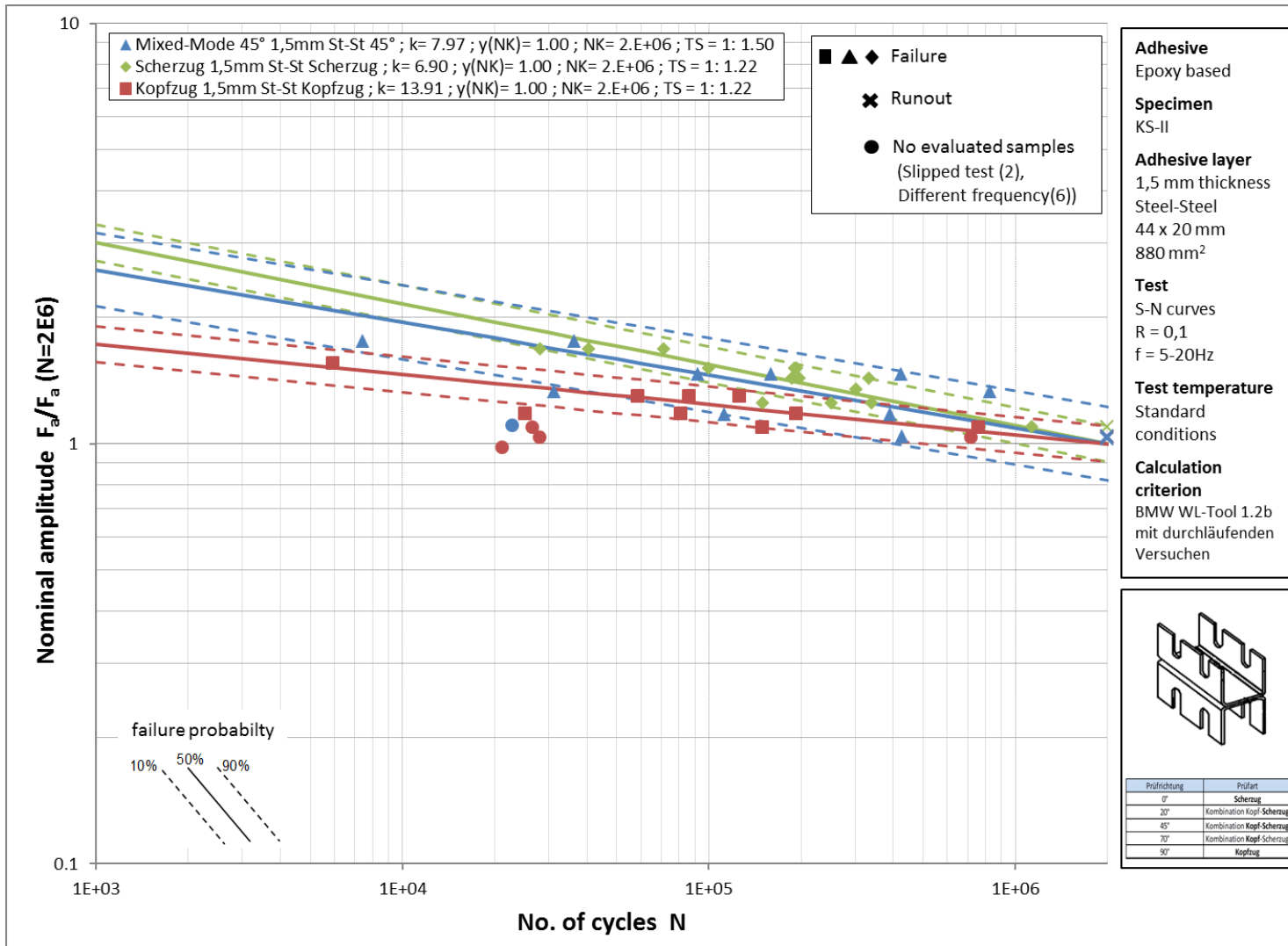


Figure 5-1: S-N curves for KS-II test, pure tension (KZ), pure shear (SZ) and Mixed Mode with 45° resultant force angle (45°)

---

Figure 5-1 shows that failure of adhesives submitted to fatigue loadings studies strongly does depend on the loading type. The slopes of the pure shear and the pure tension stress state have a very high difference. That means that a smaller variation on the tension stress would affect the joint lifetime to a greater extent than a variation the shear stress. As a conclusion of this study, it is possible to affirm that the loads that cause a tensile stress would be more significant for the strength of the joint than the ones that introduce shear stress. Because of that, the design of adhesive joints should try to avoid, as much as possible, tensile stresses.

Another remarkable point of this figure is the scatter of the tests. For pure tension or pure shear state, this scatter is smaller than for the mixed-mode load. This high scatter could create lower accuracy on the proposed methods.

---

### 5.1.2 Analysis of cup-shaped specimen

---

For this specimen there is only one type of load, which is a combination of forces in the three directions. To find the direction, the components of the unit force are explained in detail in Annex A.2. The orientation of it is  $60^\circ$  with respect to the x direction in x-y plane and  $20.35^\circ$  with respect to the x-y plane. The reference is shown in the figure 5-2:

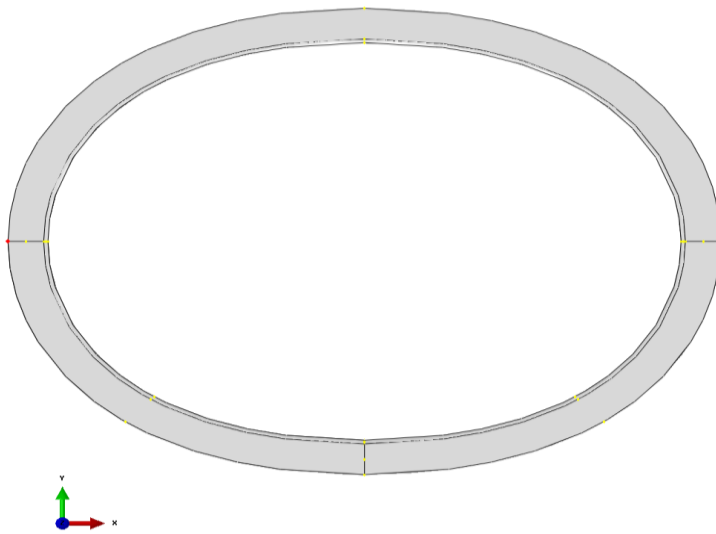


Figure 5-2: Reference components for cup-shaped adhesive layer specimen

Positive z-coordinate orientated towards the bowl substrate, negative z-coordinate towards the plate substrate.

9 samples were tested, which resulted in 8 failed samples and 1 runout.

Figure 5-3 exposes the S-N curve of this specimen.

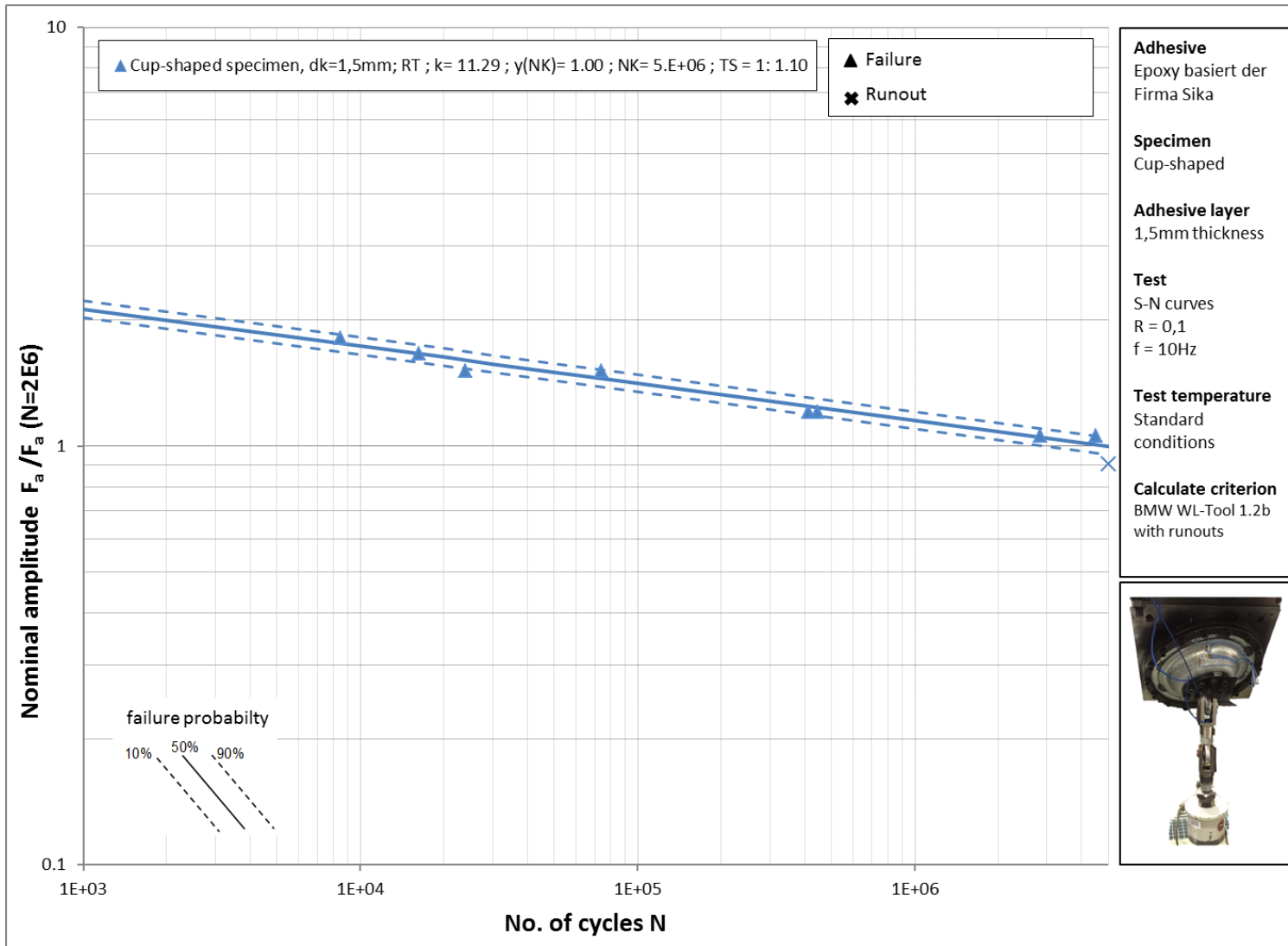


Figure 5-3: S-N curve for Cup-shaped specimen

The nomenclature to describe the S-N curve is the same as in figure 5-1. The scatter of this samples is much lower than for KS-II samples, TS = 1:1.10 in comparison with TS = 1:1.22 or 1:1.50. A lower scatter in test data is a vital basis to achieve a higher grade of accuracy in latter simulation.

### 5.1.3 Analysis of butt-jointed cylinder specimens

Four different types of load for this specimen were experimentally investigated: pure torsion, pure tension, and a combination of the two with and without phase shift. The tested samples for each type are specified in table 5-2:

Table 5-2: No. of samples for each loading type for the butt-jointed cylinder specimens

Type of Load	No.	No. Valid test		No. Not Valid test
		Failure	Runout (non-failure)	
Pure tension	15	15	0	0
Pure torsion	15	15	0	0
Combination without phase shift	18	16	2	0
Combination with phase shift	16	16	0	0

In this case the dependent variable to determinate the S-N curves is the nominal stress for axial load and the nominal shear stress at the border for torsional load. The ratio between the nominal tension stress and the nominal shear stress is always constant between the tests with a combined load. This ratio is:

$$r_{\sigma/\tau} = \frac{\sigma}{\tau} \quad (5.1)$$

$$r_{\sigma/\tau} = 1.39 \quad (5.2)$$

Equations (5.1) and (5.2) give the correlation between force and stress for the tested samples:

$$\sigma = \frac{F}{\pi R^2} \quad (5.3)$$

$$\tau = \frac{2M}{\pi R^3} \quad (5.4)$$

$$r_{M/F} = \frac{M}{F} = \frac{\tau R}{\sigma 2} = 3.6 \text{ mm} \quad (5.5)$$



---

The ratio  $r_{M/F}$  is used in this master thesis to scale unit force simulations. In the case of the combined torsion and tension loads, the ratio is used for moment-force scaling.

The S-N curves of this test are exposed in figure 5-4:

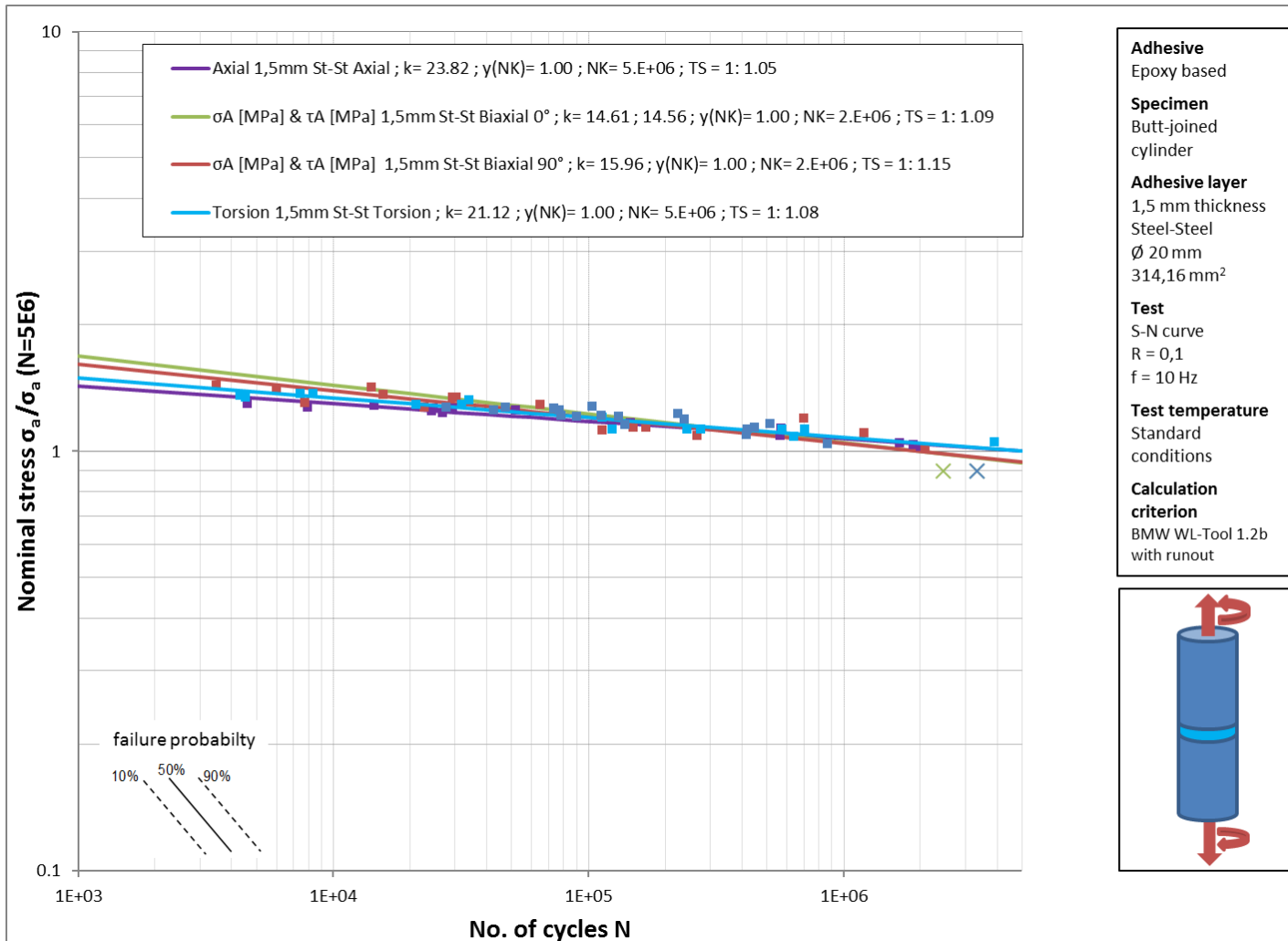


Figure 5-4: S-N curve 50% survival probability lifetime curve for butt-joined cylinder specimens

The scatter in the experiments is low,  $TS = 1:1.15$ . The slope is flatter than for other specimen tests. That means that a variation in the testing force affects the lifetime of the adhesive joints strongly.

The comparison of the combined loads with and without phase shift shows that for a combined load with phase shift the lifetime is shorter than without phase shift. The tested adhesive denotes a very small difference between concerning phase shift. It is possible to observe, that the highest difference of stress for the same number of cycles is lower than 10%. It can be observed that the difference decreases with an increase of cycle number.

A study of the creep behaviour of these samples under cyclic loading is presented. This study is needed to evaluate the possible damage and creep behaviour of the joints. Displacement sensors were used during testing in order to systematically detect the creep effects. The sensors recorded the rotation and the axial displacement of the samples. Figure 5-5 shows exemplarily the behaviour of the samples.

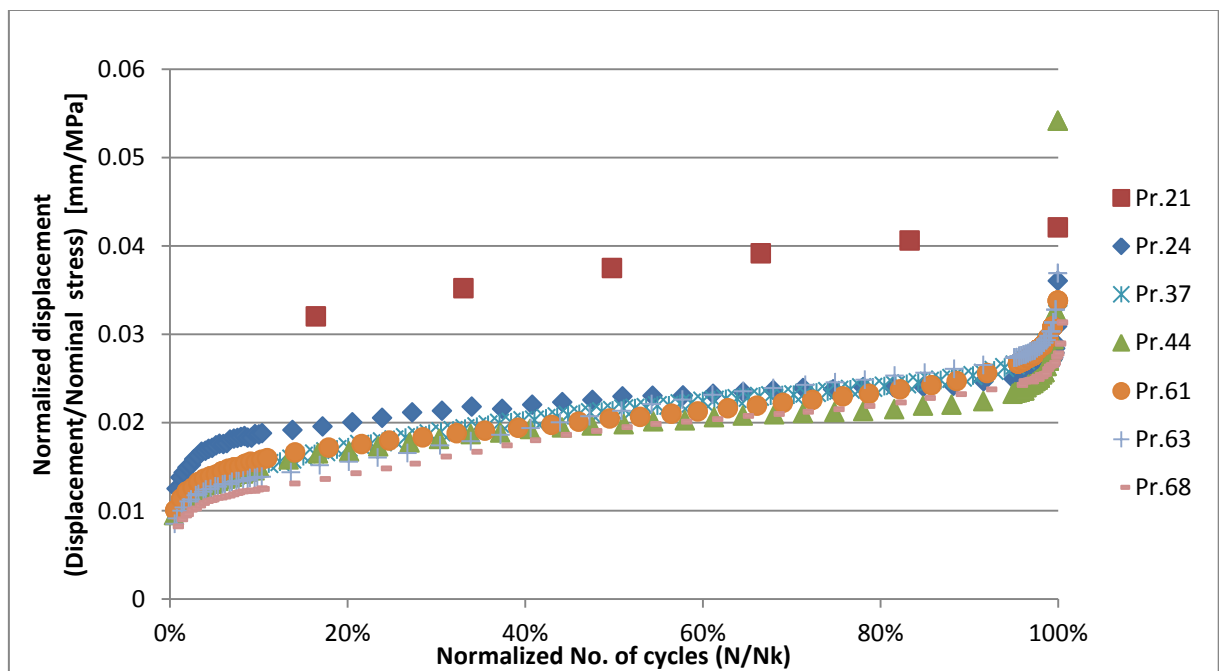


Figure 5-5: Average displacement of samples under pure torsion load before failure

Figure 5-5 shows that the displacement has 3 phases for all the tests. The first phase covers the first 5% of the lifetime. In this phase the rotation increases quickly. The second phase lasts between 5% and the 98% of the lifetime cycles. The increase of the rotation is linear in this phase. The last phase consists of crack initiation and quick propagation until failure of the joint.

The deformation can originate from creep effects of the adhesive, since test were performed at an  $R=0.1$ . That means that a constant mean stress affects the sample. Alternatively the stiffness loss of the adhesive could originate from crack propagation.

In this case, as it is shown in literature of the creep behaviour (2.1.1 Determination of the adhesive properties), it is considered as creep behaviour.

This can also be affirmed with figure 5-6:

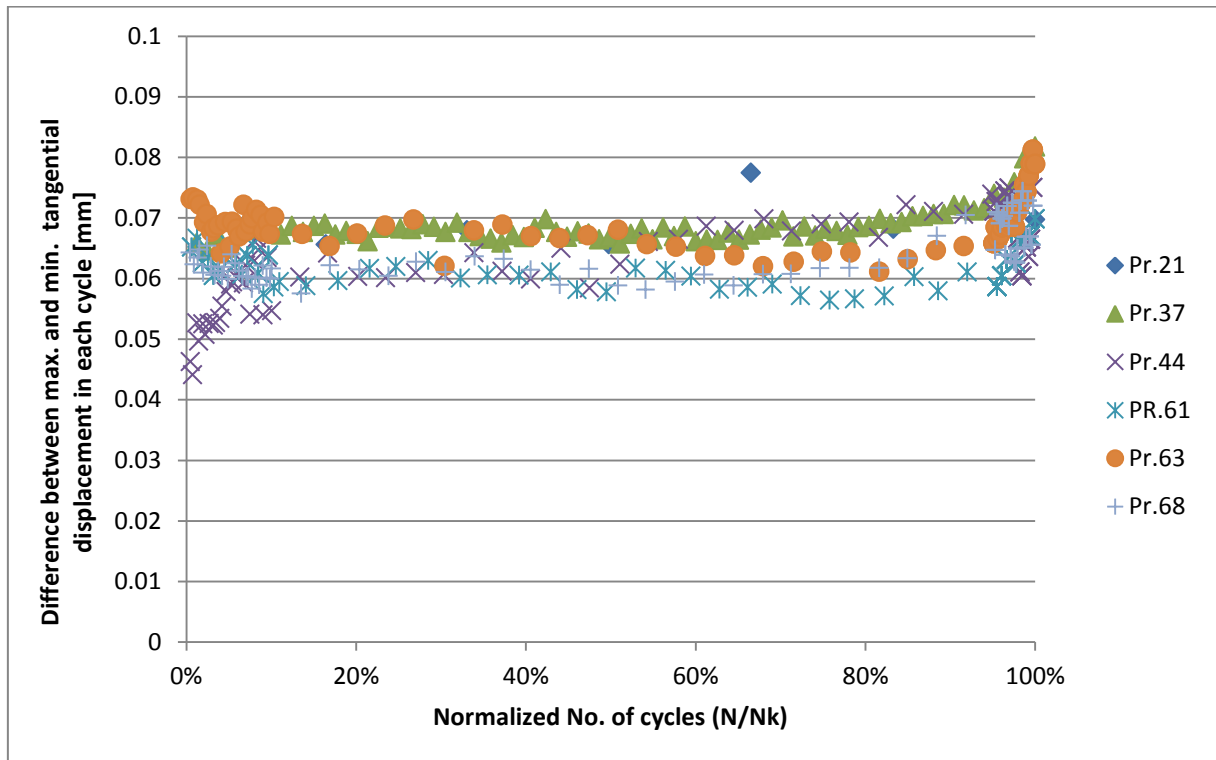


Figure 5-6: Stiffness trends of the adhesive joint during pure torsion load

Figure 5-6 illustrates the difference between the maximal and minimal displacement during a cycle, corresponding to the values of maximal and minimal load. With this variable it is possible to determine the stiffness evolution of the adhesive joint. Up to a lifetime of 95% the stiffness remains constant, no stiffness degradation of the joint is visible. At the end of the test a quick stiffness degradation occurs due to the creation and propagation of cracks.

In the case of axial loads, the results are confusing, because not all the experiments show the same behaviour, possibly due to movements of the sensor during fatigue testing. One sensor is placed arbitrarily around the steel cylinder. This set up only records properly if the crack or failure of the adhesive is placed in the vicinity of the sensor. In the case of failure at a different position, the cylinder can flex and the sensor cannot properly record the axial displacement. This is denoted in figure 5-7:

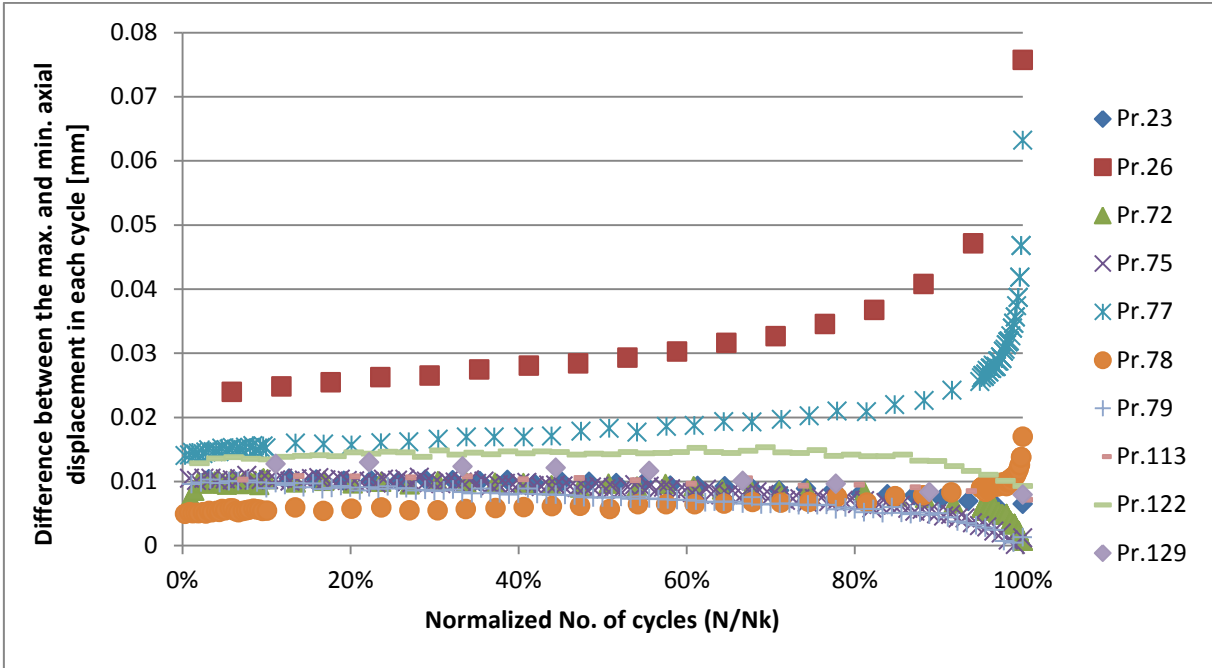


Figure 5-7: Stiffness trends of adhesive joint during axial load

Some of the samples show a high decrease of stiffness and others an increase. A measured increase in stiffness does not seem to be coherent.

## 5.2 Validation of the Finite Element Models

In this chapter the results of the finite elements models created are compared with the test data, in order to verify their suitability and validate the modelling data. The use of the finite element models (FEM) is necessary to obtain the stress distribution on the adhesive layer.

The validation is based on three different specimen types. The KS-II model used was previously validated with other test in [Her14]. The cup-shaped specimen, during the testing, the samples had strain gauges in some points of the substrate, in order to properly compare the real test with the simulated results. In the case of the butt-joined cylinder specimens, the force-displacement or moment-tangential displacement curves obtained from quasi-static test are compared with the curves obtained from simulation.

---

## 5.2.1 Cup-shaped specimen validation

---

This model is validated by the comparison of the measured strain (strain gauge on the samples) and the strain data from simulation. The strain gauges can be seen in figure 5-8:



Figure 5-8: Location of the strain gauges on cup-shaped specimens

All the gauges are unidirectional except for the gauge 4 that features two in-plane strains and the interaction between them. The gauges 2 and 5 are placed in a 15° line with respect to the front line as depicted in figure 5-8, are placed in a 30° in a line with respect to the front line.

The comparison between the measured and the obtained values from the simulation are displayed in figure 5-9:

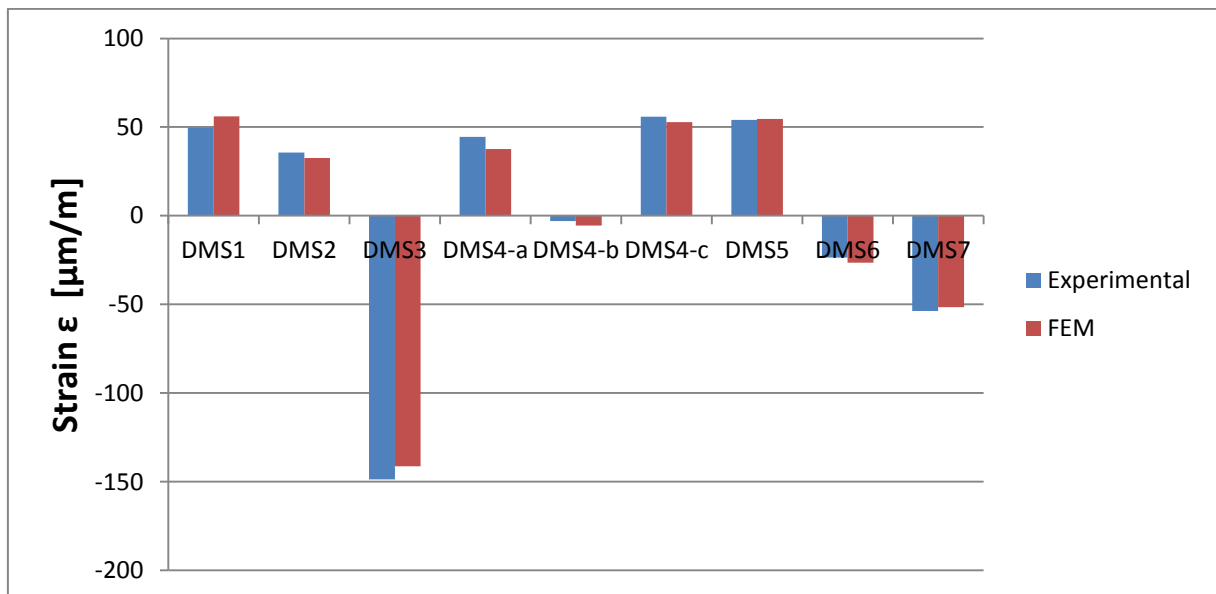


Figure 5-9: Validation of the measured and the simulated strain

Figure 5-9 affirms that the behaviour of the simulation compares well to the test measurements. Hence, the simulation describes the behaviour of the joint properly.

## 5.2.2 Butt-joined cylinder specimen validation

To realize this validation, the load-displacement curve of the quasi-static test is used.

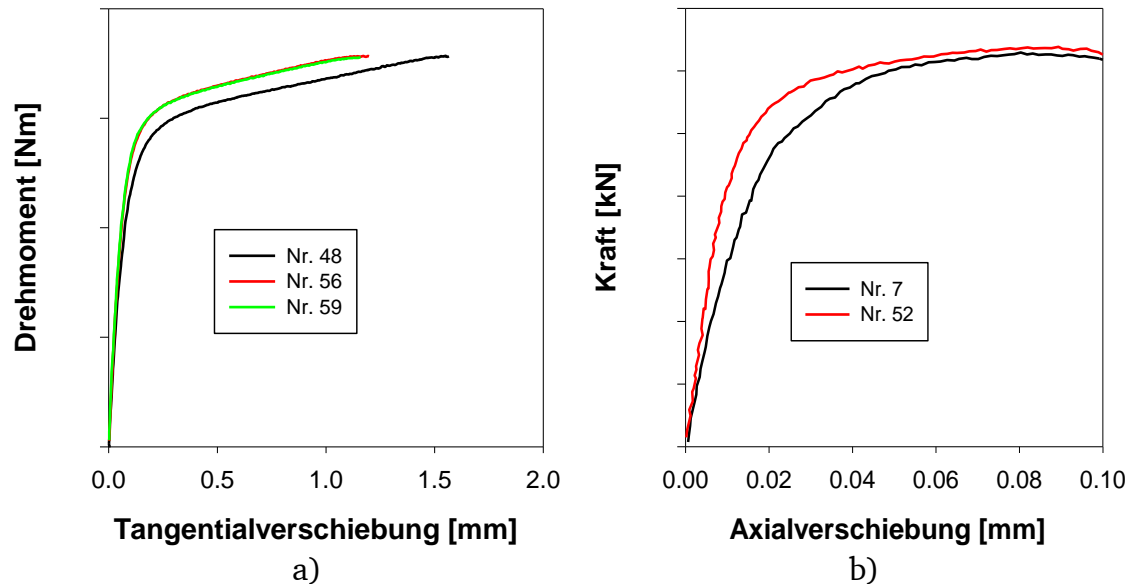


Figure 5-10: Stiffness behaviour of the quasi-static tests; a) pure torsion, b) pure tension

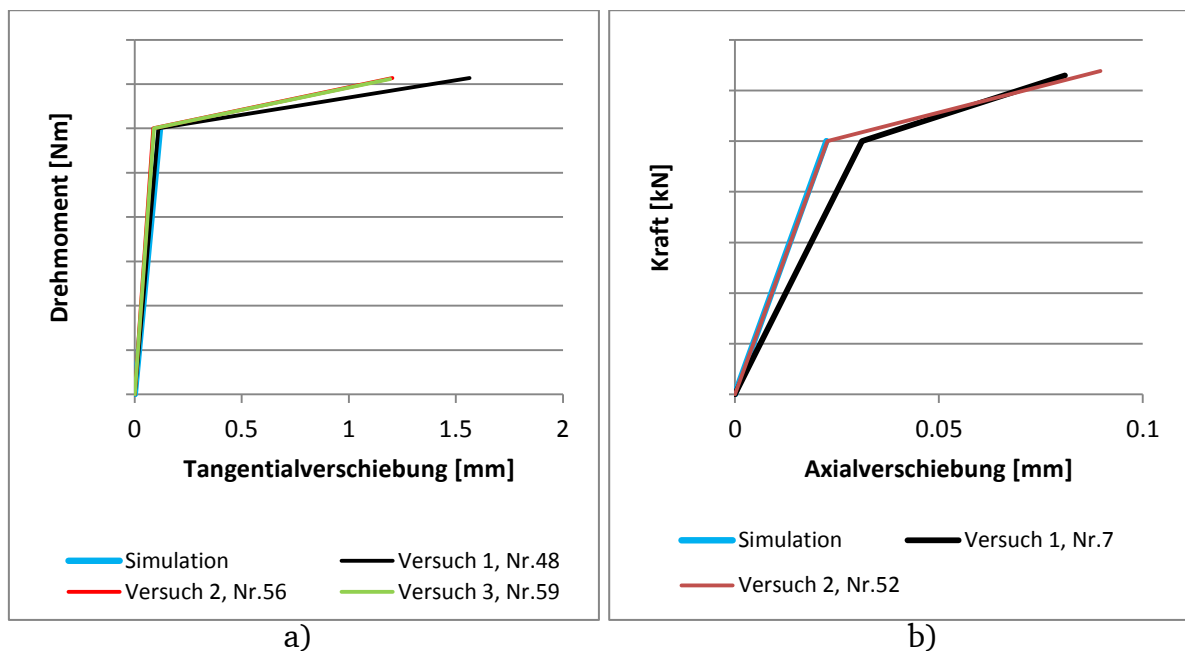


Figure 5-11: Comparison between the elastic stiffness of the simulation and the tests; a) pure torsion, b) pure tension

Figure 5-10 illustrates that adhesive joints have two different material behaviour zones, the linear-elastic material behaviour and a zone of non-linear behaviour. In fatigue simulations the linear-elastic behaviour is the zone considered for the simulation, because during the fatigue test, the force applied to the joint is significantly lower than the yield strength.

---

Because of this reason, the validation was done in the linear-elastic behaviour of the test. Figure 5-11 shows the good correlation between test and simulation, validating the FE model of the butt-joined cylinder specimens. The y-axis is not represented with quantitative values due to confidentiality terms.



---

## 6 Application of stress approaches

---

The approaches explained in the state of art (chapter 2.3.2) are elaborated in this chapter, using the stress distribution of the adhesive layer obtained from the FEA.

Approaches are based on a maximal stress criterion. The butt-joined cylinder specimens with a phase shift of  $90^\circ$  are not considered in these approaches. They are studied with another approach in a separate chapter.

The two failure criteria based on stress approaches considered in this work are:

- Critical distance approach (*Spannungsabstandsansatz*)
- Stress averaging approach (*Spannungsmittelungsansatz*)

These methods are compared using the stress state of the specimens modelled with CAE software Abaqus in a quasi-static load state. The hypothesis of using the quasi-static stresses to calculate the lifetime of the joints is based on the elastic behaviour of the adhesive and the adherend before the fatigue failure and on the generic process of fatigue simulation using unit load cases in combination with load-time-history signals. During the testing the behaviour of the bonded joint can be considered linear-elastic.

The investigation consists of two parts. The first one consists of the comparison of the two methods using two different types of reference stresses, the principal stress and the equivalent elliptic stress. The stresses are evaluated for two million cycles ( $N=2 \cdot 10^6$ ) and a 50% survival probability.

The second part derives master S-N curves with different approaches and reference stresses, taking all fatigue testing specimens' results into consideration. In order to compare the different methods, the scatter of the master S-N curve and the robustness of the methods are considered as the reference.

As it is explained on the state of art, these two methods are widely used in lifetime calculation for metallic materials. The main objective from this thesis is to analyse the suitability of these methods for adhesive materials and joints similar to published work [Sch14]. The stress distribution is always taken from the middle plane of the adhesive to avoid the contact singularities that appear in the FEA due to the contacts between two materials with a big stiffness difference (chapter 4). A more detailed explanation can be found in the doctoral thesis about fatigue calculation of adhesive joints of *H. Schmidt* [Sch14].

---

---

## 6.1 Comparison of stress approaches for a lifetime of two million cycles

---

The two stress approaches are compared at the point of two million cycles ( $N=2 \cdot 10^6$ ). With the according stress distribution the strength and lifetime of adhesive joints is evaluated. Two types of stresses are considered: the principal stress, because it represents the maximal tension stress in the adhesive, and an equivalent stress named equivalent elliptic stress, which gives high accuracy results in stress-based methods for quasi-static loads [Tre12][Sch05].

The idea of these approaches is to find a point at a certain edge distance of the piece, which can be used as a reference stress value to calculate properly the lifetime of the joint.

---

### 6.1.1 Critical distance approach

---

The aim of this approach is to find a point, which can be used as a reference stress point. To find it, the discretization of the adhesive layer is very fine (0.1 mm).

---

#### Critical distance approach evaluation with KS-II specimens

---

First of all, the KS-II tests have been studied to have a general view of the results. Several paths have been studied for the KS-II tests in order to compare the results and find which one has a better relation between accuracy and easiness. The three directions studied are:

- **Path 1,  $z = 1.7$  mm:** Transverse direction with respect to the shear load, which passes through the highest maximum principal stress for pure tension and mixed-mode 45° loading state.
- **Path 2,  $z = 22$  mm:** Transverse direction with respect to the shear load, which passes through the highest maximum principal stress for pure shear stress loading state.
- **Path 3,  $x = 1.3$  mm:** Parallel direction with respect to the shear load, which passes through the highest maximum principal stress for pure tension and mixed-mode 45° loading state.

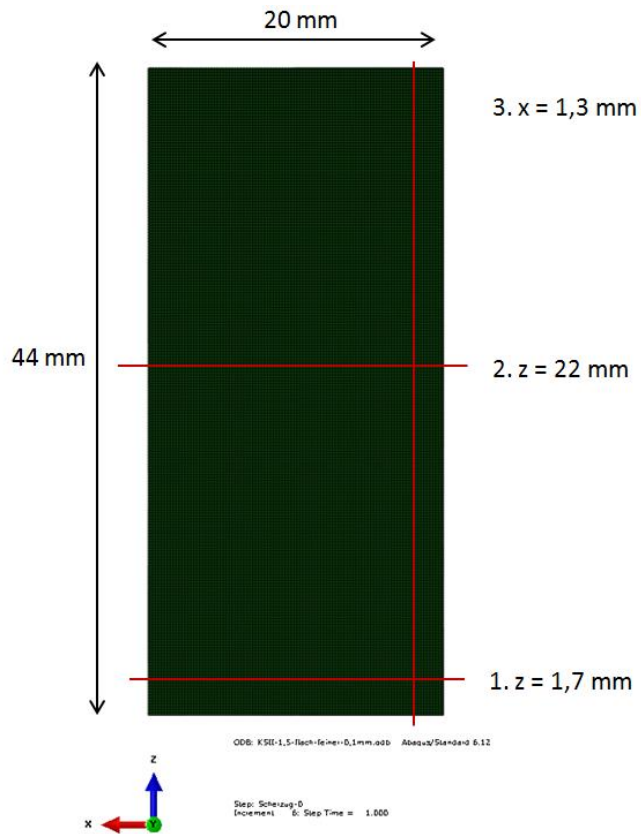


Figure 6-1: Middle plane of the adhesive with the three paths studied in KS-II specimen

**Path 1, z = 1.7 mm**

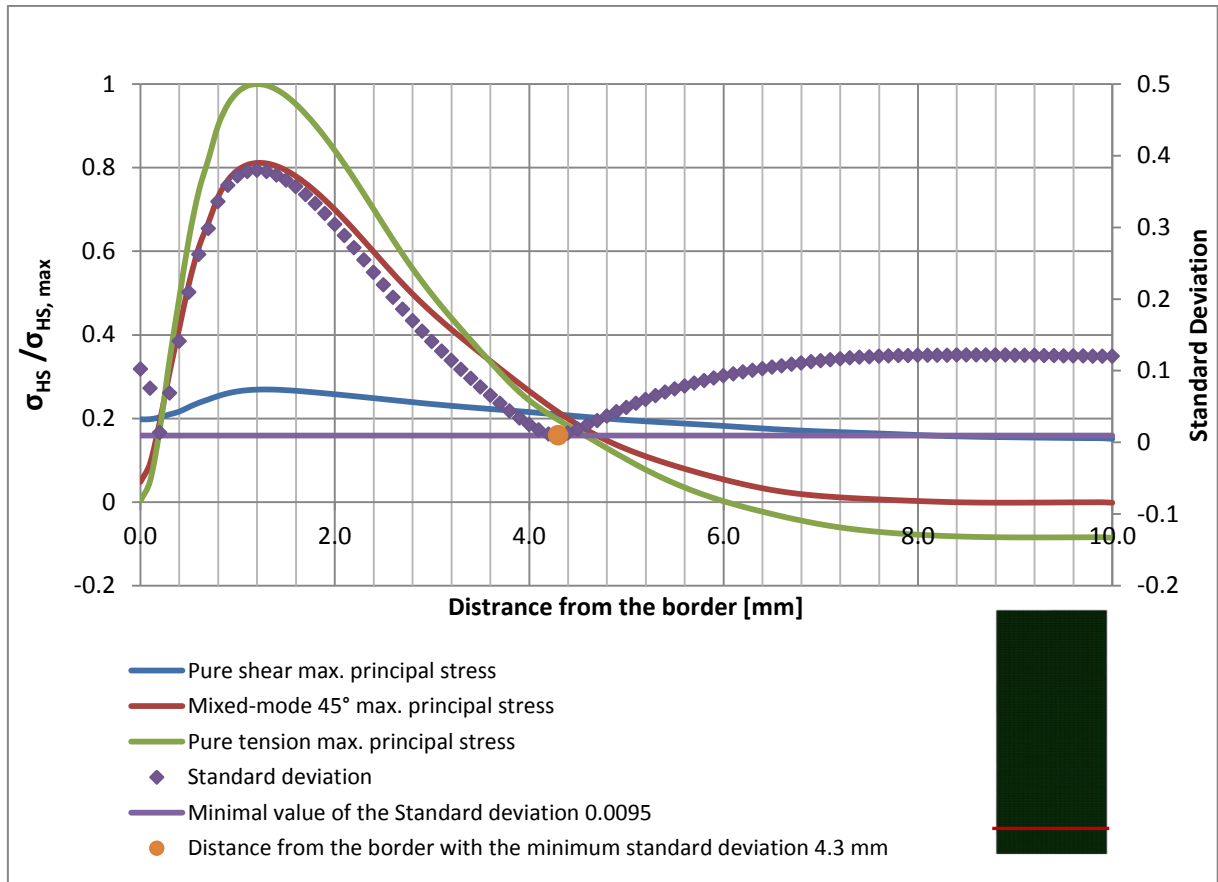


Figure 6-2: Stress distribution along path 1 for critical distance approach

Figure 6-2 shows the stress distribution of the three different load cases along the first path studied ( $z = 1.7$  mm, figure 6-1).

The maximum distance considered is 10 mm, because the width of the adhesive layer is 20 mm and the stress distribution is symmetric. The standard deviation serves as evaluation criteria. There are two points with similar standard deviations, at 0.2 mm and 4.3 mm. In this case as a reference the 4.3 mm point would be taken into account because the standard deviation of the points close to it has smaller standard deviation, and in 0.2 mm, the points next to it have a higher variability. These approaches are not exact and for this reason, it is important that the results converge in an interval with a tolerable low standard deviation.

Path 2, z = 22 mm

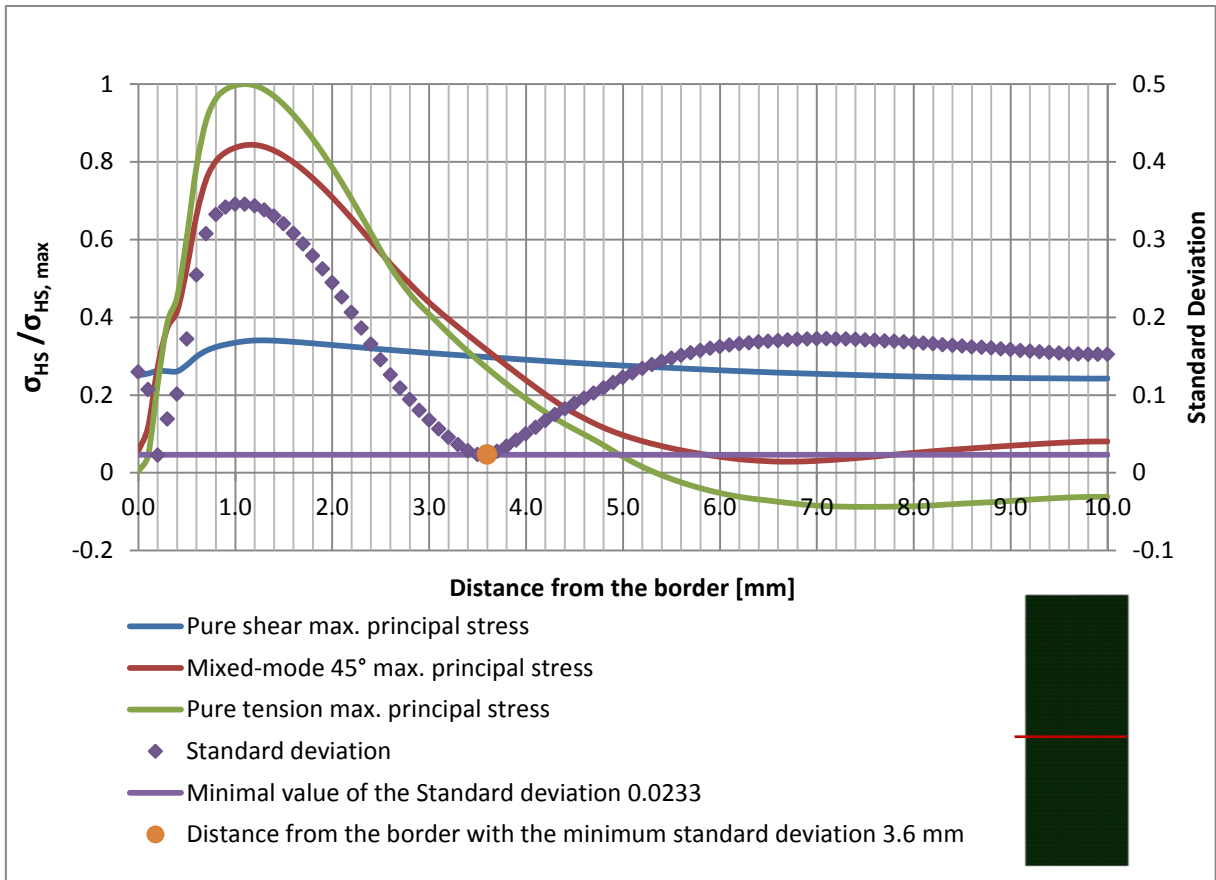


Figure 6-3: Stress distribution along path 2 for critical distance approach

In this path, the results are similar to the path 1. In this case at 0.2 mm and at 3.6 mm the standard deviation is minimal. As in the last case, the best option is to pick the 4 mm because the points close to it have lower standard deviation as in the point at 0.2 mm.

### Path 3, x = 1.3 mm

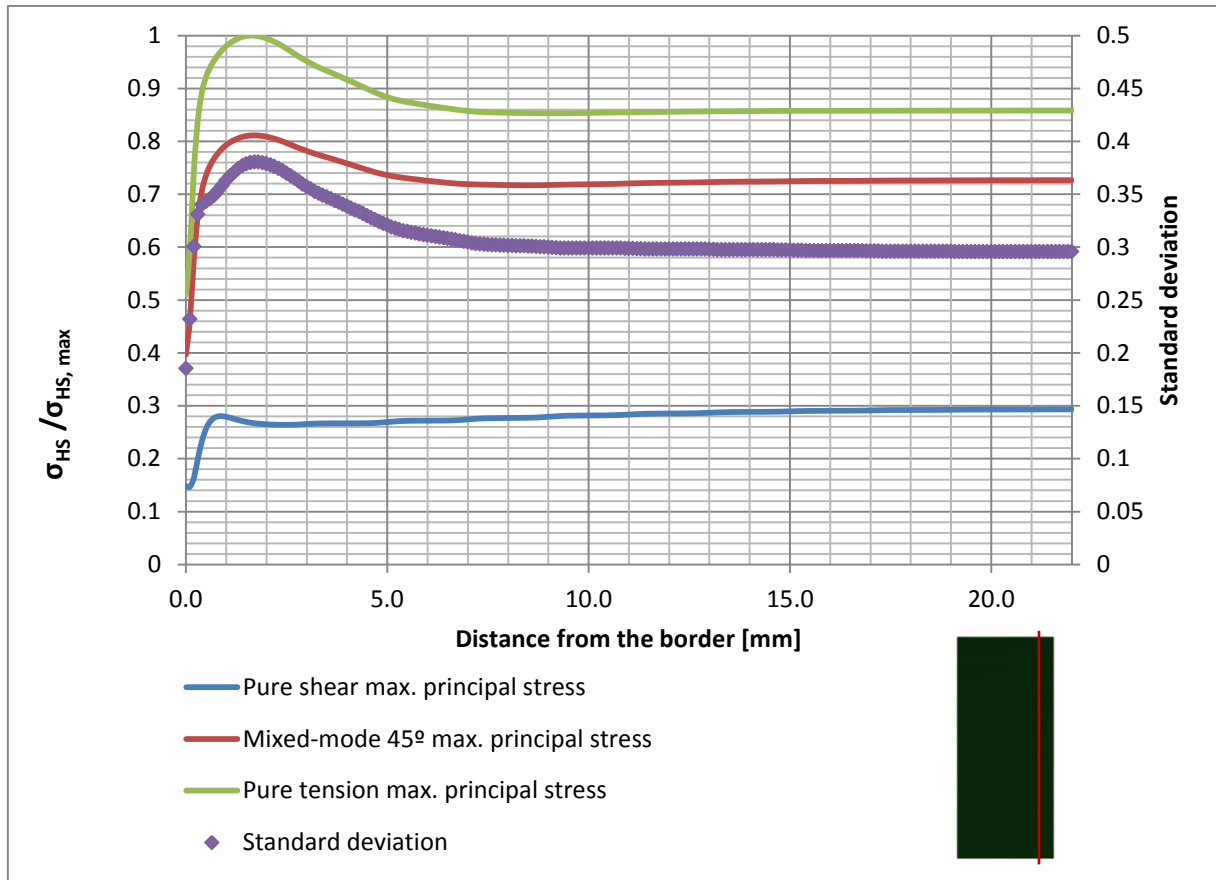


Figure 6-4: Stress distribution along path 3 for critical distance approach

In this case, any point shows a comparable principal stresses for different loading types. The variation along the path is very small.

Path 3 is completely discarded, because there is any point with a significant low difference between the principal stresses of the loading types. Path 1 has a lower minimal standard deviation, but direction 2 is easier to use because it represents the middle of the adhesive connection. The stress distribution of other specimen geometries is analysed for both paths.

---

#### Comparison of the critical distance approach between KS-II and cup-shaped specimens using the maximum principal stress

---

The KS-II and cup-shaped specimens are investigated in conjunction. This decision is based on the loading types and geometries of the joint for automotive industry. The adhesive joints of automotive industry are loaded mainly with tension and shear stresses at the car body. The butt-joined cylinder specimens introduce a torsion load, which represents a rather academic stress state. A last step compares the three different geometries.

---

These specimens are going to be presented and compared with the absolute distance from the edge of the adhesive layer as a reference to determine a unique reference point. The direction in the adhesive layer of the cup-shaped specimen is determined as the path along their width, which passes through the point with its highest value of maximum principal stress. As in the KS-II, that is analysed in the middle plane of the adhesive, to avoid contact singularities of the FE Model.

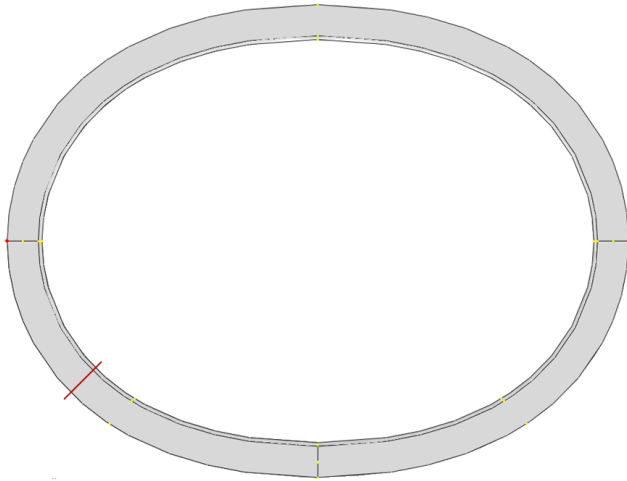


Figure 6-5: Path of the stress distribution (red line) for the cup-shaped specimen

## Absolute distance

The next figures show the stress distribution of the KS-II and cup-shaped specimens along the path:

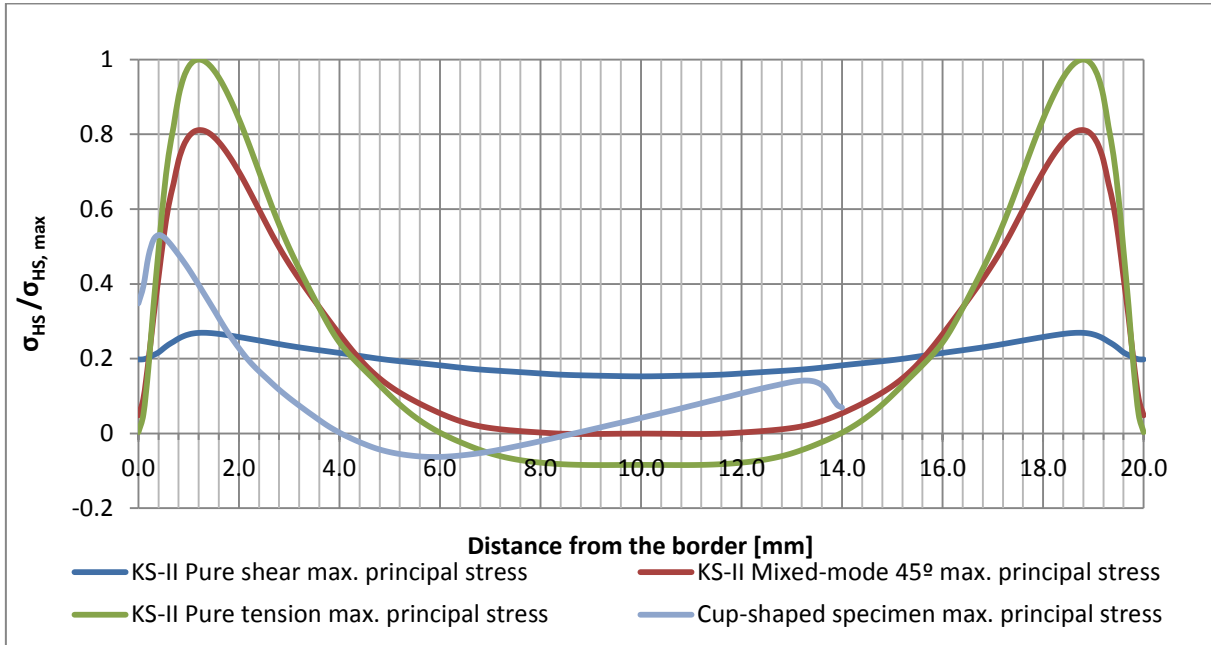


Figure 6-6: Maximum principal stress distribution of KS-II (along path 1) and cup-shaped specimens

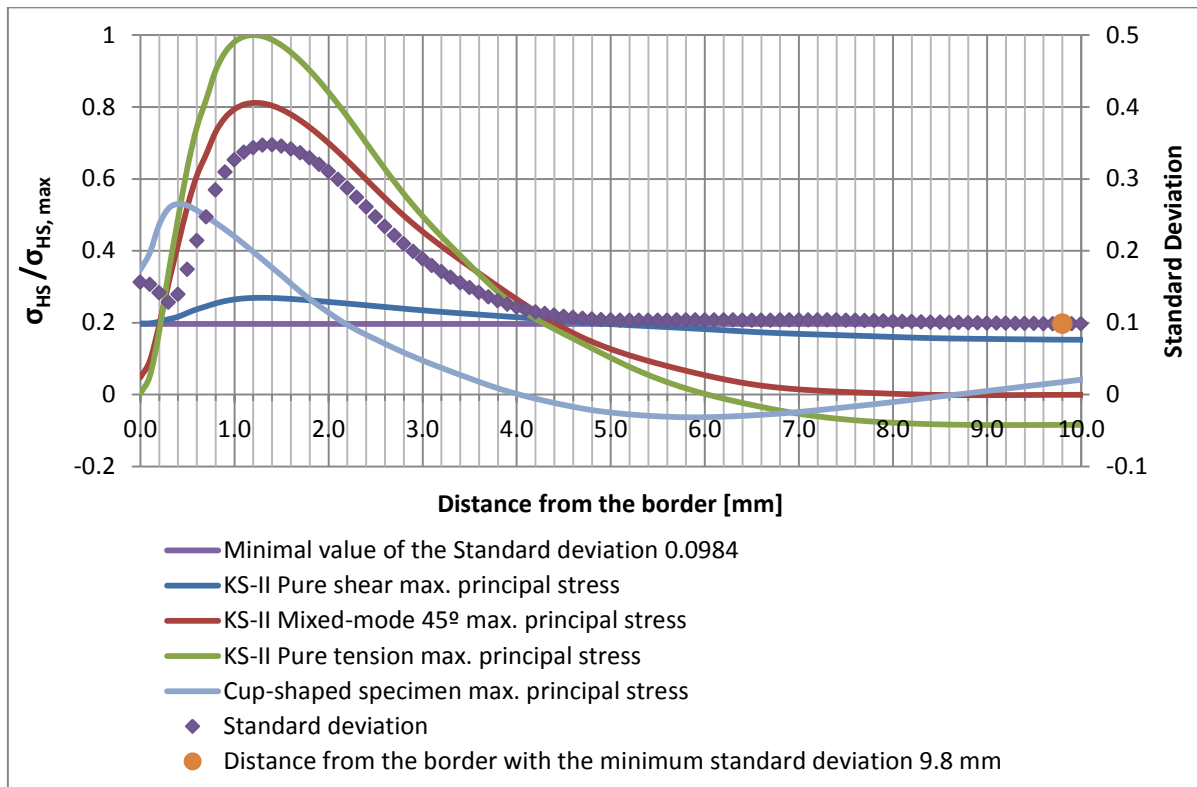


Figure 6-7: Comparison of the stress distribution between KS-II at path 1,  $z = 1.7$  mm, and cup-shaped specimen using the critical distance approach



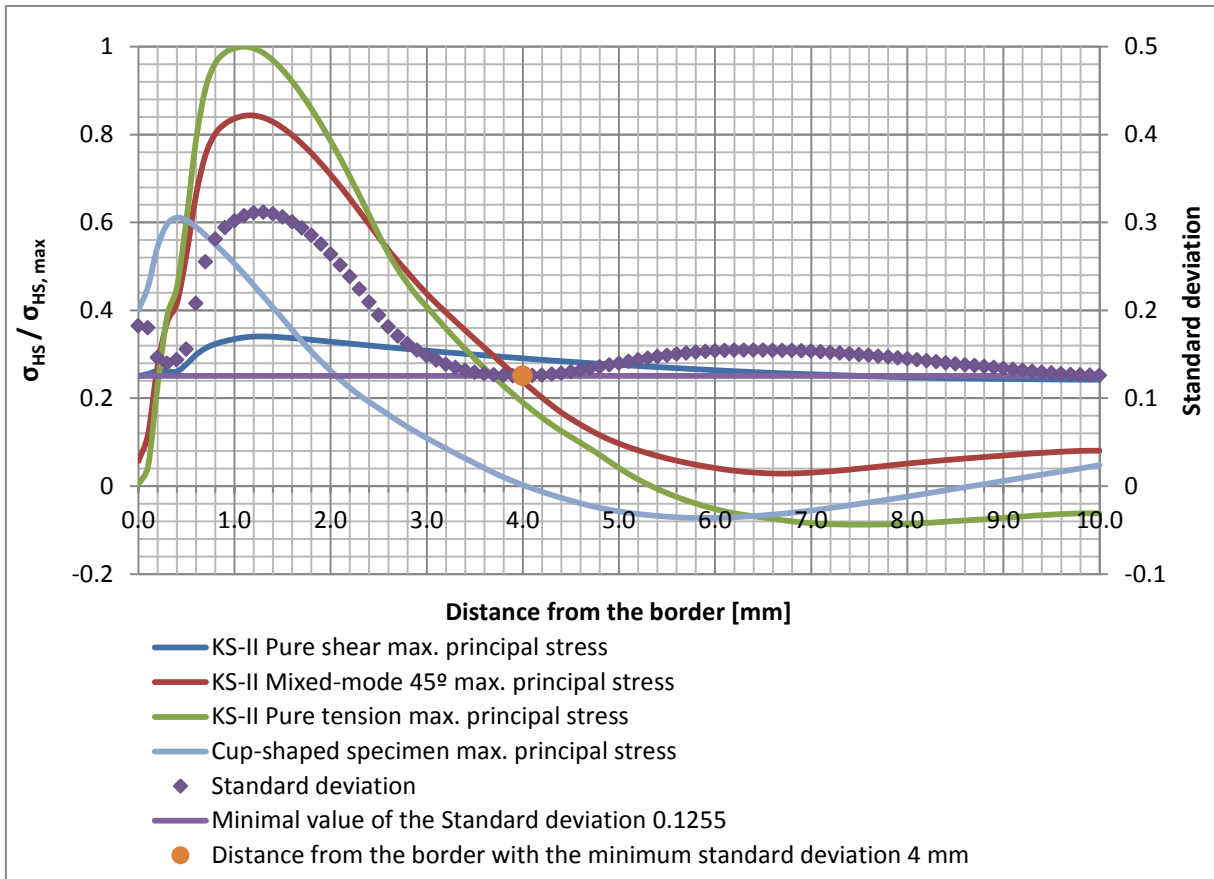


Figure 6-8: Comparison of stress distribution between KS-II at path 2,  $z = 22$  mm, and cup-shaped specimen using the critical distance approach

In both cases, the standard deviation reaches a minimum in a defined point. However, the obtained standard deviation is still very high. Hence, absolute distance from the edge of the adhesive is not a good indicator to determine the critical distance. As it is possible to observe on figure 6-7 and figure 6-8, the cup-shaped specimen has a qualitative similar stress distribution compared to the KS-II specimen loaded with a mixed force, but with a distance gap.

### Introduction to distance hypotheses

With these results, three hypotheses are proposed to minimize the gap between the two different specimens due to their different width:

- Constant gap: The distance to the point reference is a property of the material, but instead from the border this distance is determined from the point with highest value of maximum principal stress (hot spot) [Tay00].

- Relative distance: The adhesive joints are continuum joints and the stress distribution can be influenced by the total width of the joint. Instead of evaluating this distance in absolute terms, a relative term is used based on the total width of the adhesive.
- Stress scaled relative to the width: With the same base as the relative distance, the maximum stress and its distribution can be influenced by the total width of the adhesive. Instead of taking the stress values directly, a term with a stress scaled through the total width is used.

The hypotheses are further investigated. The next figures show the stress distributions using these hypotheses along path 1:

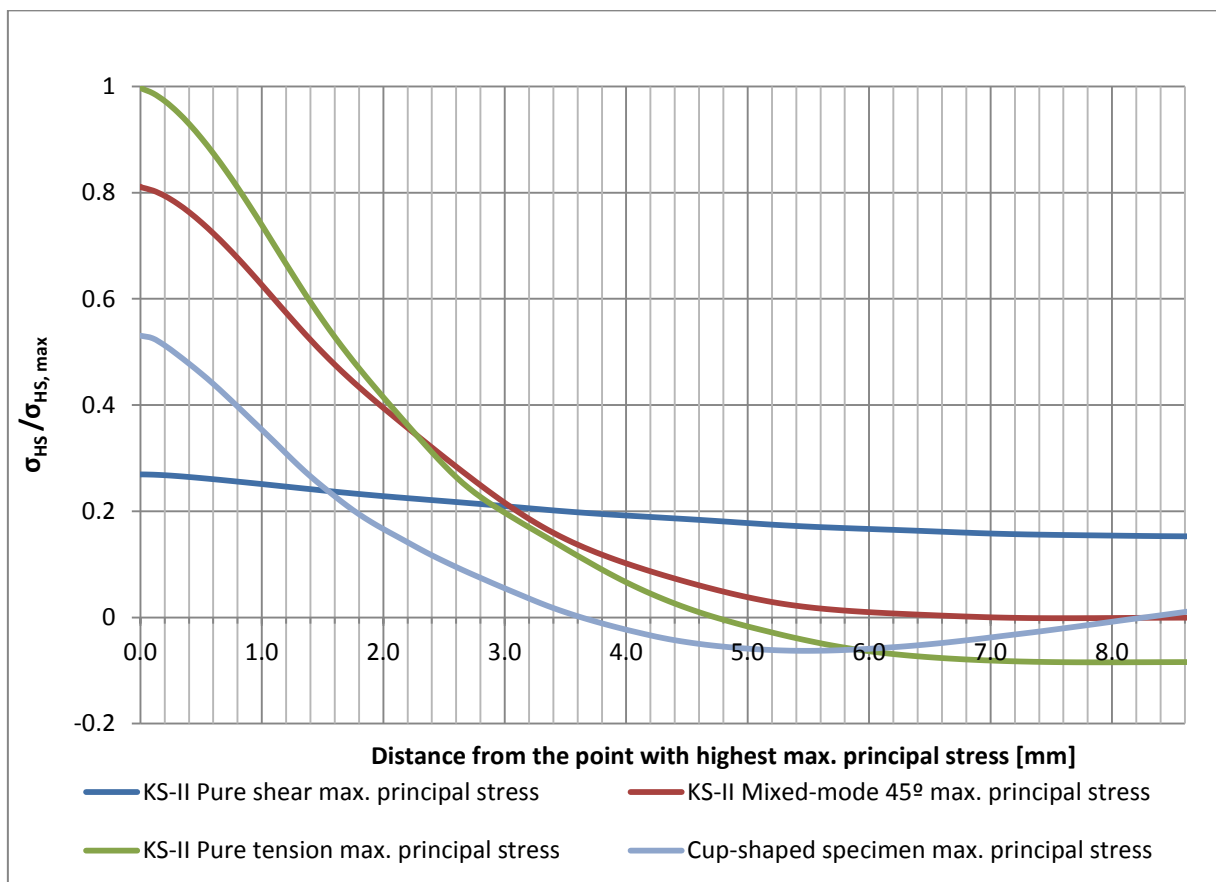


Figure 6-9: Maximum principal stress distribution of KS-II (along path 1) and cup-shaped specimens with constant gap from the point with highest maximal principal stress

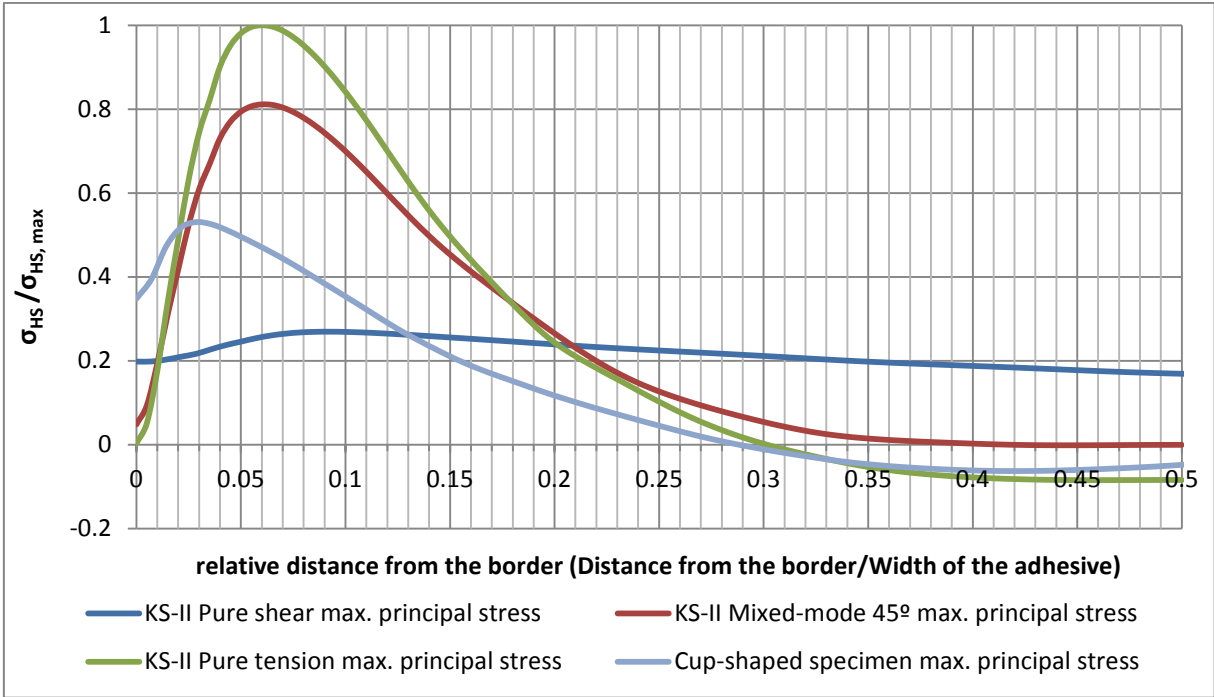


Figure 6-10: Maximum principal stress distribution of KS-II (along path 1) and cup-shaped specimens considering a relative distance

There is also the possibility that the two hypotheses are combined. The next figure shows this possibility:

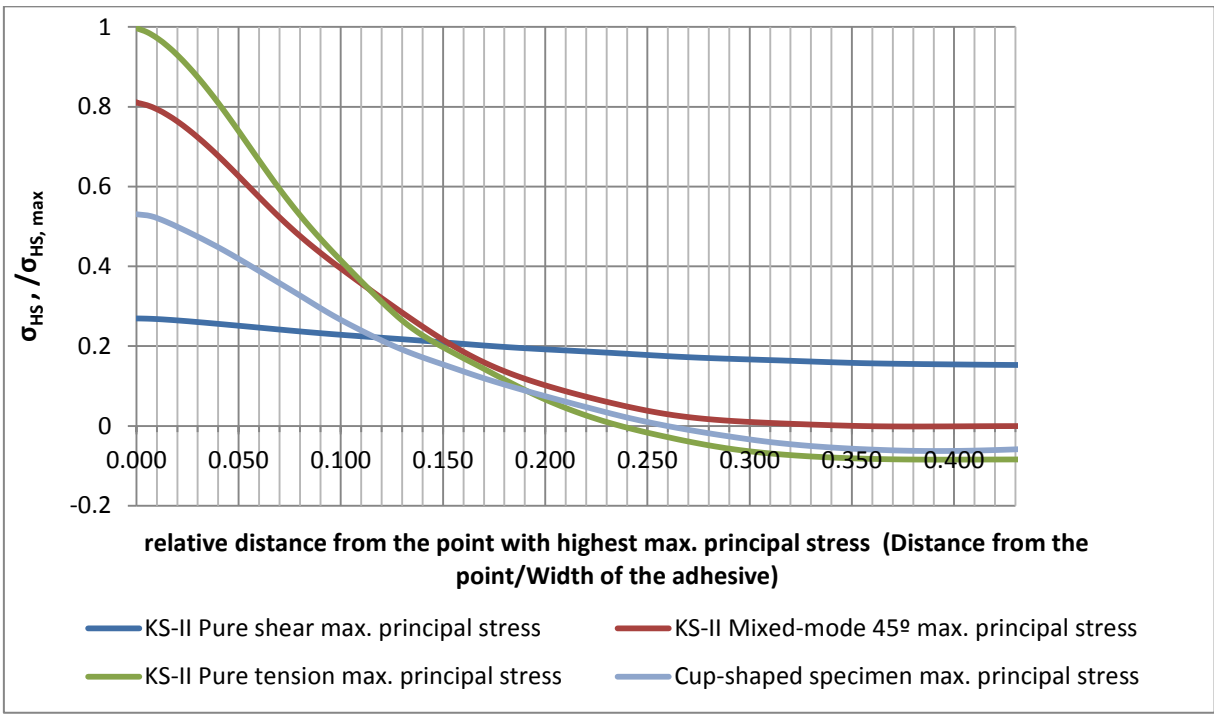


Figure 6-11: Maximum principal stress distribution of KS-II (along the path 1) and cup-shaped specimens with a constant gap distance from the point with highest max. principal stress and considering a relative distance

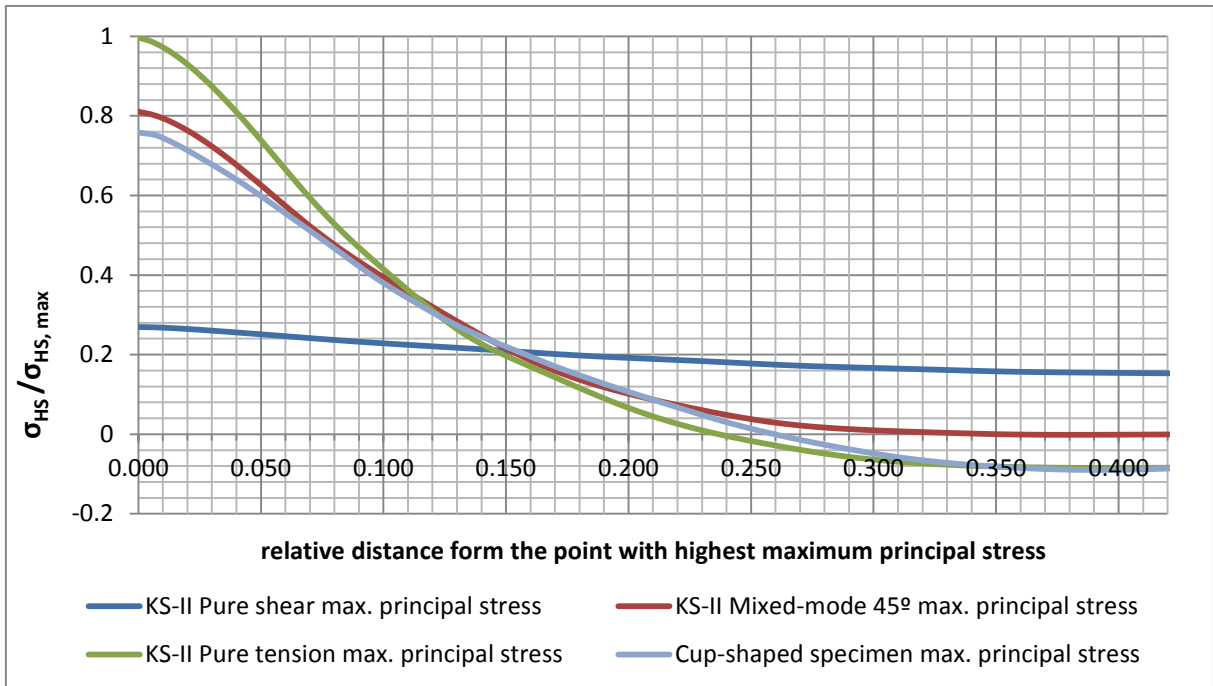


Figure 6-12: Maximum principal stress distribution of KS-II (along the path 1) and cup-shaped specimens applying the three hypotheses

It is possible to observe that the best solution is using the three hypotheses together. There it is possible to find a point at a relative distance from the maximal stress in each specimen from approximately 14%, with respect to the total length (distance = length of the adhesive · 0.14).

The next figures compare the hypotheses along path 2:

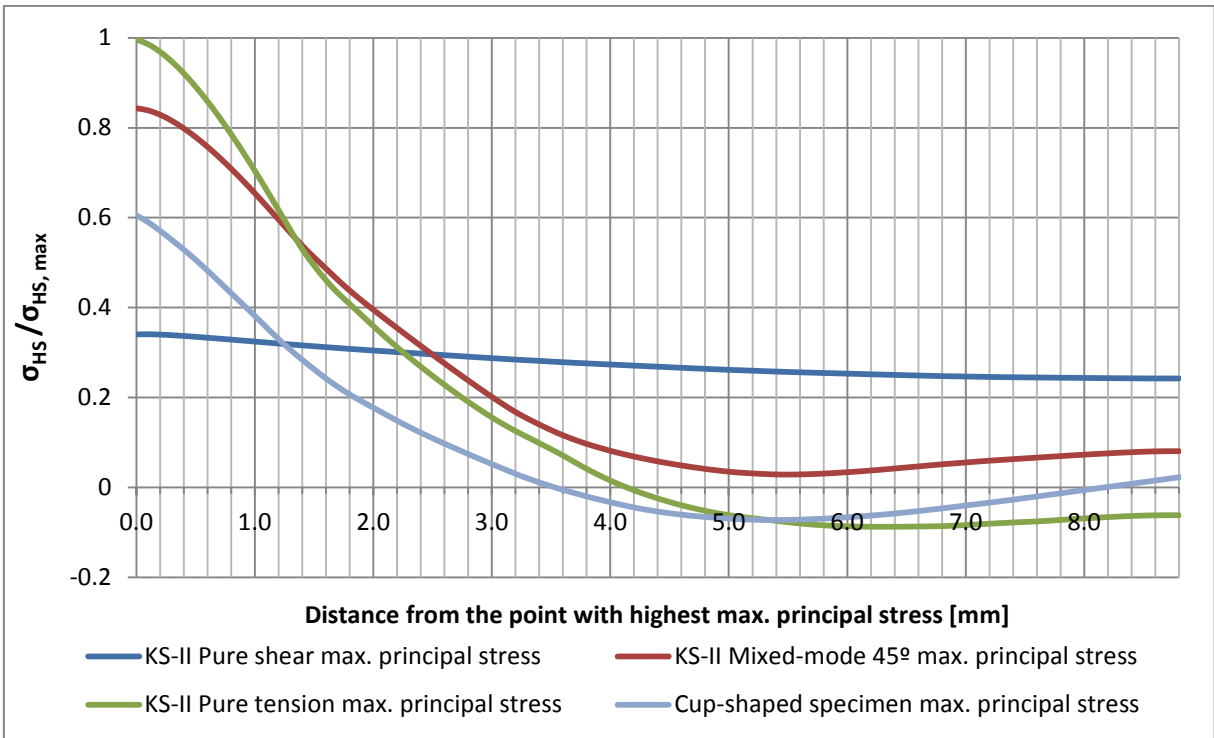


Figure 6-13: Maximum principal stress distribution of KS-II (along path 2) and cup-shaped specimens considering a relative distance

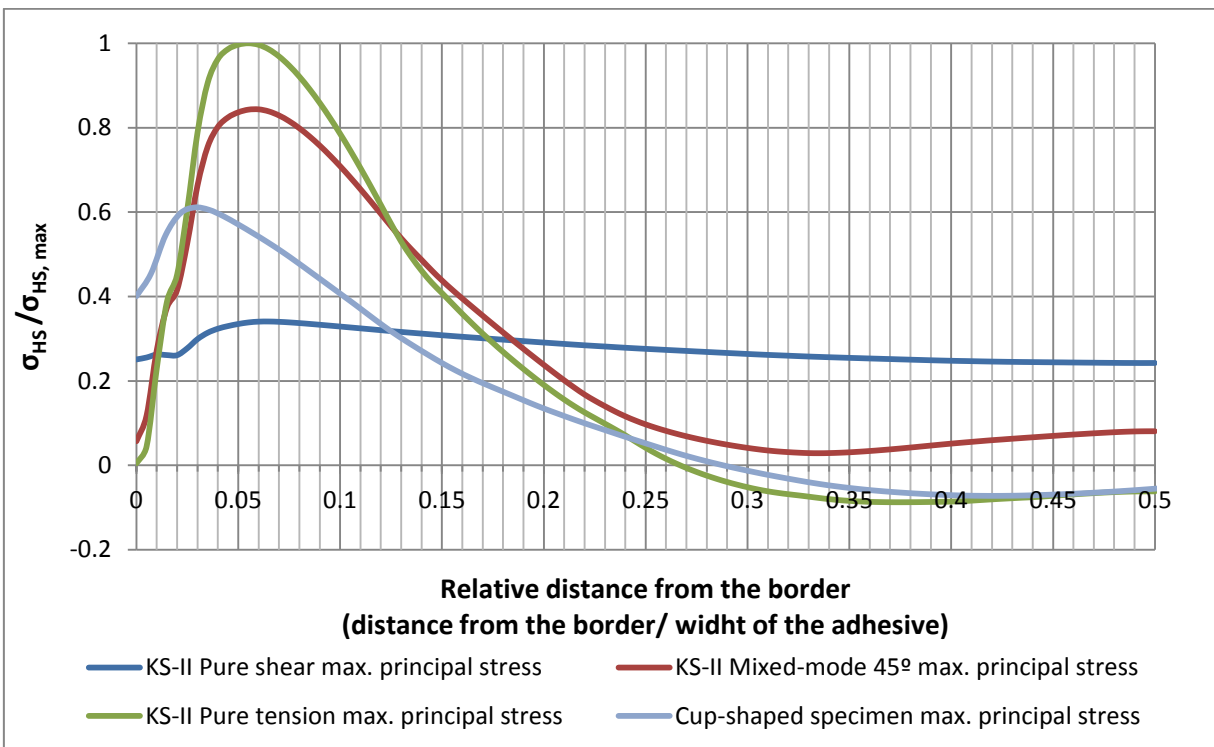


Figure 6-14: Maximum principal stress distribution of KS-II (along the path 2) and cup-shaped specimens with a constant gap distance from the point with highest max. principal stress and considering a relative distance

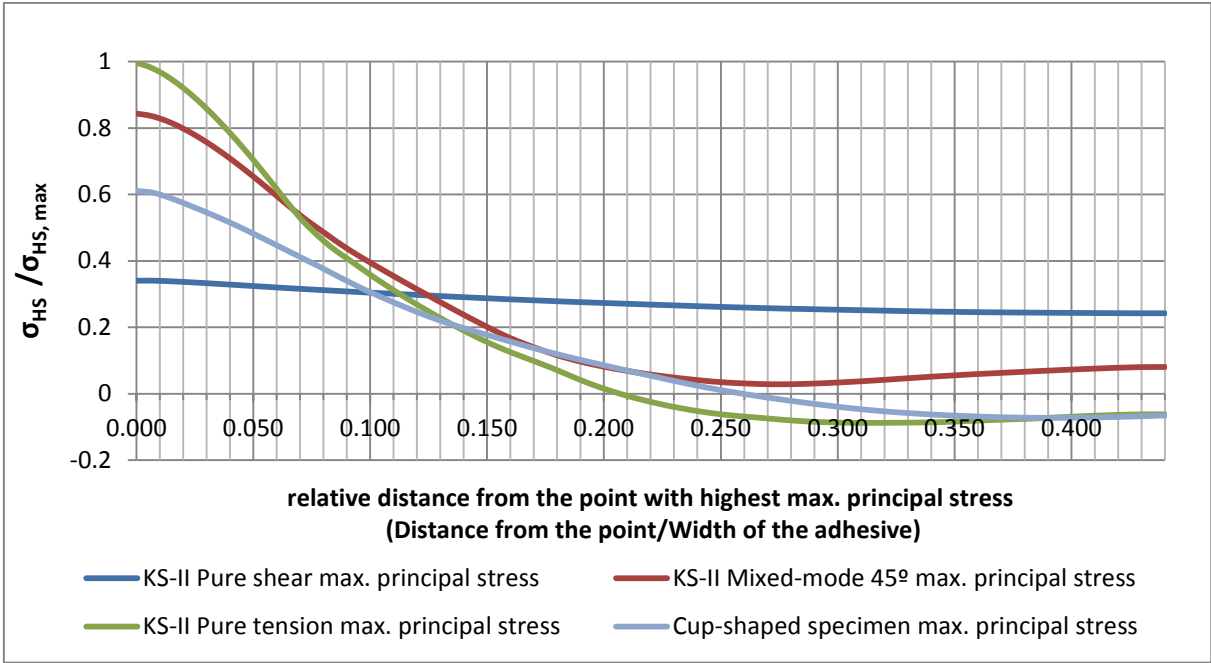


Figure 6-15: Maximum principal stress distribution of KS-II (along the path 2) and cup-shaped specimens with a constant gap distance from the point with highest max. principal stress and considering a relative distance

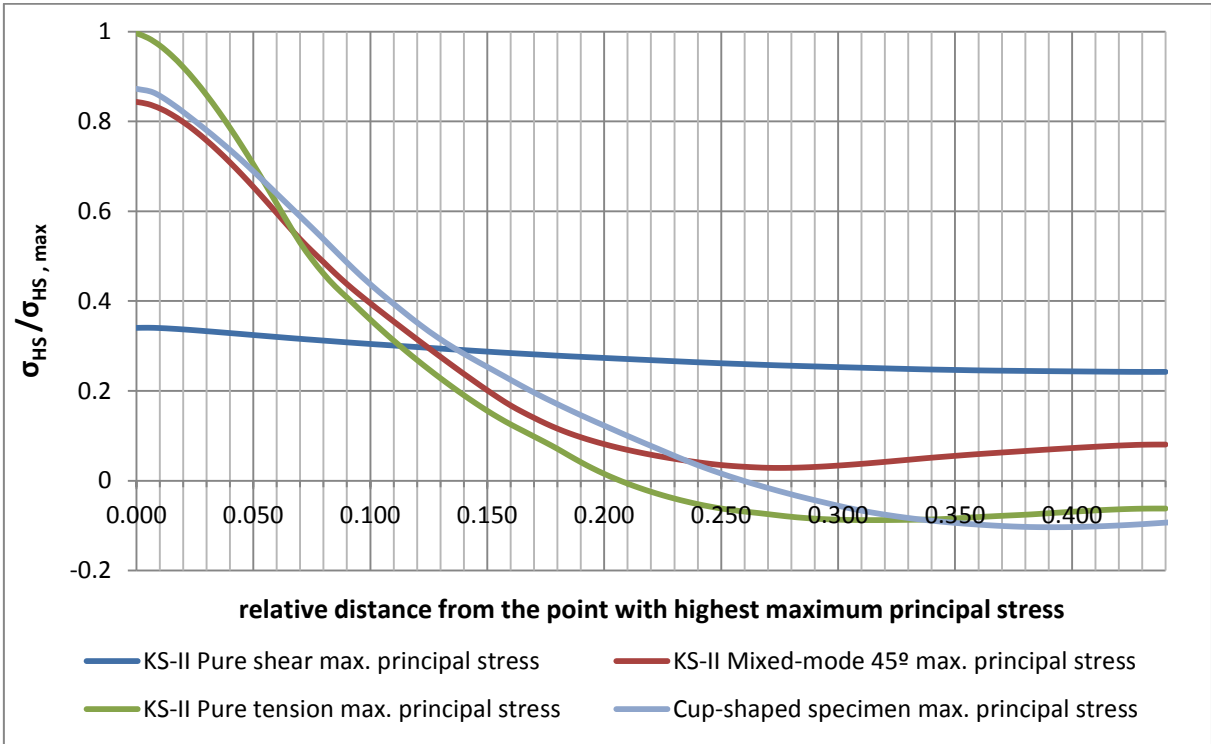


Figure 6-16: Maximum principal stress distribution of KS-II (along the path 2) and cup-shaped specimens with applying the three hypotheses

The application of the three hypotheses gives the best result, as in path 1, but with lower convergence of the loading cases. The optimal reference point in this case is approximately around 12% of the total length from the point with highest maximum principal stress.

The solution is better for the path 1 of the KS-II specimens than for the path 2. Because of this reason only the best solution is showed. Moreover, the path 1 is the path which passes through the point with highest maximum principal stress for pure tension and mixed mode. That correlates with the stress distribution path of cup-shaped specimen.

**Comparison of the critical distance approach between KS-II, cup-shaped and butt-joined specimens using the maximum principal stress**

In the chapters before, the stress distribution of the KS-II and the cup-shaped specimens were illustrated. Due to their similar geometries and loading types, the curve of maximum principal stress distribution is similar. Both start with an increase in the value until they reach a maximum, and then they decrease until almost zero. They are compared with the stress distribution of the butt-joined specimens. The first important difference between them is that the butt-joined specimens are loaded with tensile, torsion loads and a combination of them. The other specimens are loaded with tensile, shear and a combination of them. The second difference is the geometry of the specimen. In KS-II and cup-shaped specimens, the adhesive layer has a rectangular plan section and butt-joined specimens have a round section. The figure 6-17 shows the maximum principal stress distribution of the butt-joined specimen along the middle layer:

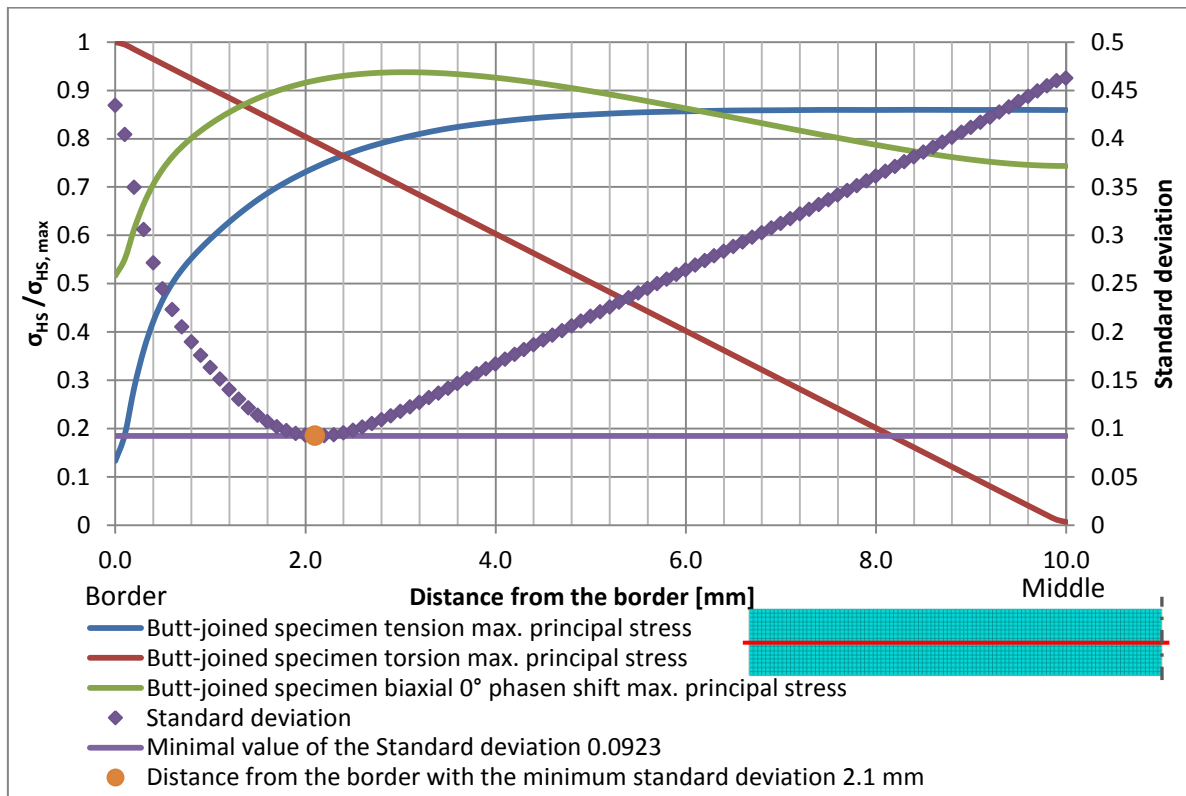


Figure 6-17: Max. principal stress distribution of the butt-joined specimen along the middle layer

Figure 6-17 illustrates the stress distributions of the butt-jointed specimens. The torsion stress has a linear distribution. The maximum lies at the border of the adhesive layer and decreases to zero in the middle. The pure tension stress has a low value at the border and then it converges to a maximum in the middle of the adhesive. The stress distribution of the combined load case results in a distribution with low values that reach a maximum around 3 mm from the border and then decrease to a lower value than the pure tensile stress.

Figure 6-18 exposes the stress distributions of the three specimens:

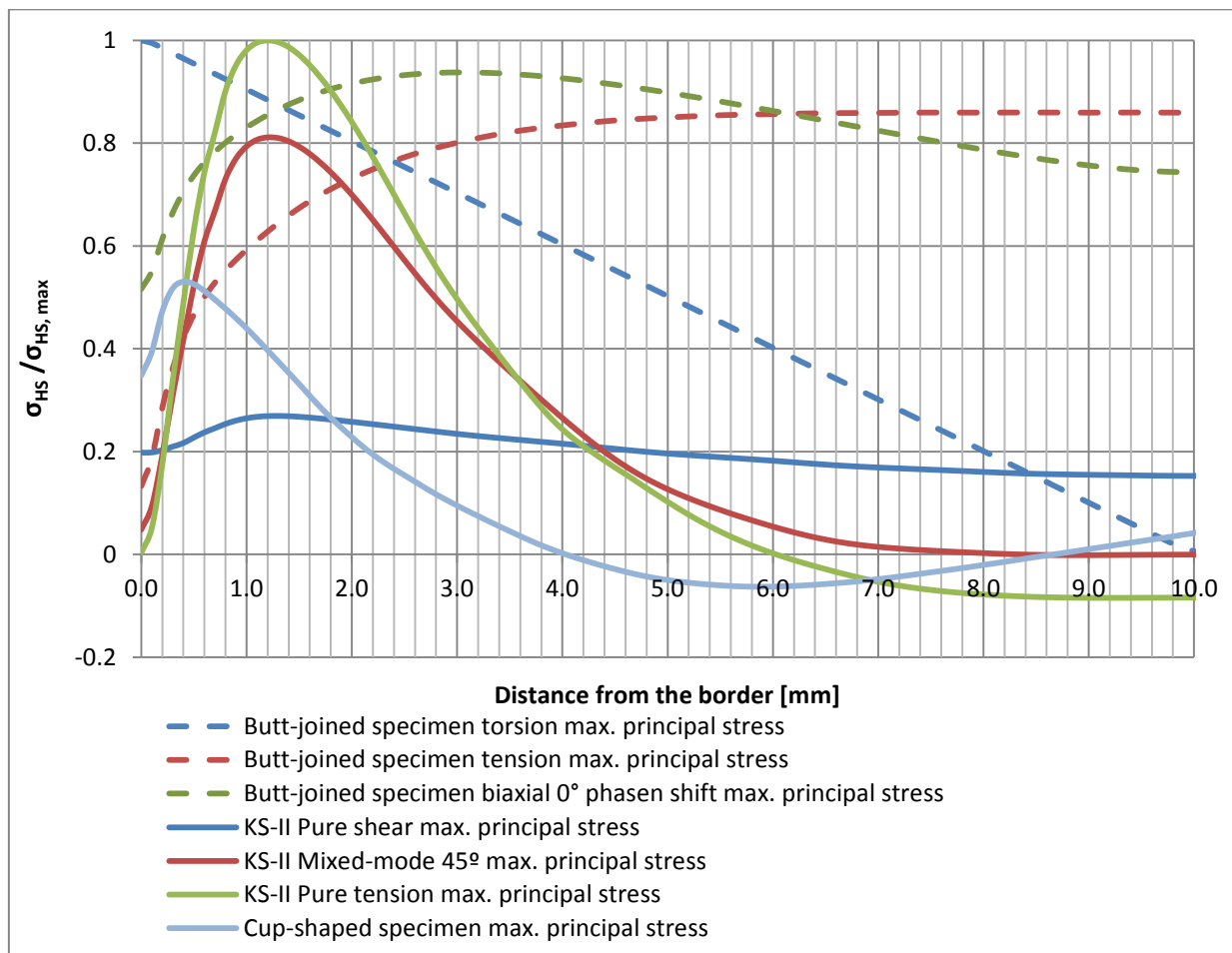


Figure 6-18: Maximum principal stress distribution of the three specimen types along the middle layer

In figure 6-18, all maximum principal stress distributions are shown. The different behaviour of the butt-jointed specimens compared to the KS-II and the cup-shaped specimens is obvious.

Because of the different distributions, it is not possible to find a common distance for evaluating. Figure 6-18 shows that the stress distribution highly depends on the geometry of the piece and the type of applied load. The butt-jointed specimen is an academic geometry and its stress distribution differs from typical automotive components.



---

---

## Determination of the equivalent elliptic stress parameters

---

The equivalent elliptic stress is a combination of the first invariant of the stress tensor ( $I_1$ ) and the second invariant ( $J_2$ ) of the deviator tensor. The equation is:

$$\tau_{ell} = \sqrt{J_2 + a \cdot I_1 + b \cdot I_1^2} \quad (6.1)$$

The parameters  $a$  and  $b$  have to be determined in order to obtain a proper equivalent stress. The method to find these parameters is as follows:

1. Determine the parameter  $b$  through adhesive material constants.

$$b = \frac{1}{6} \frac{1 - 2\nu}{1 + \nu} = \frac{1}{6} \frac{1 - 2 \cdot 0.45}{1 + 0.45} = 0.0115 \quad (6.2)$$

2. Determine the Beltrami stress in pure shear stress (*Scherzug*) and pure tension (*Kopfzug*):

$$\tau_{v,Belt}^2 = J_2 + b \cdot I_1^2 \quad (6.3)$$

3. The difference between the Beltrami and the equivalent elliptic stress is the parameter  $a$ . Because of this reason, with a linear regression in a graphic  $\tau_{v,Belt}^2 - I_1$  it is possible to find it:

$$\tau_{v,Belt}^2 = \tau_{ell} - a I_1 \quad (6.4)$$

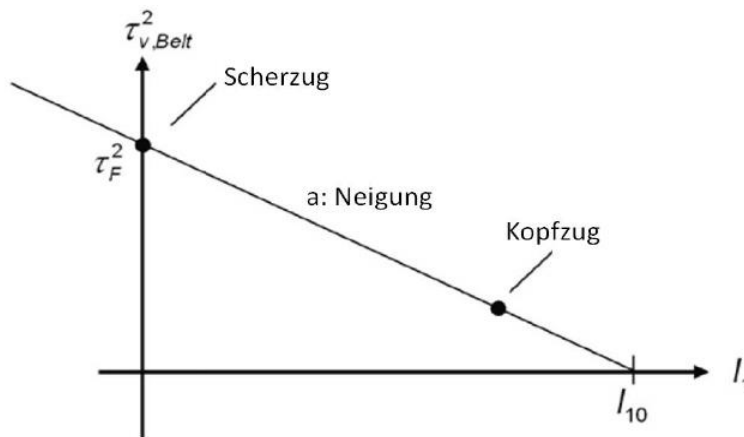


Figure 6-19: Graphic Beltrami stress- first invariant to find the  $a$  parameter [Tre12]

This method has to be applied in a defined point of a test geometry where both loading states are realized. Because of this reason five different points of KS-II specimen's adhesive layer are considered to find a suitable reference point to determine the parameter. The investigated points are:

1. The points, which have the highest stress values of principal stress for pure tension and pure shear. ( $x = 1.2$  mm;  $z = 1.7$  mm for pure tension,  $x = 1.3$  mm;  $z = 22$  mm for pure shear)(figure 6-22, green)
2. The point with a maximum principal stress with pure shear stress load. In this case, all the stresses to determinate the parameters are extracted from this point ( $x = 1.3$  mm;  $z = 22$  mm) (Figure 6-15, red)
3. The middle point of the adhesive, for all the stresses ( $x = 10$  mm;  $z = 22$  mm)(figure 6-22, blue)
4. The point over the line  $z = 1.7$  mm, which the standard deviation of the principal stresses is minimum, for all the stresses ( $x = 4.5$  mm)(figure 6-22, purple)(Reference figure 6-3)
5. The point over the line  $z = 22$  mm (middle of the adhesive), which the standard deviation of the principal stresses is minimum, for all the stresses( $x = 3.6$  mm)(figure 6-22, orange) (Reference figure 6-2)

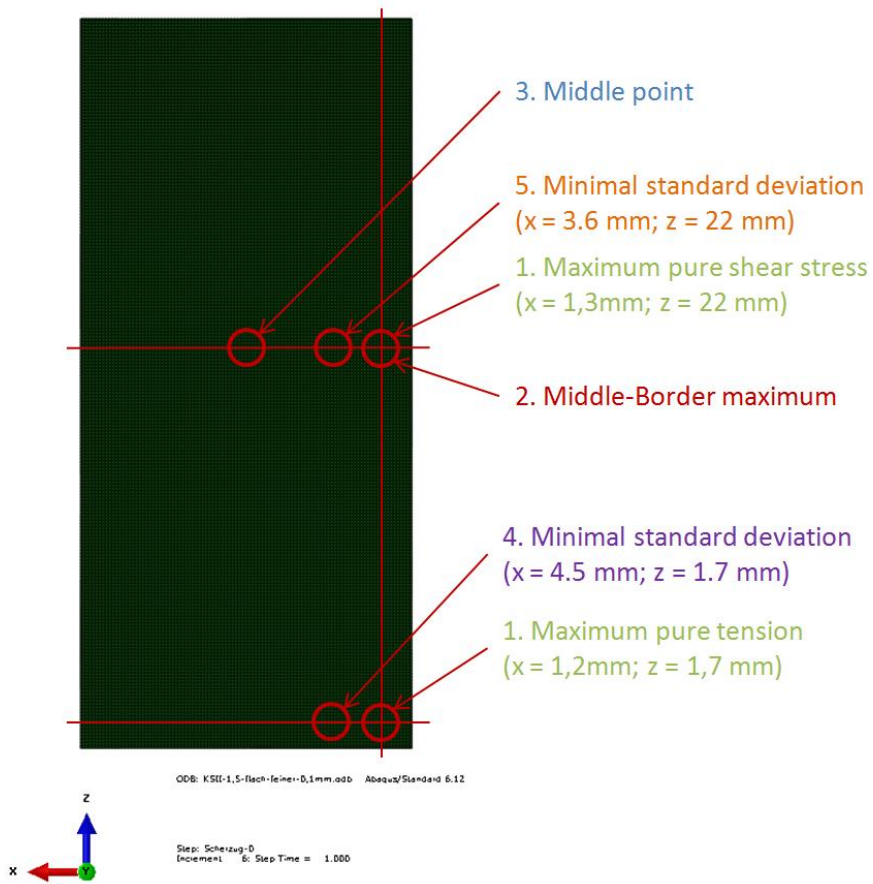


Figure 6-20: Five points to determinate the equivalent elliptic stress parameters

The linear regressions of the evaluated points are:

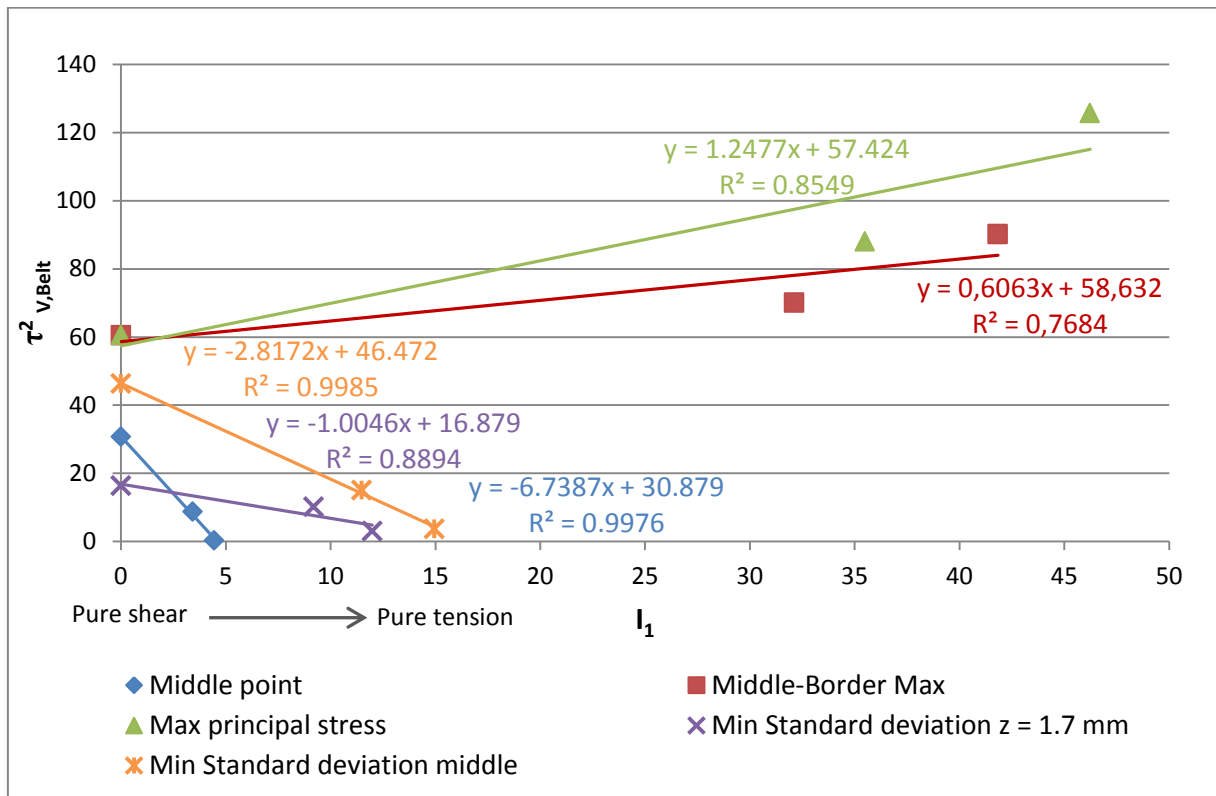


Figure 6-21: Graphic Beltrami tension - first invariant to determinate  $a$  parameter. From left to the right the points with same colour are from: pure shear, mixed-mode and pure tension

Figure 6-21 shows that the parameter  $a$  is preferably determined from the middle point, with a very good linear correlation, or at the point with minimal standard deviation along the middle line ( $x = 3.6$  mm;  $z = 22$  mm).

In this case, to evaluate which one is the best option, a graphic is needed to establish a relation between the square root of the second invariant and the first invariant. It shows the maximum stress rate before failure [Tre12].

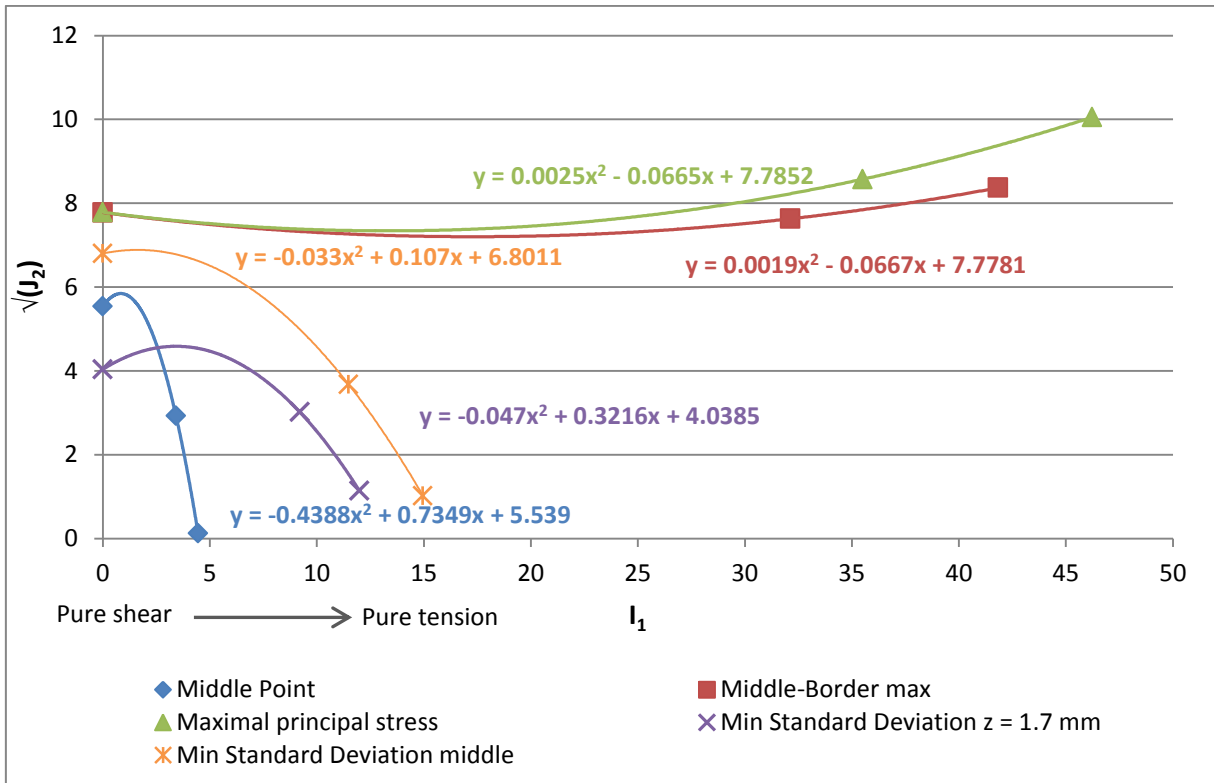


Figure 6-22: Graphic  $\sqrt{J_2} - I_1$  that determines the maximum stress state combination. From left to the right the points with same colour are from: pure shear, mixed-mode and pure tension

Figure 6-22 shows a minimal standard deviation along the middle width. In this case, the middle point curve does not represent the real strength of the adhesive, because their maximum value of first invariant is very low.

To conclude this chapter, the parameters determined are:

Table 6-1: Values of the equivalent elliptic stress parameters

a [MPa]	2,81
b [-]	0.0115

### Comparison between KS-II and cup-shaped specimens using the equivalent elliptic stress

The parameters are determined on a point along the middle width, because of that the comparison between the KS-II and cup-shaped is done using the middle path as the reference path of the KS-II specimen. For the cup-shaped, the path goes through the maximal principal stress, as done for the maximum principal stress comparison (figure 6-5).

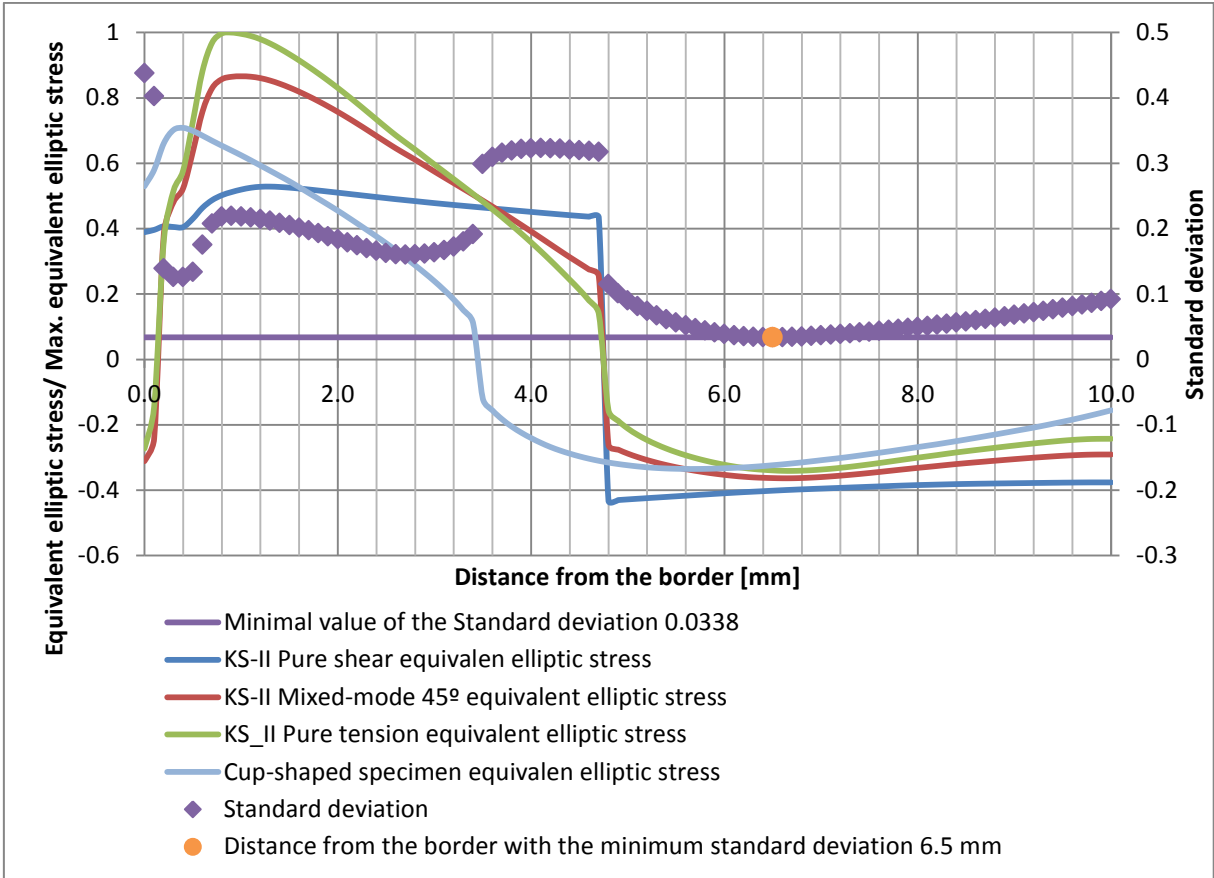


Figure 6-23: Comparison stress distribution between KS-II and cup-shaped specimens respect equivalent elliptic stress

As it is expected, the three different loading states of the KS-II specimen are passing through the same point at a distance of 3.6 mm, because it was used as reference point of the equivalent elliptic stress. The standard deviation after 5 mm is relatively slow, but this stress cannot be considered as critical because it is a compression stress, which is not critical for the adhesive joint. The reference point has to be a point with positive tensile stress with a significant lower standard deviation. In this case there is any point that fits with these requirements. The same distance appears between the tensile stress distribution of the combined load of the cup-shaped specimen and the KS-II distribution. Because of that, the same hypotheses proposed for the principal stress are considered (page 59).

**Introduction of several distance hypotheses for the critical distance approach**

As realized in the previous chapter with the maximum principal stress, two hypotheses are applied:

- Constant gap
- Relative distance

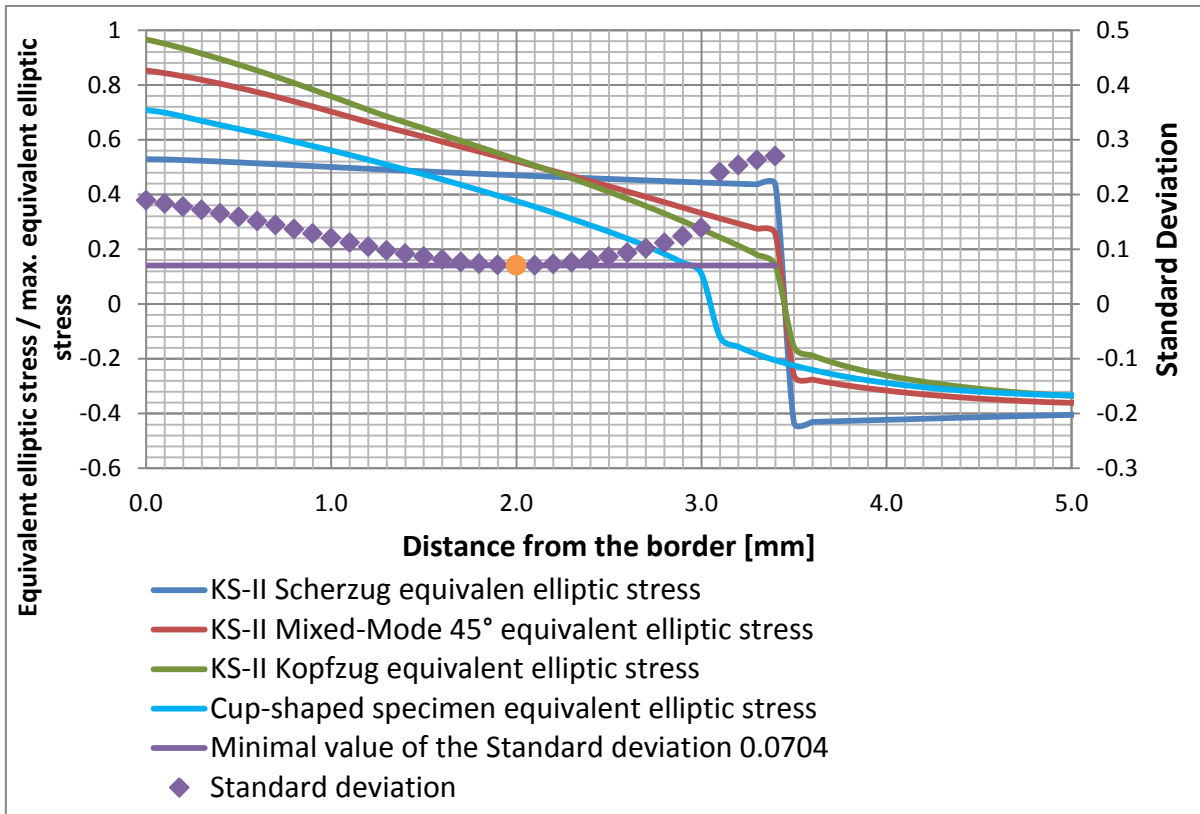


Figure 6-24: Equivalent elliptic stress distribution of KS-II and cup-shaped specimens with constant reference distance from their maximal stress point

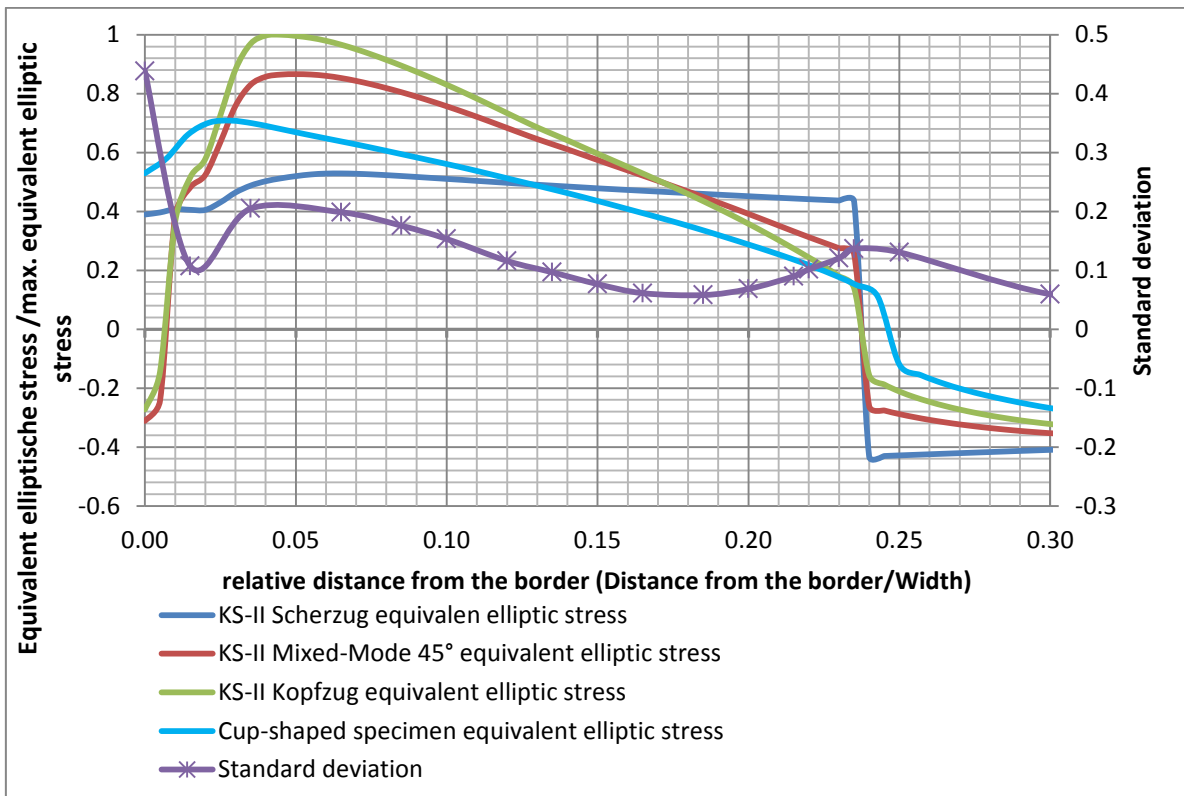


Figure 6-25: Equivalent elliptic stress distribution of KS-II and cup-shaped specimens with relative distance

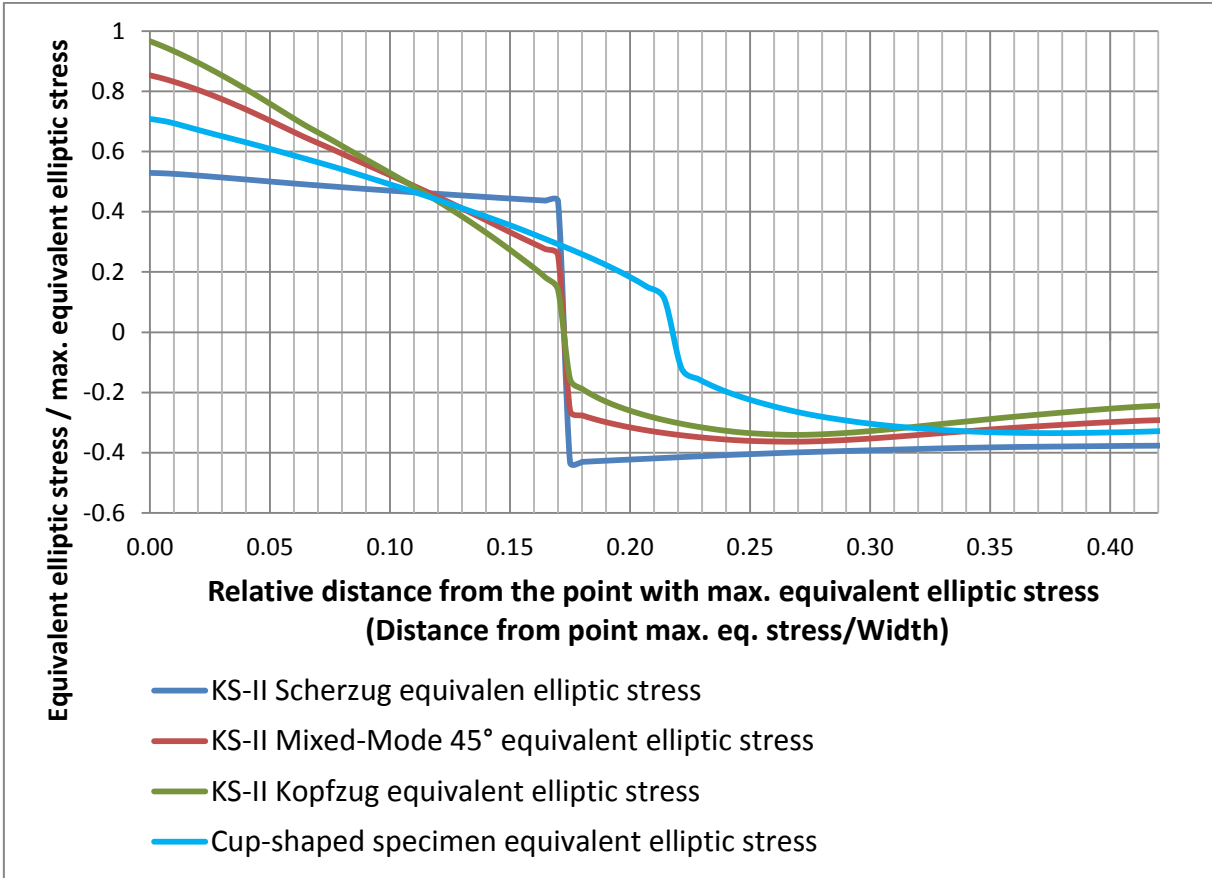


Figure 6-26: Equivalent elliptic stress distribution of KS-II and cup-shaped specimens with a constant reference distance and relative distance

Figure 6-26 and figure 6-27 shows that both hypotheses could be used, because the best solution is when both are taken into account (figure 6-28). The second approach (relative distance, figure 6-26) shows a smaller difference between the KS-II specimens and the cup-shaped specimens. In contrast, figure 6-27 shows a smaller distance and a balanced distribution.

### 6.1.2 Stress averaging approach

The stress averaging approach is applied to the samples. The stress averaging approach determines an effective stress that is an average stress. The concepts of this approach are widely explained in chapter 2.3.1.

In this section, the comparison is directly done between the KS-II and the cup-shaped specimens. In the previous chapter has been seen that the stress distribution of the two specimens are qualitatively similar.



## Stress averaging approach evaluation with KS-II specimens

As realized with the critical distance approach, the KS-II specimens are studied firstly to obtain an overview of the possible results. KS-II specimens are used because they have similar geometry with cup-shaped specimens and they have three different loading types.

The paths along the adhesive middle layer of the KS-II specimens to study this approach are the same as in figure 6-1 (page 53).

### Path 1, $z = 1.7 \text{ mm}$

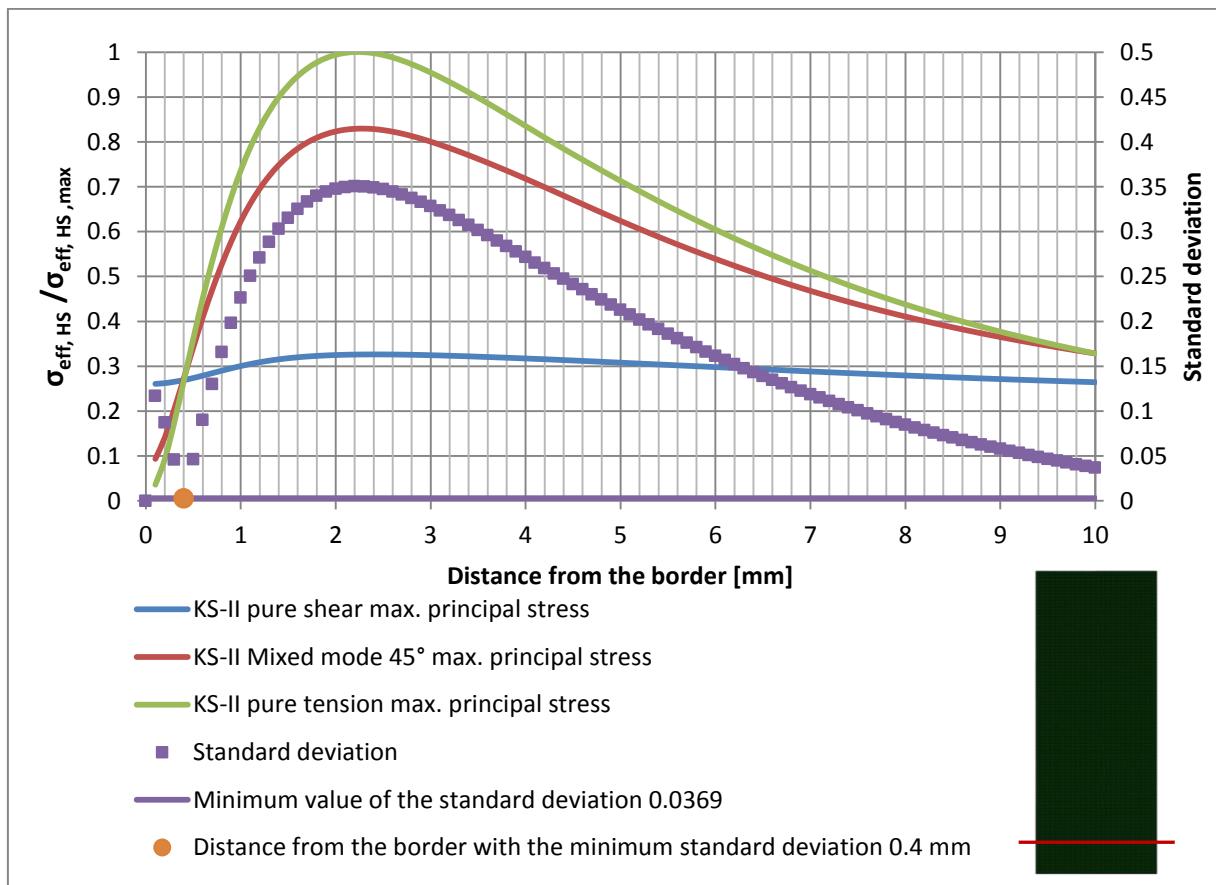


Figure 6-27: Stress distribution along path 1 for stress averaging approach

In figure 6-27 it is possible to observe that the point of minimum standard is placed at 0.4 mm, but the standard deviation of the points around increase strongly. The values do not converge in this point. The curves seem to converge in the vicinity of 10 mm. The stress distributions are symmetric and because of that this hypothesis cannot be valid. The possible solution to apply this approach is that that the figure 6-27 shows the stress distribution on a specific point of two million cycles. The distance varies depending on the number of cycles, due to the different slopes of the S-N curves for each loading type (figure 5-1, page 39). The pure shear loading type has the lowest slope value  $k$ , which means that it has the highest

increase of stress with a decreasing number of cycles. That means that for other points along the S-N curve, the pure shear curve increases more than the pure tension and mixed mode curves. In this case, the three curves converge in a point before 10 mm distance (symmetric axis distance). With a decrease of the lifetime, the distance from the border of the reference point also decreases.

**Path 2, z = 22 mm**

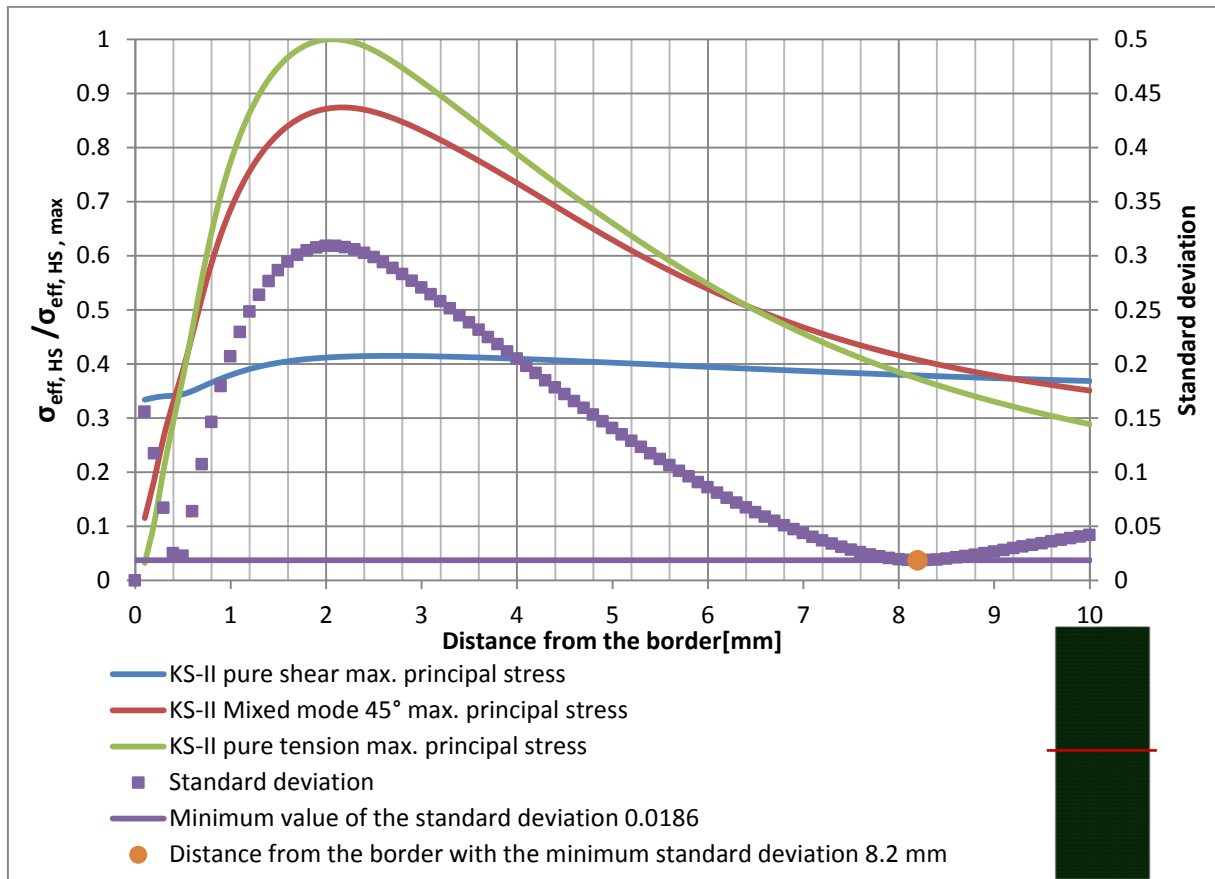


Figure 6-28: Stress distribution along path 2 for stress averaging approach

In figure 6-28 the three curves of the effective stress average form the maximum principal stress converge in a zone where the standard deviation is valid to apply the method. This zone is between 7 mm and 10 mm from the border, with a minimum value of standard deviation on 8.2 mm. As explained before, due to the difference on the slopes of the S-N curves between the loads, this interval depends on the number of cycles. The distance decreases with a decrease of lifetime.

Figure 6-28 shows another point where the three equivalent average stresses cross each other with a low standard deviation, at a point 0.5 mm from the border. In this case, the curves only cross but there is no convergence of the three curves. The differences with the other point are

that the interval reduces to two or three points, making it more difficult to apply a method because it strongly depends on the chosen point. On the other hand, when it is an interval, the results obtained from this method are robust to the application point.

**Path 3, x = 1.3 mm**

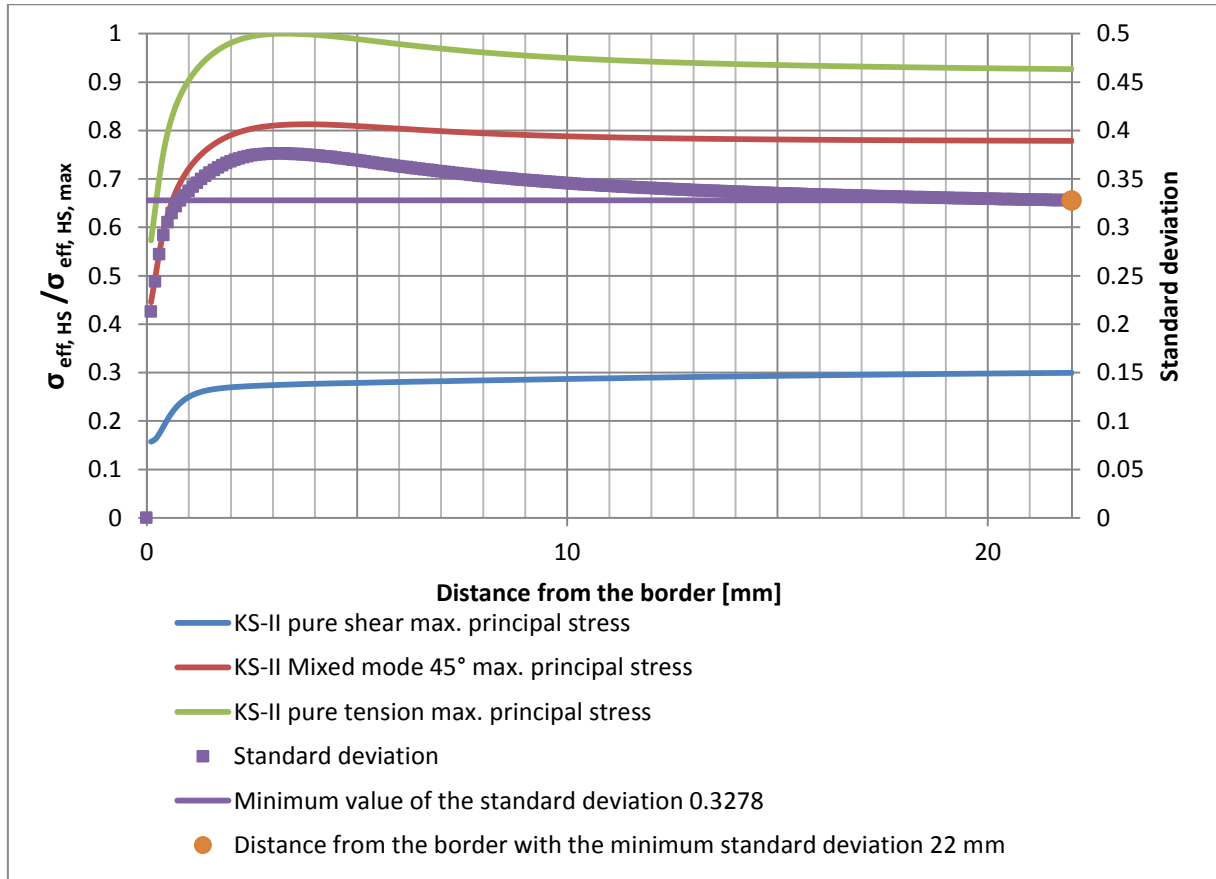


Figure 6-29: Stress distribution along path 3 for stress averaging approach

Figure 6-29 shows that, similar to the critical distance approach, the path 3 is not valid for the stress averaging approach. The effective stress curves do not converge in any point and the distance between their values are high, as can be determined from the high value of the standard deviation.

## Comparison of the stress averaging approach between KS-II and cup-shaped specimens using the maximum principal stress

From the previous comparison of the equivalent stress average along the chosen paths, it is possible to determinate that the path 1 and 2 are valid to compare with other specimens. The stress distributions on the third path do not converge in any distance between the different loading types, a requirement to properly apply this method.

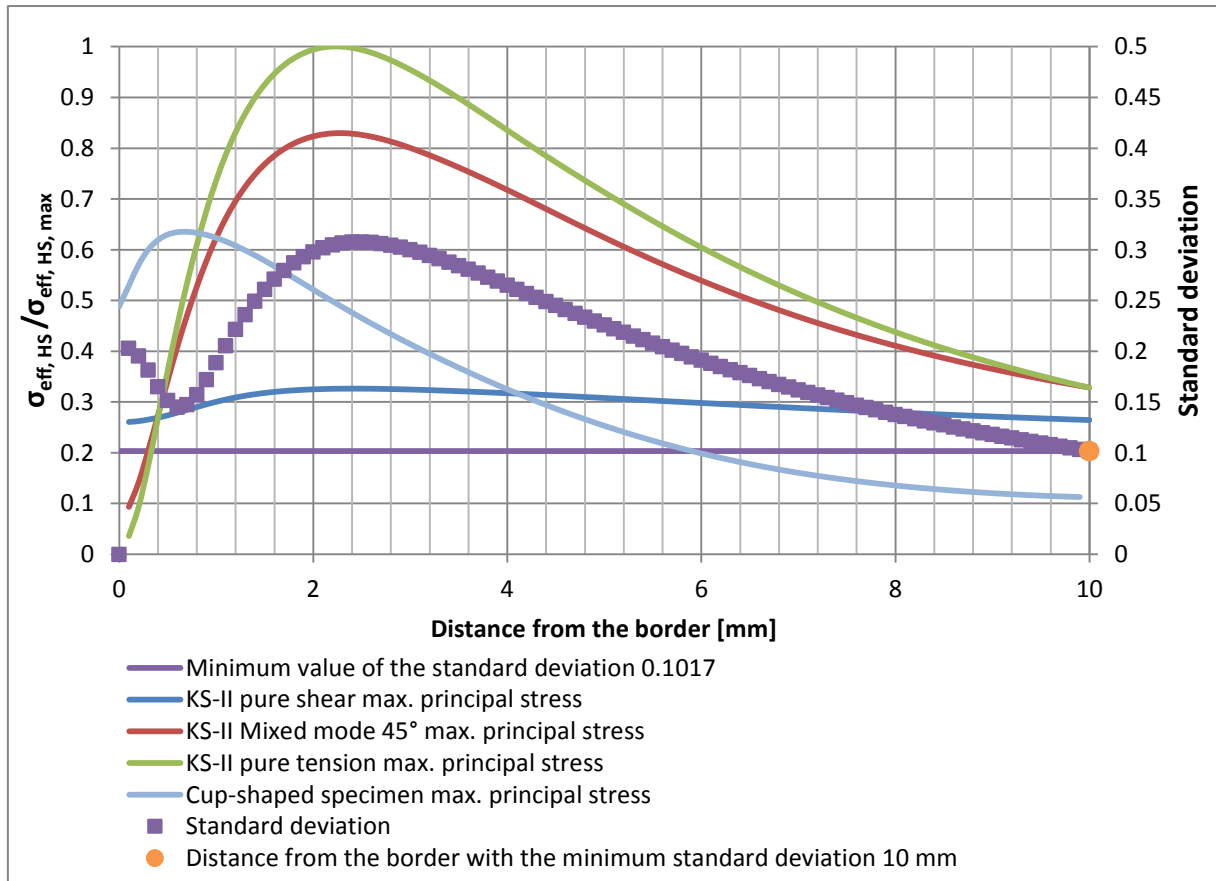


Figure 6-30: Comparison of the stress distribution between KS-II at path 1,  $z = 1.7$  mm, and cup-shaped specimen using the stress averaging approach

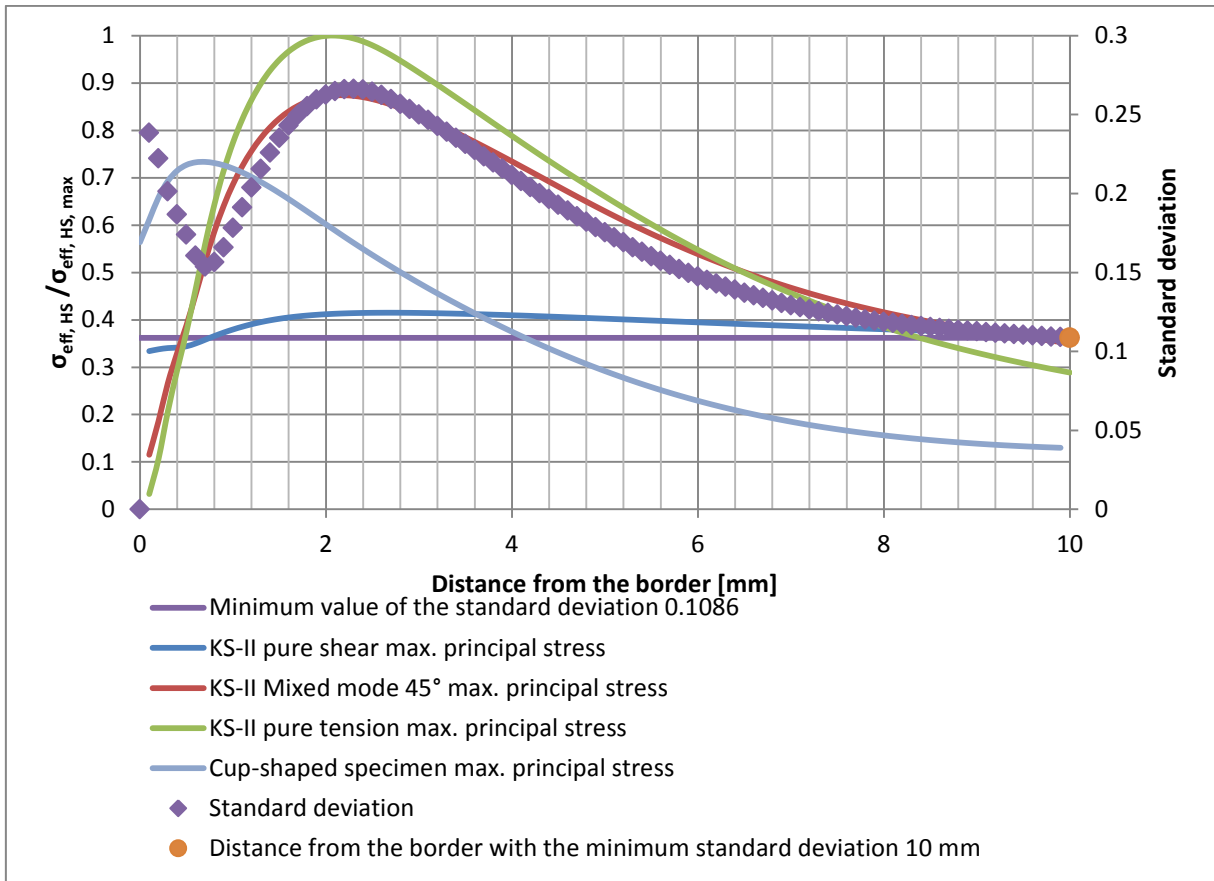


Figure 6-31: Comparison of stress distribution between KS-II at path 2,  $z = 22$  mm, and cup-shaped specimen using the stress averaging approach

Figure 6-30 and figure 6-31 shows that the stress average has a similar distribution. Despite that, the stress distributions of the two specimens do not converge.

As realized with the critical stress approaches, several hypotheses are being compared to obtain parameters to converge these similar distributions.

### Introduction of distance hypotheses for the stress averaging approach

As applied in previous chapters, three different hypotheses based on the total width of the adhesive layer are taken into account:

- Constant gap
- Relative distance
- Stress scaled relative to the width

The next figures show the stress distribution applying these hypotheses:

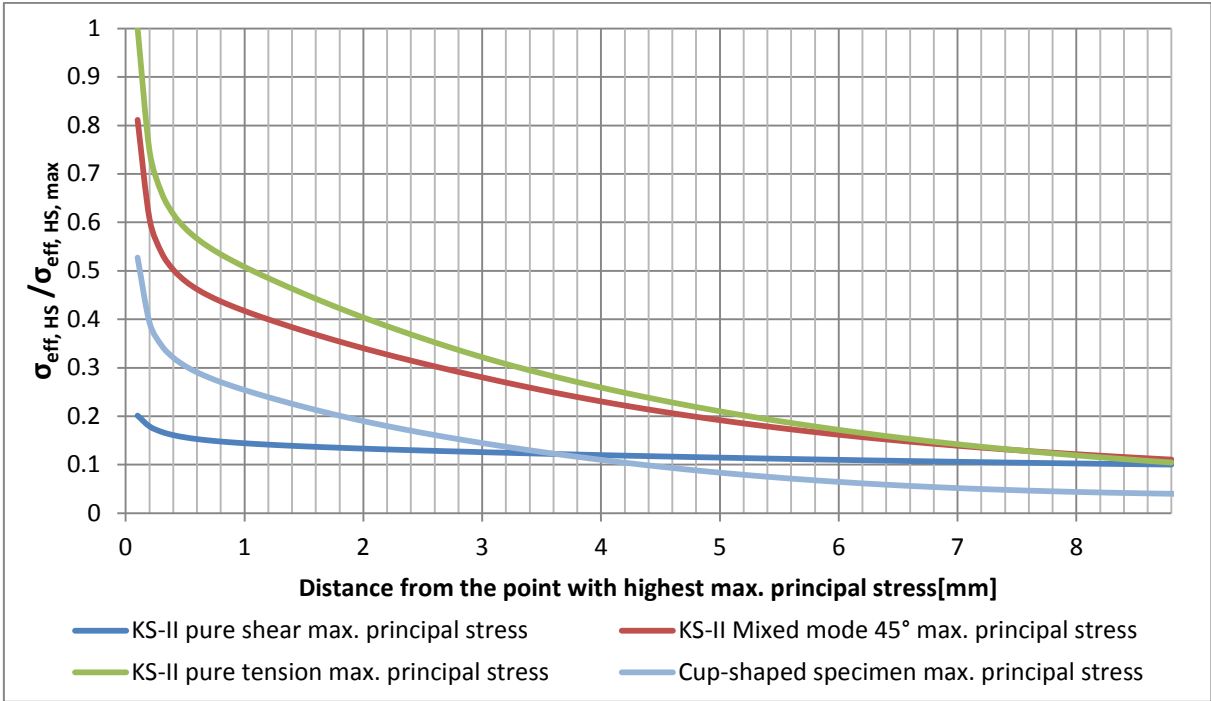


Figure 6-32: Average of maximum principal stress distribution of KS-II (along path 1) and cup-shaped specimens with constant gap from the point with highest maximal principal stress

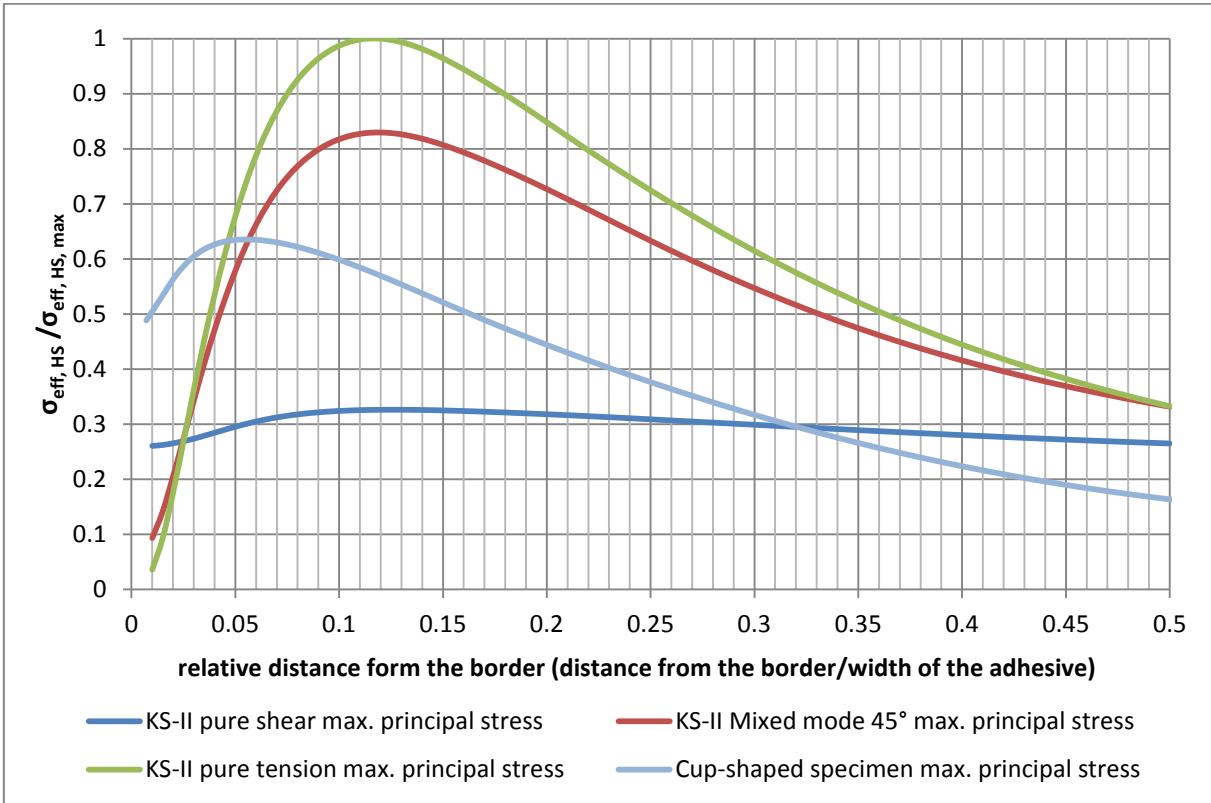


Figure 6-33: Average of maximum principal stress distribution of KS-II (along path 1) and cup-shaped specimens considering a relative distance

The results of the average stress distribution from figure 6-32 and figure 6-33 show that the two hypotheses separately adjust the curves between the both specimens, but they are not

close enough to valid the method. The next figure shows the average stress distributions applying together the two hypotheses.

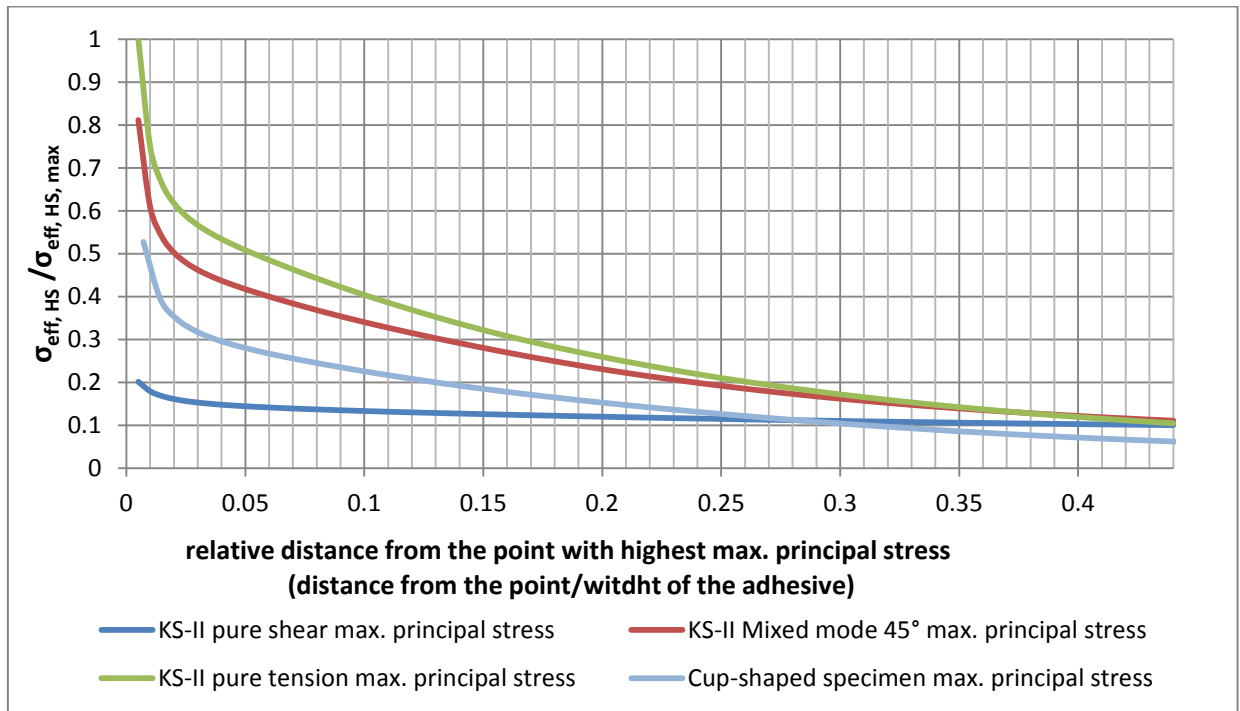


Figure 6-34: Average stress distribution of KS-II (along the path 1) and cup-shaped specimens with a constant gap distance from the point with highest max. principal stress and considering a relative distance

Figure 6-34 shows that the curves do not converge in one point, but the distances are considerably reduced.

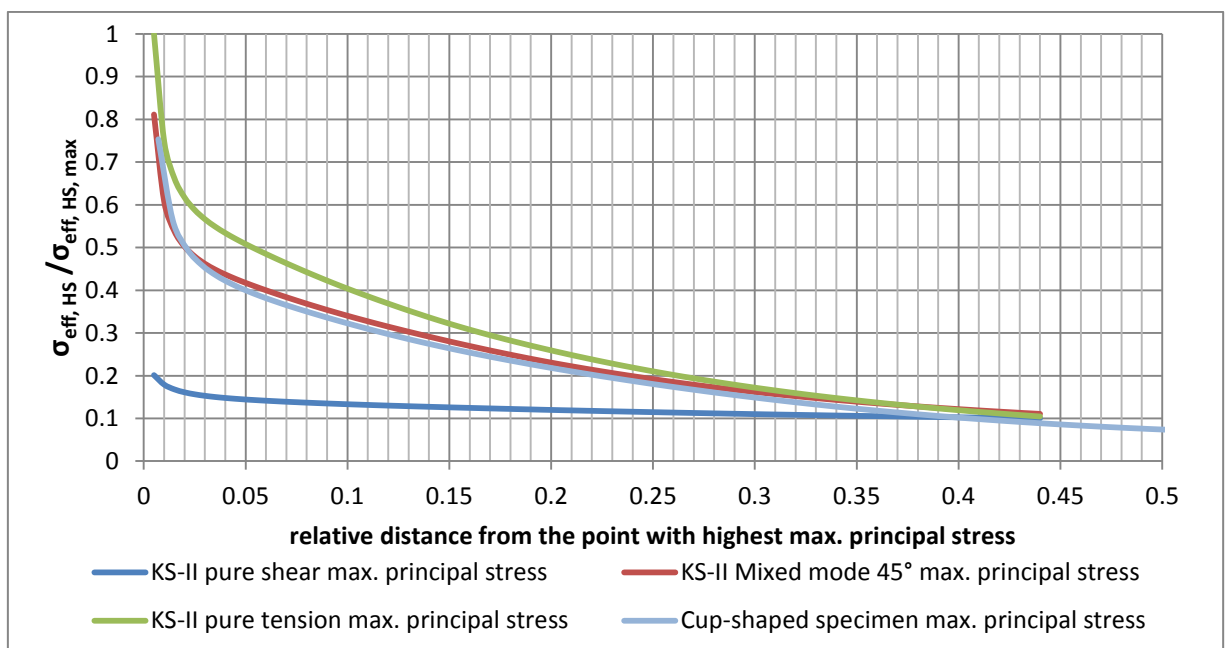


Figure 6-35: Average stress distribution of KS-II (along the path 1) and cup-shaped specimens applying the three hypotheses

---

In figure 6-35 it is possible to observe that applying the hypothesis that the peak stress also depends on the adhesive layer width, the two mixed-mode loads are almost the same curve. That is a very positive results of the hypotheses applied.



---

---

## 6.2 Comparison of stress approaches in a master S-N curve

---

A master S-N curve for adhesive joints is investigated.

The function to calculate this master S-N curve is the same that was used previously to calculate the S-N curves of the samples in chapter 5.1. The function is developed in Matlab software and it is based on a maximum likelihood approach. It is named BMW Wöhlerlinie-tool *version 1.2b*.

The stress values to calculate this S-N curve are obtained from the finite element models explained in chapter 4.

To evaluate the results of the master S-N curves two aspects are evaluated. The first one is the minimum scatter of the S-N curve. This value determines the accuracy of the results obtained. The second aspect is the interval where this method is valid (robustness). The results of the method applied can be strongly influenced by the location where they are applied.

---

### 6.2.1 Critical distance approach

---

In this chapter, the critical distance approach is studied based on a master S-N curve. Several variants are studied based on the results obtained on the previous chapter 6.1.1. In this case, two parameters are varied. One of these parameters is the two different equivalent stresses, the maximum principal stress and the equivalent elliptic stress. On the other hand, three different hypotheses are also proposed and compared. They were previously explained:

- Constant gap
- Relative distance
- Stress scaled relative to the width

The next figure 6-36 summarised the results of this variants in a graphic:

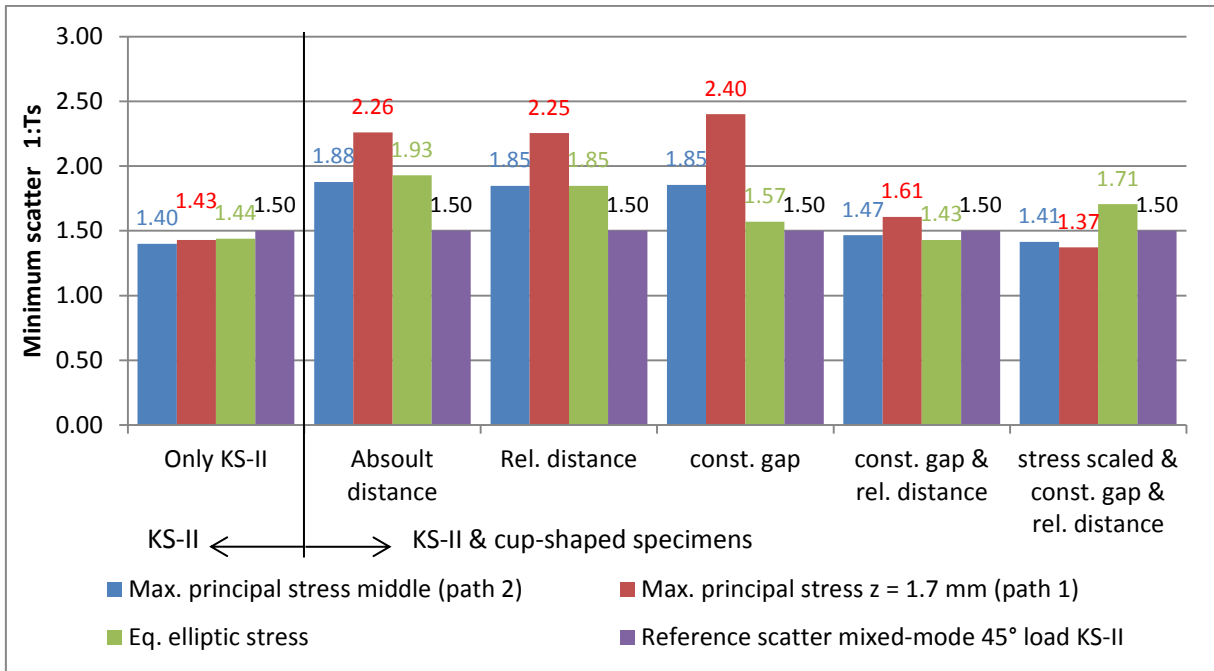


Figure 6-36: Minimum scatter of the different parameters applying the critical distance approach

In this case three different types are compared between them, two different paths along the KS-II specimen using the maximum principal stress and one using the equivalent elliptic stress. The purple bars are used as a reference. They represent the scatter of the KS-II loaded with a mixed-mode load with an angle of 45°. This value is obtained from figure 5-1. The group only KS-II is the minimum scatter of the master S-N curve using only the values obtained from the KS-II simulation. In the rest, the stress-state of the cup-shaped specimen is evaluated with the KS-II specimen.

From figure 6-36 it is possible to observe that the reference stress that changes more with the hypotheses is the stress distribution of path 1. Moreover, it is the one with a minimum scatter applying all the hypotheses. This result is coherent because the reference stresses of the cup-shaped specimen are the one along the path with highest value of maximum principal stress and path 1 contains the highest value of maximum principal stress for pure tension and mixed-mode load.

Figure 6-37 compares the interval where the method can be used:

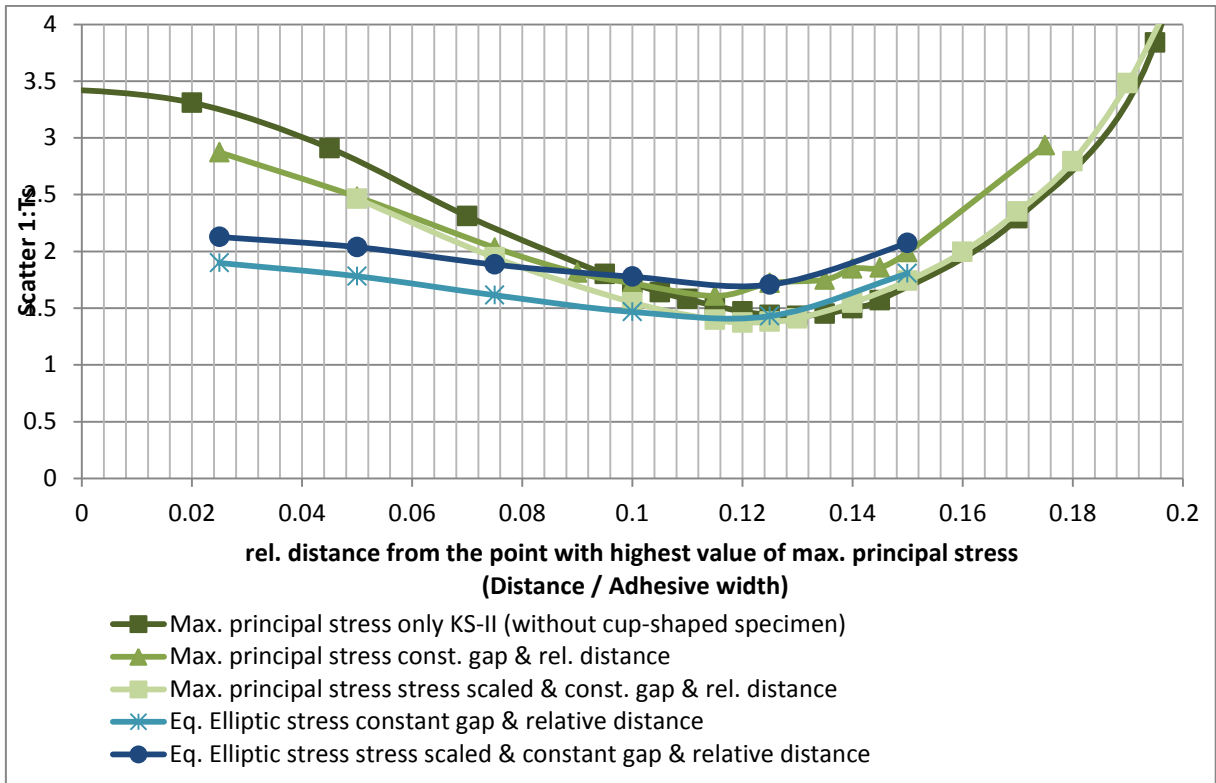


Figure 6-37: Scatter values along the distance applying the critical stress distance approach

In figure 6-37 it is possible to observe the robustness of this method. From experience and other test realized by BMW Group with adhesive joints, it is considered a reasonable scatter until a value of  $T_s = 1:2$ . With this limit is possible to observe that this interval is around 1 mm. This figure is also giving the information that applying the hypotheses does not change the reference point. That means that the cup-shaped specimen adapted to the KS-II reference curve. Another aspect to remark is that in this case, the equivalent elliptic stress is less influenced by the location of this distance due to their flatter curve.

## 6.2.2 Stress averaging approach

In this approach, based on the results obtained by the previous chapters, only the stresses of path 1 are taken as reference. With this evaluation it is possible to compare the two methods. Figure 6-38 exposes the results of this method:

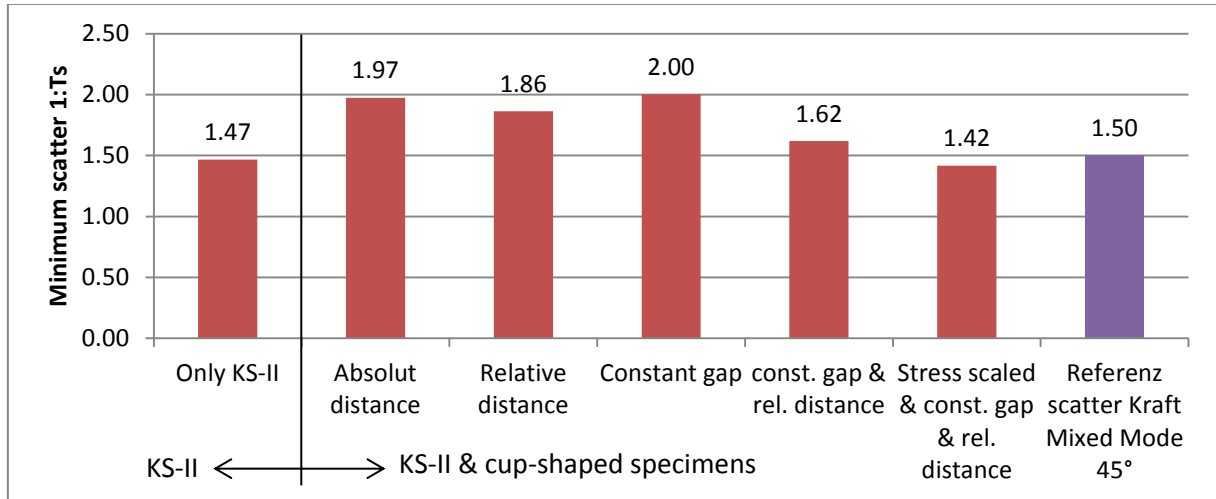


Figure 6-38: Minimum scatter of the master S-N curve for the several hypotheses using the reference stresses of path 1 applying the stress averaging approach

The minimum scatter is similar to the previous method exposed as well as the results of the different hypotheses. The valid results are applying the relative distance and constant gap hypotheses and applying the three of them previously mentioned. The interval width is a factor in these methods that determinates the reliability of them. Figure 6-39 illustrates that:

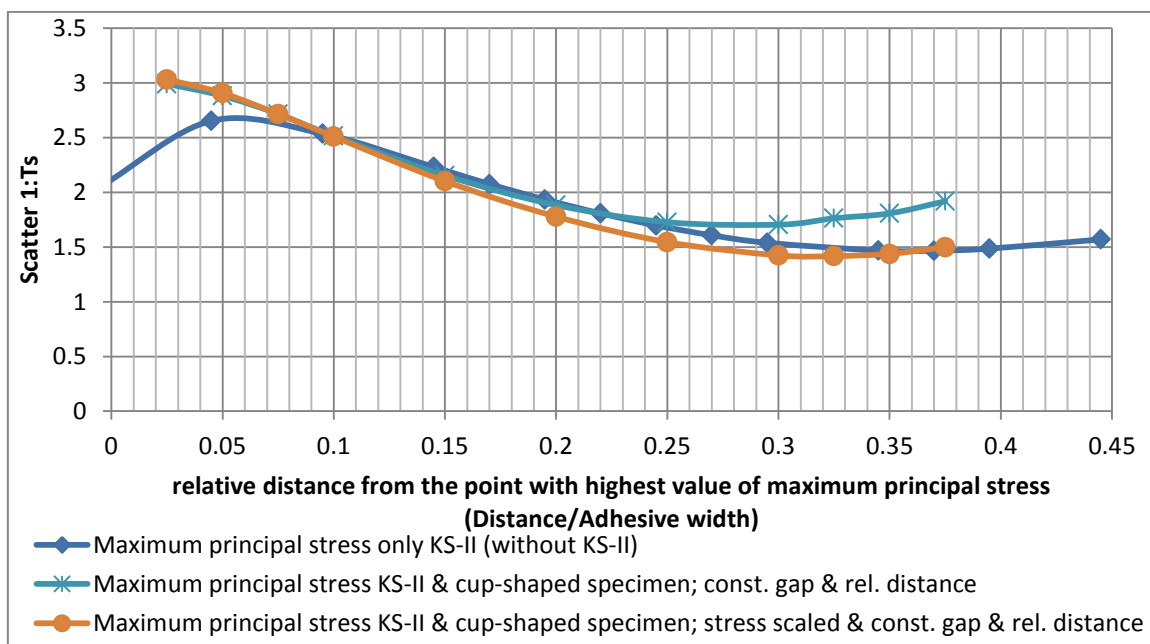


Figure 6-39: Scatter values of the master S-N curve along the path 1 applying the stress averaging approach

From the figure 6-39 it is possible to observe that the interval valid to apply the method is wide. That is a positive aspect of this approach, because it is less influenced by the local point chosen (robust). In this case, the best solution with the both specimens (KS-II and cup-shaped) displaces approximately slightly the optimum point from the single KS-II master S-N curve. But the influence of this displacement does not strongly affect the result due to the flatness of the scatter curve.

### 6.2.3 Comparison of the applied approaches

To conclude this chapter a comparison between the two approaches is realized. The comparison is based on the scatter obtained of the master S-N curves for the three loading types of the KS-II specimen and the mixed-mode load of the cup-shaped specimen. In the case of the KS-II the reference stresses are the stresses along the path with the highest value of maximum principal stress (along path 1). The stresses reference of the cup-shaped specimen is also the perpendicular path along the joint with the highest maximum principal stress. This comparison is evaluated with the maximum principal stress (HS).

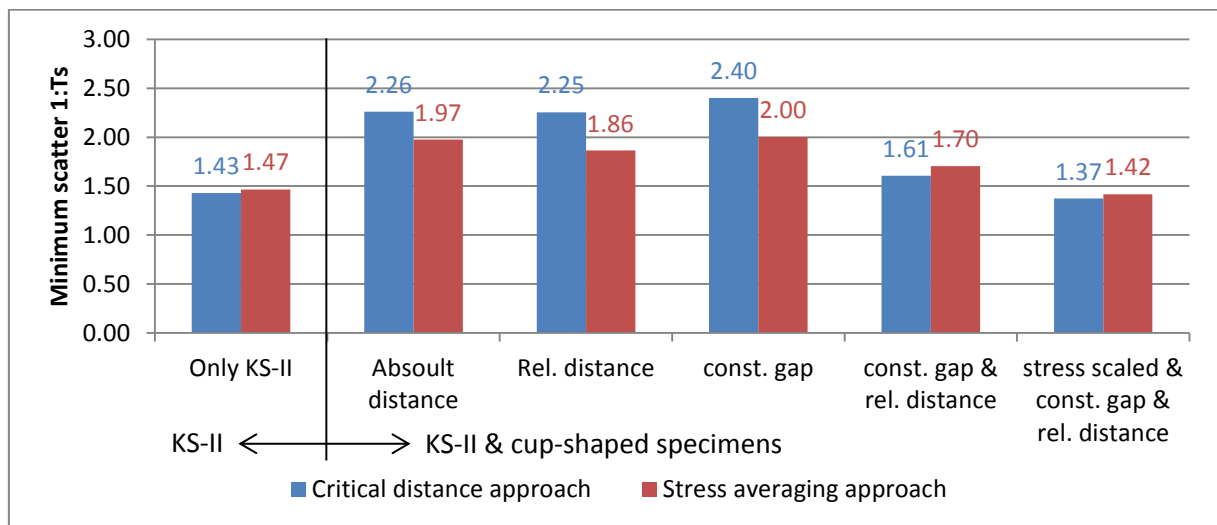


Figure 6-40: Comparison of the minimum scatter between the two approaches

The figure 6-40 summarise the results of the both approaches. It is possible to observe that the single hypotheses cannot improve properly the results, but the combination of the relative distance and the constant gap hypotheses reaches reasonable results. Further improvement achieved when the hypothesis of scaling the stress is applied. In terms of minimum scatter the stress averaging approach may give smoother results, but in absolute terms they are very similar.

The next step is to compare the interval where this method is valid in the both cases. This is summarized in the figure 6-41:

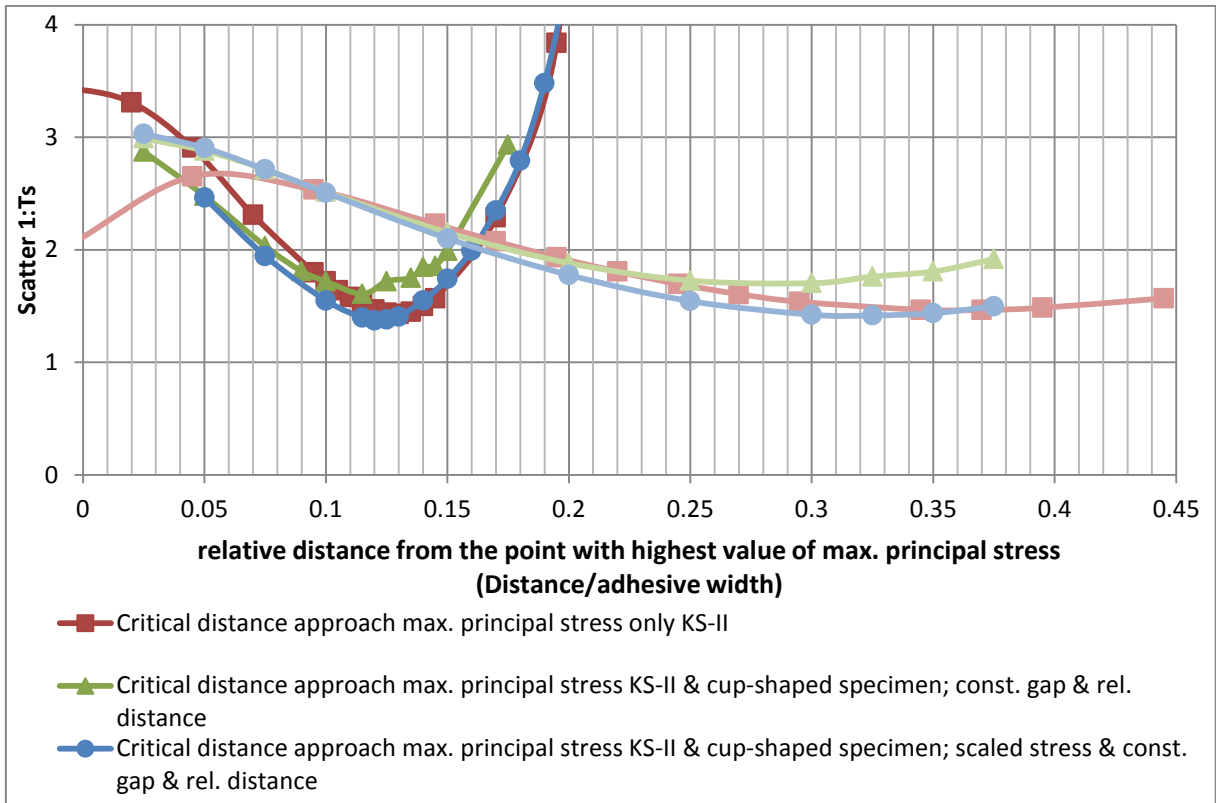


Figure 6-41: Scatter values of the approaches along the distance

In the figure 6-41 it is possible to observe the location where the two methods are valid and its scatter along their optimum point. In this case is very clear that the interval of the stress averaging approach is much wider than the critical stress distance.

To resume and conclude the reliability of the two approaches is that with the hypotheses considered the both approaches can be valid to evaluate an adhesive joint with the same material and with similar geometry. It is reached a good correlation value between the two specimens. But the stress averaging approach has less influence on the local point chosen as the critical distance approach.

---

## 7 Evaluation of the butt-joined specimen submitted to non-proportional loading

---

The last chapter contains the fatigue evaluation of the non-proportional load type for butt-joined specimen. As exposed in the chapter 3.5, one of the four loading types in butt-joined specimen is a composition of torsion and tensile stress with a 90° phase shift. For this type of load applying a proportional method as used before is not recommended, because the stress tensor is not proportional. The stress tensor is dependant of the phase and it is not constant during the cycle. That can produce a change of the maximum principal stress direction during the cycle and create sequences inside the cycle. In these cases one of the suitable methods to realize a fatigue study is the critical stress plane.

The method is detailed explained in chapter 2.2.5'. For further information see [Sus10].

The first step to evaluate the test is to define the stress tensor dependent on the phase. The global tensor for each point is the sum of the stress state of each point of pure tension and pure torsion state, taking into account the phase shift. Because of this last reason, the global tensor is dependent on the phase  $\varphi$ .

$$[\sigma(\varphi)_{total}] = [\sigma(\varphi)_{pure\ tension}] + k \left[ \sigma(\varphi - \pi/2)_{pure\ torsion} \right] \quad (7.1)$$

$$\text{where } k = r_{M/F} = 3.6$$

$$[\sigma(\varphi)_{pure\ tension}] = \cos(\varphi) \cdot [\sigma_{pure\ tension}] \quad (7.2)$$

$$[\sigma(\varphi)_{pure\ torsion}] = \cos(\varphi) \cdot [\sigma_{pure\ torsion}] \quad (7.3)$$

$$[\sigma(\varphi)] = \begin{bmatrix} \sigma_x(\varphi) & \sigma_{xy}(\varphi) & \sigma_{xz}(\varphi) \\ \sigma_{xy}(\varphi) & \sigma_y(\varphi) & \sigma_{yz}(\varphi) \\ \sigma_{xz}(\varphi) & \sigma_{yz}(\varphi) & \sigma_z(\varphi) \end{bmatrix} \text{ where } \varphi \in T \quad (7.4)$$

The stress tensor  $\sigma(\varphi)$  is considered as nominal tension force. With this description is possible to scale easily the tensor to obtain the real stress-state, due to the linear-elastic behaviour of the adhesive joints. The parameter  $r_{M/F}$  represents the constant relation between the force and moment. It is previously described in equation (5.5) (page 42). The next step is to find the

---

critical stress plane for each studied point. In this case a *Matlab* subroutine (iterative algorithm) is programmed to find the critical stress plane in each point. The critical plane found is defined as the plane in which the variance of tensile stress is maximal. For other materials, like steel in [Sus10] and [Sus13], the critical plane is the one with maximum variance of shear stress, because on fatigue steel test the shear stress is the critical stress state. In the case of adhesive, as could be seen in the chapter 5.1, the critical stress is the tensile stress. Because of this reason it is decided that the critical plane is the plane with a maximum variance of tensile stress.

The iterative algorithm increases the angles  $\phi$  and  $\theta$   $10^\circ$  from  $0^\circ$  to  $180^\circ$  (according symbolism adopted in figure 2-13, page 24). The other half is not calculated because they have the same value with different sign. For each possible plane the variance of the tensile strength is calculated using also a phase interval of  $10^\circ$  from  $0^\circ$  to  $360^\circ$ . Then the algorithm compares the variance of normal stress and takes the one with maximum value.

That means that in total there are 324 possible planes. The variance is calculated from 36 points. This iteration is realized in each node of the middle adhesive layer with 0.1 mm element length. After found the plane with maximal variability of the tensile stress, the angle  $\alpha$  is calculated with another iteration based on the direction with maximal variability of the shear stress inside the critical plane ( $\phi$  and  $\theta$  fixed).

The results obtained are accord the stress distribution seen previously in the figure 6-17 (page 65). The critical stress state near the symmetric axis is the direction of the tension force, because in the middle of the adhesive is where the tensile strength is maximal. Otherwise, near the border the orientation of the critical plane is orientated to the shear stress.

Once the critical stress plane is found for each point, the tensile and shear stresses are defined. Then a damage accumulation method is applied. The method consists in applying a rain-flow matrix to simplify the subsequence inside the cycle to one equivalent stress amplitude, as it is applied in FEMFAT 5.1 program [Mag15]. After that, the PALMGREN-MINER rule, with the reference S-N curves from the pure loads, damage accumulation estimation is realized. In this particular case, due to the particular stress distribution and loads on the sample, there is any subsequence inside the cycle. All the critical planes have perfect sinusoidal behaviour during the cycle. This is the consequence of apply two different pure loads as torsion and tension load, which tensors components combine between them without modifications or sums. Because of this reason, the rain-flow matrix can be avoided and it is



possible to apply the damage accumulation method with the stress amplitude of the sinus curve obtained from the tensile and shear stress of the critical plane.

The damage accumulation method applied is the PALMER-MINER rule. S-N curves obtained in chapter 5.1.3 from pure tension and pure torsion load are established as the reference curves. The damage accumulation is calculated on the 16 butt-joined samples loaded with this non-proportional loading type (all of them failed).

The results below exposed are the point along the middle layer with maximum damage accumulation.

Table 7-1: Maximum damage accumulation for the 16 butt-joined samples with combined loads with phase shift

$F_a$ [kN]	3.02	2.88	3.3	3.39	3.44	3.53	3.2	3.39
$D_{exp}$	0.395	0.030	0.035	0.263	0.194	0.139	0.053	0.272

$F_a$ [kN]	3.62	3.58	3.25	2.88	2.79	2.74	2.83	2.55
$D_{exp}$	0.151	0.449	0.215	0.027	0.101	0.015	0.014	0.022

This point of maximum damage accumulation is situated all the time near the revolution axis (1.7 mm from the revolution axis), where the tensile stress is higher. This result can be explained by two theories. The first one is that the tensile strength is the critical stress-state for the adhesive and it fails where the tensile stress is maximal. The other option is that in this particular case, the torsion stress is very low in comparison with the maximum torsion stress that the joint can support (Figure 5-4, page 44). But the tensile stress is near the maximum tensile stress that the joint can support (near the values of pure tension force).

The values of the experimental damage accumulation are between 0.4 and 0.014. These values can be found similar in literature, for example in [Sch14]. But this total damage varies strongly because of the flat slope of the S-N curves.

---

---

## 8 Conclusions

---

This work is a study of different methods to evaluate structural adhesive joints submitted to cyclic loads with constant amplitudes. It is based on the experimental results of three different specimens: KS-II, cup-shaped specimen similar to the real components and butt-joined cylinder specimens.

To avoid differences on the specimens the three types are joined with the same adhesive and the same thickness. The substrates of the specimens are steel to secure a cohesive rupture of the joint. The three specimens are loaded with constant variable amplitude with a stress ratio of  $R=0.1$ , which generates a tensile mean stress.

The first study of the thesis is the evaluation of the tests to determinate the S-N curves for every specimen and loading type and their behaviour under cyclic loads with tensile mean stress. With this first study it is possible to observe the high values of the slope of S-N curve respect to the metallic materials. It is also shown that the tensile stress is more critical on the adhesive joint than the shear stress. The non-proportional load is an aspect that has a high influence in metals but it is a new investigation direction for adhesive joints. From the results obtained with this butt-joined specimen, the S-N curve of the non-proportional load is very similar to the one obtained for the proportional load. The butt-joined specimens were used to study the creep behaviour of the adhesive and the possible reduction of their stiffness. From the experiments it could be seen that there is a creep effect due to the positive mean stress, but there is no loss of stiffness.

Two different approaches widely used in the fatigue analysis of metallic components and welds were compared to develop a reliable method to evaluate the lifetime of adhesive joints. The two methods are stress-based approaches named critical distance approach and stress averaging approach. The stresses to compare these specimens are obtained through FEM. In this study several hypotheses based on the total width of the adhesive are applied to evaluate their influence on the method. These hypotheses are based on the similar distribution of tension perpendicular to the joint direction. The two approaches achieved a good correlation to evaluate the adhesive joints. Despite the high accuracy of the results, the stress distance approach has higher influence of the chosen point than the critical distance approach.

It is also compared the accuracy of the results using the maximum principal stress and an equivalent stress named elliptic stress based on the tensor invariants. This equivalent stress gave good results for quasi-static failure assessment of adhesives, because it considers the hydrostatic component of the stress. Despite the good results obtained from this equivalent

---

stress, it has several drawbacks for application. One of them is the necessity to experimentally determine its parameters. They have to be determined through the stress-state of a reference point and they are strongly influenced by it. The results can vary strongly because of the determination of these parameters, reducing the accuracy and reliability of the method.

A damage accumulation method is applied to evaluate the non-proportional load of the butt-joined specimen. This method is complex to apply in adhesive joints and does not give high accuracy results due to the high value of the S-N curve slope.

In this work the suitability of the stress-based and damage accumulation methods is realized. It has been observed the high influence of the geometry on the stress distribution on the adhesive layer and the possible influence of the total width of the adhesive as another parameter to determinate the lifetime of an adhesive joint. Further studies are needed in this field to evaluate the suitability of the current methods and specimens on adhesive joints and possible improvements of them.

---

---

## 9 Outlook

---

This work opens different direction to investigate in further studies about the lifetime prediction of adhesive joints.

One is the suitability to study this joint from a fatigue approach. Fatigue became important in the industry world due to the failure of materials under low cyclic loads. In the adhesive, the slope of S-N curve is quite flat, which means that the fatigue effect is lower. The adhesive has less difference behaviour between quasi-static load and cyclic load based on stress approaches. The outlook is to verify the suitability of simplify the fatigue approach for a quasi-static approach in adhesive joints lifetime predictions.

Another is the further studies about the creep effect of the adhesive. Creep effect has a big influence in the structures stiffness. No loss of stiffness was observed in this adhesive until the failure. The specimens were tested submitted to constant cyclic amplitudes. Other tests, with combined amplitudes, should be studied to determine this creep effect accurately.

In the same direction, further studies with non-proportional loads should be realized to study the effects of phase shift and combined loads in adhesive joints with specimens and loads similar to the automotive industry components.

---

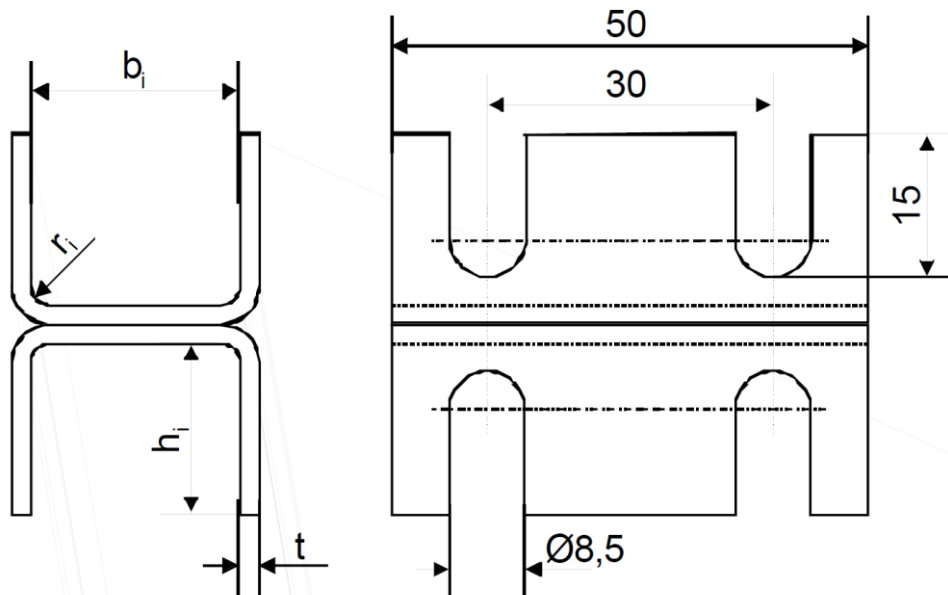
---

## Annex

---

### A. Technical drawings

#### A.1. KS-II specimen

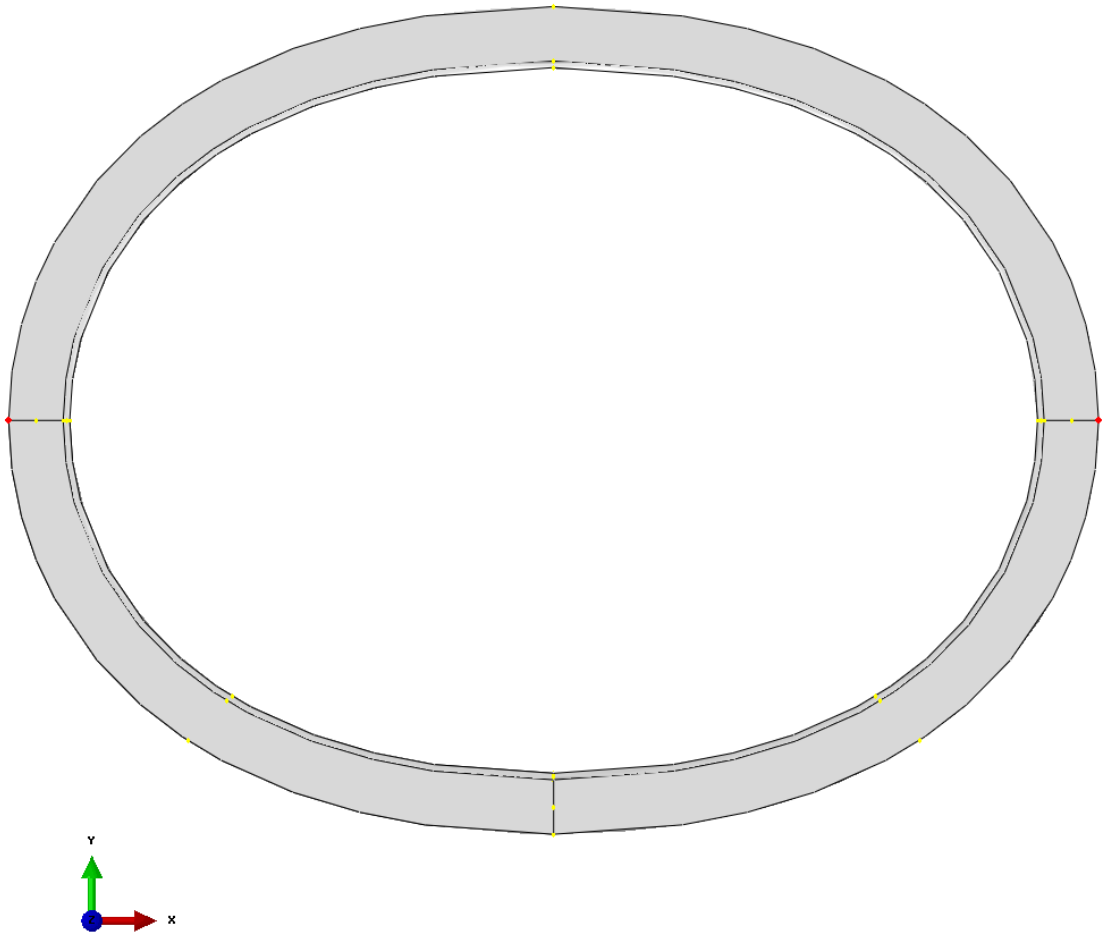


	Blehdicken [mm]			
	0,8-1,5	>1,5-2,5	>2,5-3,5	>3,5-4,5
Innenbiegeradius $r_i \pm 0,2$ [mm]	2	4	6	8
Innenweite $b_i +0,2$ [mm]	22	26	30	34
Innenhöhe $h_i \pm 0,1$ [mm]	18	22	26	30

The thickness of the metal plate is 1.5 mm

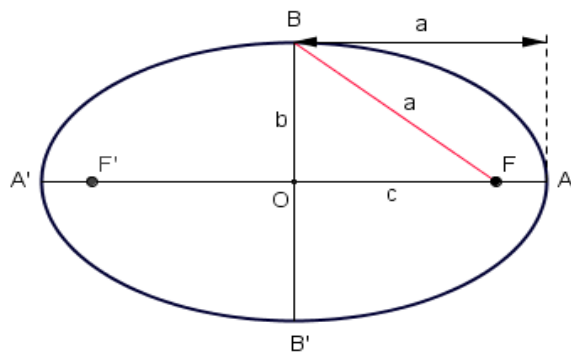
---

## A.2. Cup-shaped specimen



x	0.47191
y	0.81738
z	0.33044

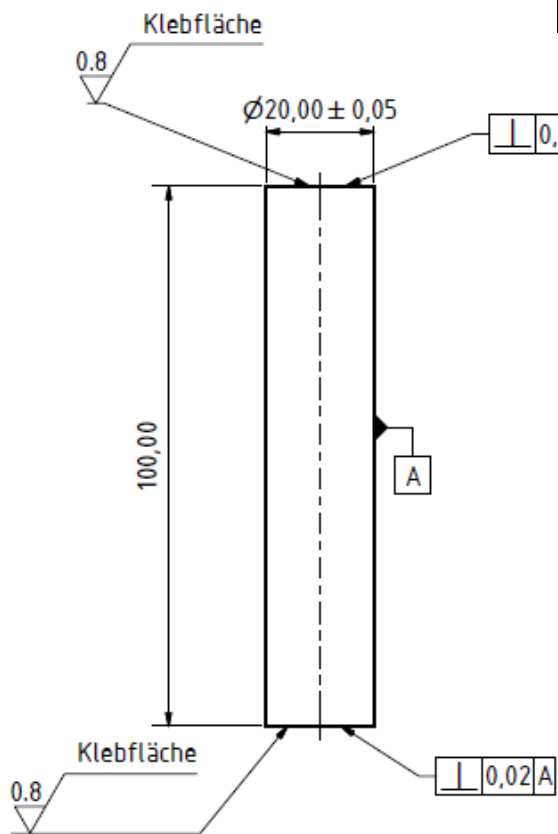
Unitary components of mixed load force in cup-shaped specimen



Oberfläche [mm <sup>2</sup> ]	9220.30
Breite Klebstoff [mm]	14
Dicke [mm]	1.5

### A.3. Butt-joined cylinder specimen

	Innenellipse	Außenellipse
a [mm]	111	125
b [mm]	81	95



Kanten scharfkantig,  
100 St.  
Material: 1.0036

---

---

## Bibliography

---

- [Aba10] **Collective of authors:** Abaqus 6.10-1-Dokumentation. ABAQUS Inc. (2010)
- [Bac08] **Bacher-Höchst, M.; Berger, C.; Sonsino, C.M.; Vormwald, M.:** *Current developments and trends on structural durability*. Mat.-wiss. u. Werkstofftech. 39, No. 10 (2008) S.680-687
- [Bet04] **Betten, J.:** *Kontinuumsmechanik*. Springer-Verlag 2004. – ISBN 978-3-540-42043-9
- [Bik68] **Bikermann, J. J.** *The Science of Adhesive Joints*. New York: Academic Press (1968)
- [Car00] **Carpinteri, A.; Spagnoli, A.:** *Multiaxial high-cycle fatigue criterion for hard metals*. International journal of fatigue 23 (2001) 135-145
- [Eul00] **Eulitz, K.G.; Kotte, K.L.:** *Damage Accumulation – Limitations and Perspectives for Fatigue Life Assessment*. In: Materials Week. München (2000)
- [Eul99] **Eulitz, K.G.:** *Beurteilung der Zuverlässigkeit von Lebensdauervorhersagen nach dem Nennspannungskonzept und dem Örtlichen Konzept anhand einer Sammlung von Betriebsfestigkeitsversuchen*. Habilitationsschrift, TU Dresden (1999)
- [FAT221] **Tölle, J.; Schmidt, H.; Hahn, O.; Hanselka, H.:** *Entwicklung einer Methode zur vergleichenden Bewertung von Schwingfestigkeitsversuchen mit gefügten Stahlfeinblechen in Abhängigkeit des Versagensverhaltens*. FAT- Schriftenreihe 221, AVIF- Projekt A233, Berlin, Paderborn, Darmstadt (2009)
- [Gas39] **Gaßner, E.:** *Festigkeitsversuche mit wiederholter Beanspruchung im Flugzeugbau*. In: LUFTWISSEN 6 (1939) S.61-64
- [Gas67] **Gaßner, E.:** *Betriebsfestigkeit*. In: Lueger Lexikon der Technik, Band Fahrzeugtechnik. Deutsche Verlagsanstalt. Stuttgart (1967)
- [Gei12] **Geiß, P.L.; Fritzsche, C.; Kleiner, F.; Peschka, M.; Rauscher, M.; Schmale, H.C.; Vogt, D.; Zanotti, A.; Weber, C.; Boldt, F., Wibbeke, M.:** *Kleben von Stahl und Edelstahl Rostfrei*. Merkblatt 382. Stahl-Informationen-Zentrum, Informationsstelle Edelstahl Rostfrei (Hrsg.). Düsseldorf (2012)
- [Gro07] **Gross, D.; Hauger, W.; Wriggers, P.:** *Technische Mechanik 4*. Springer-Verlag, 2007. – ISBN 978-3-540-22099-2
- [Hab06] **Habenicht, G.:** *Kleben Grundlagen – Technologie – Anwendung*. Springer – Verlag (2006)
- [Hah00] **Hahn, O.; Kurzok, J. R.; Oeter, M.:** *Prüfvorschrift für die LWF KS-2-Probe – Forschungsbericht*. Laboratorium für Werkstoff- und Fügetechnik, Universität Paderborn (2000)
- [Hah95] **Hahn, O.; Schulte, A.:** *Eignung des Durchsetzfügens und des Stanznietens zum Fügen höherfester Stahlbleche*. P283 Studie, Studiengesellschaft Stahlanwendung e. V., Düsseldorf (1995); ISBN – 3-93062138-X
- [Hai03] **Haibach, E.:** *Betriebsfestigkeit: Verfahren und Daten zur Bauteilberechnung*. 3. Aufl. Springer-VDI Verlag. Heidelberg (2003)
- [Hai06] **Haibach, E.:** *Betriebsfestigkeit: Verfahren und Daten zur Bauteilberechnung*. 2. Auflage, Springer- Verlag, Berlin, Heidelberg, New York (2006)



- 
- [Hai89] **Haibach, E.:** *Betriebsfestigkeit; Verfahren und Daten zur Bauteilberechnung.* VDI-Verlag. Düsseldorf (1989)
- [Har11] **Hartmann, J.; Monin, M.; Marie Lousie, A.; Ayglon, D.; Robichon, P.; Limousin, E.; Gerard, F.; Naudin, F.; Guyon, D.; Launay, A.; Büter, A.; Sonsino, C.M.:** *Influence of frequency and stress concentration on fatigue behavior of short glass-fibre reinforced polyamides.* Proceedings: International conference on fatigue design, Senlis (2011)
- [Hen11] Nach Pressemitteilung der Firma **Henkel AG & Co. KGaA** in Schweißen und Schneiden 63. Heft 10 (2011) S. 607 – 610
- [Her14] **Hernando, R.:** Praktikumsbericht (2014). BMW AG. München.
- [Her96] **Herrmann, F., Kiehn, H. und Stäblein, R.:** *Lebensdauer von Blechen mit Sicken.* Forschungsvereinigung Automobiltechnik e.V., FAT Schriftenreihe Nr. 128. Frankfurt (1996)
- [Hol04] **Hollmann, C.:** *Die Übertragbarkeit von Schwingfestigkeits-Eigenschaften im Örtlichen Konzept.* Dissertation. Technische Universität Dresden (2004)
- [Köt84] **Kötting, G.:** *Untersuchung der Klebschichtmorphologie und der beanspruchungsabhängigen Deformations- und Versagensmechanismen in der Klebfuge von Metallklebverbindungen.* Diss. Univ. Ges. Hochsch. Paderborn (1984)
- [Kre99] **Kretz, J.:** *Zur Zeitfestigkeit von Verbundträgern mit Profilbelchen.* Dissertation. Universität Kaiserslautern (1999)
- [Mag15] **Magna:** *FEMFAT 5.1 basic Theorie-Manual*
- [Mat12] **Matzenmiller, A.; Kroll, U.:** Constitutive modelling of damage in adhesively bonded joints for static and cyclic sustained loadings with constant and variable amplitudes. European Congress on Computational Methods in Applied Sciences and Engineering, Wien (2012)
- [Men11] **Menzel, S.:** *Zur Berechnung von Klebverbindungen hybrider Karosseriestrukturen beim Lacktrocknungsprozess,* Technische Universität Dresden, Dissertation, 2011
- [Min45] **Miner, M.A.:** *Cumulative damage in fatigue.* In: Journal of Applied Mechanics 12, 3 (1945) S. A159-A164
- [Neu61] **Neuber, H.:** *Theory of Stress Concentration for Shear-Strained Prismatical Bodies with Arbitrary Nonlinear Stress-Strain Law.* Trans. ASME, Journal of Applied Mechanics 28 (1961)
- [Pal24] **Palmgren, A.:** *Die Lebensdauer von Kugellagern.* In: VDI-Z 68, 14 (1924) S.339-341
- [Rad03] **Radaj, D.:** *Ermüdungsfestigkeit Grundlagen für Leichtbau, Maschinen- und Stahlbau.* Springer-Verlag. Berlin (2003)
- [Rad07] **Radaj, D.; Vormwald, M.:** *Ermüdungsfestigkeit.* 3. Auflage, Springer Verlag, Berlin (2007)
- [Rut03] **Ruther, M.; Jost, R.; Freitag, V.; Peitz, V.; Piccolo, S.; Brüdger, s.; Meschut, G.; Küting, J.; Hahn, O.; Timmermann, R.:** *Fügesystemoptimierung zur Herstellung von Mischbauweisen aus Kombinationen der Werkstoffe Stahl, Aluminium, Magnesium und Kunststoff.* BMBF- Abschlussbericht Förderkennzeichen 03N3077D1 (2003)

- 
- [Sch03] Schäfer, M.: Vorlesungsskript *Numerische Berechnungsverfahren*. Technische Universität Darmstadt (2003)
- [Sch05] Schlimmer, M.: *Methodenentwicklung zur Berechnung und Auslegung geklebter Stahlbauteile im Fahrzeugbau* – Forschungsvereinigung Stahlanwendung e.V.– Forschungsbericht (2005)
- [Sch07] Schürmann, H.: *Konstruieren mit Faser-Kunststoff- Verbunden*. Springer-Verlag (2007)
- [Sch14] Schmidt, H.: *Schwingfestigkeitsanalyse strukturelle Klebverbindungen unter Belastung mit variablen Amplituden-Doctoral Thesis*, Fraunhofer-Institut für Betriebsfestigkeit und Systemzuverlässigkeit LBF, Darmstadt (2014)
- [Sch74] Schlimmer, M.: *Fließverhalten plastisch kompressibler Werkstoffe*, RWTH Aachen, Dissertation, 1974.
- [Sil10] da Silva, L. F. M.; Öchsner, A. (Eds.): *Modelling of Adhesively Bonded Joints*. Springer- Verlag, Berlin, Heidelberg (2010).
- [Son05] Sonsino, C.M.: *Betriebsfestigkeit – Eine Einführung*. Vorlesungsunterlagen, Technische Universität Darmstadt (2005)
- [Son07] Sonsino, C.M.: *Fatigue testing under variable amplitude loading*. In: International Journal of Fatigue, Volume 29, Issue 6 (2007) S.1080-1089
- [Son08] Sonsino, C.M.: *Betriebsfestigkeit – Eine Einführung in die Begriffe und ausgewählte Bemessungsgrundlagen*. MP Materials Testing 50 (2008) 1-2, S.77-90
- [Son11] Sonsino, C.M.; Oppermann, H.: *Lässt sich bei einer Lebensdauerabschätzung die Kollektivvölligkeit berücksichtigen?* Konstruktion 6 (2011) S.1-8
- [Son12] Sonsino, C.M.; Morgenstern, C.; Streicher, M.; Oppermann, H.; Schmid, A.M.: *Corrosion fatigue of welded aluminium vehicle structures under constant and variable amplitude loadings*. Welding in the World Vol. 56 (2012) S. 97-108
- [Sta98] Stachowiak, E.: *Klebeteknik als Fügeverfahren – Einstieg für die Anwendung*. VDI Fortschrittsberichte Reihe 2 Fertigungstechnik No. 468. VDI Verlag GmbH. Düsseldorf (1998)
- [Ste12] Stemp, A.: *Validierung einer faserverbundgerechten Prüfmethode zur Kennwertermittlung von Verbindungstechniken- Diplomarbeit*, Hochschule Hof (2012)
- [Sus10] Susmel, L.: *A simple and efficient numerical algorithm to determine the orientation of the critical plane in multiaxial fatigue problems*. International Journal of Fatigue 32 (2010) 1875-1883.
- [Sus11] Susmel, L.; Taylor, D.: *A critical distance/plane method to estimate finite life of notched components under variable amplitude uniaxial/multiaxial fatigue loading*. International Journal of Fatigue 38 (2012) 7-24
- [Sus13] Susmel, L.; Tovo, R.; Socie, D.F.: *Estimating the orientation of Stage I crack paths through the direction of maximum variance of the resolved shear stress*. International Journal of Fatigue 58 /2014 94-101
- [Tay00] Taylor, D; Bologna, P.; Bel Knani, K.: *Prediction of fatigue failure location on a component using a critical distance method*. International Journal of Fatigue 22 (2000) 735-742

- 
- [Tay07] **Taylor, D.:** *The theory of critical distances: a new prespective in fracture mechanics.* Elsevier Science (2007)
- [Teu12] **Teutenberg, D.:** *Entwicklung einer Vorgehensweise zur Abschätzung der Einflüsse konstruktions- und fertigungsbedingter Toleranzen auf die mechanischen Eigenschaften von Klebverbindungen unter zyklischer Belastung.* Dissertation. Universität Paderborn (2012)
- [Tre12] **Treffler, R.:** Ermittlung eines Kriteriums zur Betriebsfestigkeitsbewertung von CFK-Stahl Klebeverbindungen, Diplomarbeit, Technische Universität München und BMW AG, München (2012)
- [Vor00] **Vormwald, M.:** *Treffsicherheit von Lebensdauerberechnungen nach dem Nennspannungskonzept und dem örtlichen Konzept.* Insitutionsbericht. Institut für Strukturmechanik. Bauhaus-Universität Weimar (2000).
- [Vor03] **Vormwald, M.; Seeger, T.:** *Betriebsfestigkeit auf der Grundlage örtlicher Beanspruchung.* Unterlagen zum gleichnamigen Seminar der Technischen Universität Darmstadt, Fachgebiet Werkstoffmechanik (2003)
- [Wal03] **Wallmichrath, M.; Sonsino, C.M.; Bruder, T.:** *Betriebsfestigkeit gefügter Bauteile.* In: Bundesministerium für Bildung und Forschung –BMBF- u.a.: Mechanisches Fügen und Kleben. Universität Paderborn (2003) S. 163-173

---

---

## Norms

---

DIN EN ISO 10365	<i>Adhesives: Designation of main failure patterns.</i> Beuth Verlag GmbH, Berlin (1995)
ISO 11003-2	<i>Adhesives: Determination of shear structural adhesives, Part 2: Tensile test method using thick adherends</i> (2001)
DIN EN 1465	<i>Adhesives: Determination of tensile lap-shear strength of bonded assemblies.</i> English version of DIN EN 1465: 2009-07 (2009)
DIN EN ISO 527-1	<i>Plastics: Determination of tensile properties. Part 1 : General principles</i> (2012)
DIN EN 9664	<i>Verfahren zur Prüfung der Ermüdungseigenschaften von Strukturklebungen bei Zugscherbeanspruchung</i> (1995)

